

TWENTY-SECOND ANNUAL CONFERENCE ON THE PHYSICS AND CHEMISTRY OF SEMICONDUCTOR INTERFACES

January 8-12, 1995

Holiday Inn and Conference Center, Old Town Scottsdale, Arizona

Program Committee:

R. M. Feenstra, *IBM*
M. Hybertsen, *AT&T*
A. Kahn, *Princeton*
G. Lucovsky, *North Carolina State*
C. G. Van de Walle, *Xerox PARC*

Consultants:

D. K. Ferry, *Arizona State*

Ex Officio

D. E. Aspnes, *North Carolina State*
L. R. Cooper, *ONR*
J. D. Dow, *Arizona State*
D. J. Wolford, *Iowa State*

Arrangements:

R. E. Allen, *Texas A&M University*

T. C. McGill, *Caltech*



SPONSOR

The Office of Naval Research

INVITED TALKS: 28 minutes of oral presentation, 12 minutes of discussion, plus poster presentation.

CONTRIBUTED TALKS: 4 minutes of oral presentation and discussion, plus poster presentation.

PLEASE ASK QUESTIONS DURING THE INVITED TALKS, BUT AFTER CONTRIBUTED TALKS.

ALL POSTERS WILL BE DISPLAYED THROUGHOUT THE MEETING DOWNSTAIRS.

Su, Mo, Tu, We, and Th denote Sunday, Monday, Tuesday, Wednesday, and Thursday. Times are 2400 hour times.

DTIC QUALITY INSPECTED 3

19950703 226

DISTRIBUTION STATEMENT A

Approved for public release;
Distribution Unlimited

Miscellaneous information

Projectors: The conference will provide transparency projectors, a 35 mm slide projector, and a video cassette recorder with television display (standard American format).

Registration: Sunday night, conference registration is opposite the hotel registration desk. After that, the conference headquarters will be downstairs in the Teakwood room. The editorial office will be downstairs in the Teakwood room. All events are at the Holiday Inn - Old Town, Scottsdale, Arizona (a suburb of Phoenix).

Meals: Breakfast is not provided by the conference, but there will be goodies at the coffee breaks, and at the poster sessions (downstairs). The conference begins with a dinner for participants, Sunday (1700) at poolside, after which there is an opening session at 1900 (7:00 p.m.) in the Banyan ballroom. Attendees are on their own for all breakfasts and for dinner on Monday and Tuesday. The conference provides dinner on Wednesday (in the Banyan ballroom). Lunches will be provided Monday through Thursday, in the bar. Persons wishing a box lunch before 1130 Wednesday should make arrangements with the hotel.

Sessions: Oral presentations are in the upstairs ballroom. Posters are in the downstairs area, and should be put up Sunday evening and removed by noon Thursday (lest they be trashed). Contributed papers are allotted 4 minutes of oral presentation (no details, please), 1 minute for questions and discussion, and a 120 cm×120 cm poster (for details). Invited papers are allotted 28 minutes of oral presentation, 12 minutes of questions and discussion, and a 120 cm×120 cm poster.

Guests: Spouses, guests, and families may buy meal tickets for the Western dinner on Sunday and the dinner banquet on Wednesday.

Safety, Maps, Restaurants, Museums, and Trips: Information on these topics follows the Conference Scientific Program.

Accession For	
NTIS	CRA&I <input checked="" type="checkbox"/>
DTIC	TAB <input type="checkbox"/>
Unannounced	<input type="checkbox"/>
Justification _____	
By _____	
Distribution / _____	
Availability Codes	
Dist	Avail and/or Special
A-1	

REPORT DOCUMENTATION PAGE

Form Approved
OMB No. 0704-0188

Public reporting burden for this collection of information is estimated to average 1 hour per response, including the time for reviewing instructions, searching existing data sources, gathering and maintaining the data needed, and completing and reviewing the collection of information. Send comments regarding this burden estimate or any other aspect of this collection of information, including suggestions for reducing this burden, to Washington Headquarters Services, Directorate for Information Operations and Reports, 1215 Jefferson Davis Highway, Suite 1204, Arlington, VA 22202-4302, and to the Office of Management and Budget, Paperwork Reduction Project (0704-0188), Washington, DC 20503.

1. AGENCY USE ONLY (Leave blank)		2. REPORT DATE 28 June 1995	3. REPORT TYPE AND DATES COVERED Final 1 April 1994 - 28 June 1995	
4. TITLE AND SUBTITLE Final Report: Twenty Second Annual Conference on the Physics and Chemistry of Semiconductor Interfaces			5. FUNDING NUMBERS G: N00014-94-1-0636	
6. AUTHOR(S) C. R. Schulte				
7. PERFORMING ORGANIZATION NAME(S) AND ADDRESS(ES) Institute for Postdoctoral Studies P. O. Box 10146 Scottsdale, AZ 85271-0146			8. PERFORMING ORGANIZATION REPORT NUMBER F1-1995	
9. SPONSORING/MONITORING AGENCY NAME(S) AND ADDRESS(ES) Office of Naval Research ATTN: ONR 251:JWK Ballston Tower One 800 North Quincy Street Arlington, VA 22217-5660 CFDA No. 12.300			10. SPONSORING/MONITORING AGENCY REPORT NUMBER	
11. SUPPLEMENTARY NOTES The view, opinions and/or findings contained in this report are those of the author(s) and should not be construed as an official Office of Naval Research position, policy, or decision, unless so designated by other documentation.				
12a. DISTRIBUTION/AVAILABILITY STATEMENT Approved for public release; distribution unlimited.			12b. DISTRIBUTION CODE	
13. ABSTRACT (Maximum 200 words) The Twenty-Second Annual Conference on the Physics and Chemistry of Semiconductor Interfaces was held in Scottsdale, AZ, and the enclosed report contains abstracts of papers presented.				
14. SUBJECT TERMS Semiconductor Interfaces			15. NUMBER OF PAGES 102	
			16. PRICE CODE	
17. SECURITY CLASSIFICATION OF REPORT Unclassified	18. SECURITY CLASSIFICATION OF THIS PAGE Unclassified	19. SECURITY CLASSIFICATION OF ABSTRACT Unclassified	20. LIMITATION OF ABSTRACT UL	

SCIENTIFIC PROGRAM FOR PCSI-22

Su1700 — Western cookout (at the pool, if weather permits).

Su1900: Opening (evening) session at 7:00 p.m. — Chairs: J. Dow, R. Allen.

Su1900 — Simulation of Quantum Well Lasers. Karl Hess. Illinois.

Su1940 — Fabrication of Sub - 50 nm Gate Length n-MOSFETs and their Electrical Characteristics. M. Ono, M. Saito, T. Yoshitomi, C. Fiegna, T. Ohguro, H. Iwai. Toshiba, Univ. Ferrara (Italy).

Mo0800 — Monday morning session — Chair: G. Lucovsky.

Mo0800 — High integrity thin SiO₂ free from contamination and surface micro-roughness. T. Ohmi, Y. Okada, T. Yabune, and K. Ohmi. Tohoku University

Mo0840 — Si/SiO₂ Interface Roughness Measured with X-ray Diffraction. K. W. Evans-Lutterodt, M.-T. Tang, M. L. Green, D. Brasen, K. Krisch, L. Manchanda, G. S. Higashi, and T. Boone. AT&T.

Mo0920 — Hydrogen Bonding Arrangements at Si-SiO₂ Interfaces. Z. Jing, G. Lucovsky, J. L. Whitten. NC State.

Mo0925 — The Initial Oxidation of Silicon(100): A Unified, Chemical Model for Thin and Thick Oxide Growth Rates and Interfacial Structure. T. K. Whidden, P. Thanikasalam, M. J. Rack, D. K. Ferry. Arizona State.

Mo0930 — Reliability of Nitrided Si-SiO₂ Interfaces formed by a New, Low-Temperature, Remote-Plasma Process. D. R. Lee, G. Lucovsky. NC State.

Mo0935 — Characterizing Wearout, Breakdown and Trap Generation in Thin Silicon Oxide. D. J. Dumin, J. R. Maddux, R. Subramoniam, R. S. Scott, S. Vanchinathan, K. J. Dickerson, S. Mopuri, S. M. Gladstone, T. W. Hughes. *Clemson*.

Mo0940 — Process Dependence of the $\text{SiO}_2/\text{Si}(100)$ Interface Structure. Z. H. Lu, M. J. Graham, S. P. Tay, T. Miller, T.-C. Chiang. *NRC, Ottawa; Northern Telecom Limited; Illinois*.

Mo0945 — Coffee Break (downstairs). Chair (post-break): L. Cooper.

Mo1015 — Scaling of Si/SiO_2 Interface Roughness. H. Iwasaki. *Osaka*.

Mo1055 — Defect Production, Degradation, and Breakdown of Silicon Dioxide Films. D. DiMaria. *IBM-Yorktown*.

Mo1135 — Oxygen-Associated Defects Near Si-SiO_2 Interfaces in Porous Si and their Role in Photoluminescence. W. E. Carlos, S. M. Prokes. *Naval Research Laboratory*.

Mo1140 — Lunch, provided by conference (in bar).

Mo1400 — Monday afternoon session — Chair: D. Aspnes.

Mo1400 — Silicon Interlayer Based Surface Passivation of Near-Surface Quantum Wells. Satoshi Kodama, Satoshi Koyanagi, Hideki Hasegawa. *Hokkaido University*.

Mo1405 — Quasi-Epitaxy of the Organic Semiconductor PTCDA on Se-Passivated $\text{GaAs}(100)$. Y. Hirose, S. R. Forrest, A. Kahn. *Princeton University*.

Mo1410 — Hydrogen Induced Modification of the Optical Properties of the $\text{GaAs}(100)$ Surface. N. Esser, P. V. Santos, M. Kuball, M. Cardona, M. Arens, W. Richter, F. Stietz, J. A. Schaefer, B. O. Fimland. *Max-Planck-Institut; TU Berlin; Universität Kassel; NIT, Trondheim*.

Mo1415 — Surface Ordering on GaAs(100) by Indium-Termination. U. Resch-Esser, C. Springer, W. Richter, N. Esser, J. Zegenhagen, P. V. Santos, M. Cardona, B. O. Finland. *TU Berlin; Max-Planck-Institut; NIT, Trondheim.*

Mo1420 — Interactions Between Vacancies on InP(110) Surfaces. M. Heinrich, Ph. Ebert, Xun Chen, M. Simon, K. Urban, M. G. Lagally. *Jülich; Wisconsin.*

Mo1425 — Structure and Dynamics of Anion and Cation Vacancies at III-V (110) Surfaces. G. Lengel, M. Weimer, J. Gryko, R. E. Allen. *Texas A&M.*

Mo1430 — Scanning Tunneling Microscopy and Spectroscopy of the Reaction of NH₃ with GaAs (110). G. Brown, M. Weimer. *Texas A&M.*

Mo1435 — Hot Electron Transport Through Metal-Oxide-Semiconductor Structures Studied by Ballistic Electron Emission Spectroscopy. R. Ludeke, A. Bauer, E. Cartier. *IBM.*

Mo1515 — Poster Viewing and Discussions. Authors of Monday and Wednesday papers should stand by and defend their posters until at least 1630. Participants are expected to provide their own dinners. The poster area will be open all evening for discussions.

Mo2000 — Rump session, topic to be announced. Chair: H. Salemink

Tu0800 — Tuesday morning session. Chair: C. Van de Walle.

Tu0800 — Interface Characterization by Scanning Tunneling Microscopy. S. L. Skala, W. Wu, K. -Y. Cheng, J. R. Tucker, J. W. Lyding, A. Scabaugh, E. A. Beam III, D. Jovanovic. *Illinois; Texas Instruments Inc.*

Tu0805 — Photomodulation Raman scattering spectroscopy of ZnSe/GaAs(001) Heterostructures Interface. H. Talaat, L. Elissa, S. Negm, E. Burstein. *Cairo, Penn.*

Tu0810 — Surface Roughness and Pattern Formation during Homoepitaxial Growth of Ge(001) at Low Temperatures. J. E. Van Nostrand, S. J. Chey, and D. G. Cahill. *Illinois.*

Tu0815 — Hydrogen-ion Treatment of AlGaAs/GaAs Near-surface Quantum Well: A New Approach to Surface Passivation. Y.-L. Chang, S. I. Yi, S. Shi, E. Hu, W. H. Weinberg, and J. Merz. *UC Santa Barbara*.

Tu0820 — The Microscopic Picture of Si(113): a Novel Surface Reconstruction, the Origin of Defects, and Adsorption Sites. Theoretical and Experimental Study. J. Dabrowski, H. -J. Mussig, G. Wolff. *Institut für Halbleiterphysik*.

Tu0900 — Band Discontinuities at Heterojunctions Between Crystalline and Amorphous Silicon. C. G. Van de Walle, Lin Yang. *Xerox PARC, Lawrence Livermore*.

Tu0905 — Electron Energy Loss Investigation of Non-Uniform Carrier Depth Profiles from Hole-Plasmon Excitation of Boron-Doped Si(111) Surfaces. J. E. Rowe, R. A. Malic, E. E. Chaban. *AT&T*.

Tu0910 — Site Specific Si 2p Core Level Spectroscopy of Si(111) 7x7: a Fundamental Assignment. G. LeLay, M. Gothelid, M. Grehk, M. Bjorkquist, V. Yu. Aristov, U. O. Karlsson. *CRMC2-CNRS; Royal Institute of Technology*.

Tu0915 — p+ Doping of Si by Al Diffusion upon Annealing AlIn-Si(111). H. J. Wen, M. Prietsch, A. Bauer, M. T. Cuberes, I. Manke, G. Kaindl. *Freie Universität Berlin*.

Tu0920 — Homoepitaxy and Controlled Oxidation of Silicon at Low Temperatures Using Low-Energy Ion Beams. J. W. Rabalais, A. H. Al-Bayati, S. S. Todorov, K. J. Boyd, D. Marton. *University of Houston*.

Tu0925 — Calculation of the Average Interface Field in Inversion Layers Using Zero-Temperature Green's Function Formalism. Dragica Vasileska-Kafedziska, Paolo Bordone, Terry Eldridge, David K. Ferry. *Arizona State*.

Tu0930 — Coffee Break. Chair (post-break): M. Hybertsen.

Tu1000 — Hydrogen Diffusion and Reactions on Si Surfaces. A. Selloni. *Geneva*.

Tu1040 — Hydrogen Desorption from Si: How Does This Relate to Film Growth? C. M. Greenlief. *Missouri-Columbia*.

Tu1120 — Cross-Sectional Scanning Tunneling Microscopy of AlGaAs/GaAs Heterojunctions: Interfacial Roughness and Alloying Effects. A. R. Smith, K. -J. Chao, C. K. Shih, Y. C. Shih, A. Srinivasan, B. G. Streetman. *The University of Texas at Austin*.

Tu1125 — Lunch, provided by conference.

Tu1305 — Tuesday afternoon session. Chair: A. Kahn.

Tu1305 — Misfit Dislocations in ZnSe-Based Films Grown on (001) GaAs Substrates. L. Salamanca-Riba, L. H. Kuo. *University of Maryland*.

Tu1345 — Na/Carbon-Rich β -SiC(100) Surface: Initial Interface Formation and Metallization. F. Semond, P. S. Mangat, V. Yu. Aristov, P. Soukiassian. *Centre D'Etudes de Saclay, Universite de Paris-Sud, Northern Illinois*.

Tu1350 — High-Brightness Light-Emitting Diodes Grown by MBE on ZnSe Substrates. D. B. Eason, Z. Yu, W. C. Hughes, C. Boney, J. W. Cook, Jr., J. F. Schetzina, G. Cantwell, W. C. Harsch. *NC State, Eagle-Pitcher*.

Tu1355 — Deep Level Formation at ZnSe/GaAs(100) Interfaces. A. D. Raisanen, L. J. Brillson, A. Franciosi, L. Vanzetti, L. Sorba. *Xerox Wilson Center; Laboratorio TASC-INFM; University of Minnesota*.

Tu1400 — Study of Reconstruction at Interfaces of CdSe/ZnTe Superlattices by Total Energy Calculation. S.-F. Ren, Z. -Q. Gu, Y. -C. Chang. *Illinois State; Institute of Semiconductors; Illinois*.

Tu1405 — Accommodation of Strain in Ultra-Thin InAs/GaAs Films. J. C. Woicik, J. G. Pellegrino, S. H. Southworth, P. S. Shaw, B. A. Karlin, K. E. Miyano. *National Institute of Standards; Brooklyn College*.

Tu1410 — Withdrawn.

Tu1415 — First Principles Studies of MBE Growth, Band Offsets at Heterojunctions, and Surface Oxidations Using Gaussian Dual-Space Density Functional Theory. X. J. Chen, J. Hu, B. Tsai, A. Mintz, W. A. Goddard III. *Caltech*.

Tu1420 — Explanation of the Origin of Electrons in the Unintentionally Doped InAs/AlSb System. J. Shen, H. Goronkin. *Motorola*.

Tu1425 — Study of Abruptness and Band Alignments at InAs-GaSb Interfaces. M. W. Wang, D. A. Collins, R. W. Grant, R. M. Feenstra, T. C. McGill. *Caltech; Rockwell International; IBM*.

Tu1430 — Ballistic Electron Emission Microscopy of Strained and Relaxed In_{0.35}Ga_{0.65}As/AlAs Interfaces. Mao-long Ke, D. I. Westwood, S. Wilks, S. Heghoyan, A. Kestle, C. C. Matthai, B. E. Richardson, R. H. Williams. *UWCC, Cardiff*.

Tu1435 — Strain Dependence of the Valence-Band Offset in Arsenide Compound Heterojunctions Determined by Photoelectron Spectroscopy. C. Ohler, J. Moers, A. Forster, H. Luth. *Jülich*.

Tu1440 — Poster Viewing and Discussions. *Authors of Tuesday and Thursday papers should stand by and defend their posters until at least 1600. Participants are expected to provide their own dinners. The poster area will be open all evening for discussions.*

We0700 — Wednesday morning, no session. *Hike, sightsee, sleep, or shop. Persons climbing Camelback Mountain should leave hotel by 0700 (in cars).*

We1130 — Box Lunch provided by conference. *Please notify hotel if you wish to pick your lunch up earlier (in the morning). The Poster Viewing room will be open all morning.*

We1300 — Wednesday afternoon session. *Chair: D. Wolford.*

We1300 — Optoelectronic Devices Based on GaN/AlGaN Heterojunctions. A. Khan. *APA Optics*.

We1340 — Electron Microscopy Characterization of GaN and AlN Films Grown by MBE on Different Substrates. Zuzanna Liliental-Weber, Hyunghul Sohn. *Lawrence Berkeley Laboratory.*

We1345 — MBE Growth and Properties of GaN Films on GaN/SiC Substrates. W. C. Hughes, W. H. Roland, M. A. L. Johnson, J. W. Cook, Jr., J. F. Schetzina, J. Ren, J. A. Edmond. *NC State; Cree Research, Inc.*

We 1350 — The Barrier Height at the Valence Band Discontinuity in GaAs/GaN Heterostructures. X. Huang, T. S. Cheng, S. E. Hooper, T. J. Foster, L. C. Jenkins, C. T. Foxon, J. W. Orton, P. C. Main, L. Eaves. *University of Nottingham.*

We1355 — Auger Electron Spectroscopy, X-ray Diffraction and Scanning Electron Microscopy of InN, GaN and GaAsN Films on GaP and GaAs(001) Substrates. L. C. Jenkins, T. S. Cheng, C. T. Foxon, J. W. Orton, S. E. Hooper, S. V. Novikov, D. E. Lacklison. *University of Nottingham; St. Petersburg.*

We1400 — UHV-TEM Study of the Growth and Relaxation of SiGe on Si(001). F. K. LeGoues. *IBM-Yorktown.*

We1440 — MBE Grown Si/SiGe and Devices. U. König. *Daimler-Benz.*

We1520 — Coffee break and poster viewing. Chair (post-break): R. Feenstra.

We1550 — Measurements of Local Strain Variation in $\text{Si}_{1-x}\text{Ge}_x/\text{Si}$ Heterostructures. L. D. Bell, A. M. Milliken, S. J. Manion, W. J. Kaiser, R. W. Fathauer, W. T. Pike. *Caltech.*

We1555 — Surface and Interface Roughness Anisotropy of $\text{Si}_{1-x}\text{Ge}_x/\text{Si}$ Superlattices. C. Teichert, Y. H. Phang, L. J. Peticolas, J. C. Bean, M. G. Lagally. *University of Wisconsin-Madison; AT&T.*

We1600 — Ge/Si Superlattices Grown by Sn Surfactant-Mediated Molecular Beam Epitaxy. X. W. Lin, Z. Liliental-Weber, J. Washburn, E. R. Weber, A. Sasaki, A. Wakahara, T. Hasegawa. *Lawrence Berkeley Laboratory; Kyoto University.*

We1605 — Effect of Interface Roughness on Mobility of Si/SiGe Heterostructures. R. M. Fecunstra, M. A. Lutz, Frank Stern, K. Ismail, J. O. Chu, B. S. Meyerson. *IBM.*

We1610 — In Situ Ballistic-Carrier Spectroscopy on Epitaxial CoSi₂/Si(111) and (100). H. Sirringhaus, E. Y. Lee, H. von Känel. *Zürich.*

We1615 — Formation of the Ce/Si(111) and Ce/CaF₂/Si(111) Interfaces. H. J. Wen, I. Manke, A. Hohn, A. Bauer, M. Prietsch, G. Kaundl. *Freie Universität Berlin.*

We1620 — Poster viewing and discussions.

We1830 — Dinner provided by conference in oral-presentation room.

We2000 — Poster Viewing and Discussions.

Th0800 — Thursday morning session. Chair: R. Allen

Th0800 — Interface Roughness in GaAs-AlAs Heterostructures: The Role of Ga Surface Segregation. G. S. Spencer, J. Menendez, L. N. Pfeiffer, K. W. West. *Arizona State.*

Th0805 — Optical Study of Heterointerfacial Growth Interrupts in Type-II GaAs/AlAs Superlattices by Time-Resolved PL-Imaging. T. Chang, L. P. Fu, F. T. Bacalzo, G. D. Gilliland, K. K. Bajaj, A. Antonelli, R. Chen, D. J. Wolford, J. Klem, M. Hafich. *Emory University; Iowa State University; Sandia National Laboratory.*

Th0810 — XPS Study of the MnS/ZnSe Valence Band Discontinuity. L. Wang, S. Sivananthan, R. Sporken, R. Caudano. *Illinois-Chicago, Namur (Belgium).*

Th0815 — Spatially Resolved Internal Photoemission by Near-field Optics. J. Almeida, T. dell'Orto, C. Coluzza, G. Margaritondo, O. Bergossi, M. Spajer, and D. Courjon. *Lausanne, Besancon.*

Th0820 — Near-field Optical Characterization of Quantum Wells and Nanostructures. H. Hess. *AT&T*.

Th0900 — Doping and Composition Fluctuations in Epitaxial Semiconductors. H. W. M. Salemink, M. B. Johnson, P. M. Koenraad, M. Pfister, and S. F. Alvarado. *IBM-Zürich and Eindhoven*.

Th0945 — Direct Sublattice Imaging in Compound Semiconductor Heterostructures. A. J. McGibbon, S. J. Pennycook, D. E. Jesson. *Oak Ridge*.

Th0950 — Photon Channeling in the Vacuum Ultraviolet Wavelength Range. J. E. Rowe, R. A. Malic, E. E. Chaban, R. J. Chichester, C. -M. Chiang, N. V. Smith. *AT&T; Lawrence Berkeley Laboratory*.

Th0955 — A Method for the Experimental Determination of the Tensorial Component of Stress in Si-Based Structures and Devices. G. S. Loechele, N. Cave, J. Menendez. *Arizona State*.

Th1000 — Coffee Break. Chair (post-break): D. Ferry.

Th1030 — Fabrication of In-Plane Gate Quantum Structures Through Direct Schottky Interface Formation by In-Situ Selective Electrochemical Process. T. Hashizume, H. Okada, K. Jinushi, H. Hasegawa. *Hokkaido University*.

Th1035 — Polarized-CL and CL Wavelength Imaging Study of Variations in Strain in $\text{In}_x\text{Ga}_{1-x}\text{As}/\text{GaAs}(001)$. D. H. Rich, K. Rammohan, Y. Tang, R. S. Goldman, J. Chen, H. H. Wieder, K. L. Kavanagh. *University of Southern California; University of California. San Diego*.

Th1040 — The Investigation of Adsorbates on Si(110) with Photoelectron Holographic Imaging. H. Yu, H. Wu, and G. J. Lapre. *Montana State*.

Th1045 — Effects of Interface Flatness and Abruptness on Optical and Electrical Characteristics of GaAs/Al(Ga)As Quantum Well Structures Grown by Metalorganic Vapor Phase Epitaxy. Masanori Shinohara, Haruki Yokoyama, Naohisa Inoue. *NTT LSI Laboratories*.

Th1050 — Gate-Controlled Modulation of Charge Transport in Long Channel, δ -Doped, Heterojunction Hall Bar Structures. H. H. Wieder, R. S. Goldman, A. P. Young, Jianhui Chen. *University of California, San Diego.*

Th1055 — Annealing-induced Near-surface Ordering in Disordered LPE-grown $\text{Ga}_{0.5}\text{In}_{0.5}\text{P}$. J. S. Luo, J. M. Olson, M-C. Wu. *NREL, Tsing Hua (Taiwan)*

Th1100 — Surface Chemistry Evolution During MBE Growth of InGaAs. K. R. Evans, J. E. Ehret, R. Kaspi, and C. R. Jones. *Wright-Patterson*

Th1105 — Scanning Tunneling Microscopy with Large Band-gap Semiconductor Tips and Samples. W. E. Packard. *Arizona State*

Th1110 — Composition and Structure of InP and GaAs(100) Surface Phases from Time-of-Flight Scattering and Recoiling Spectrometry J. W. Rabalais, M. M. Sung, and C. Kim. *Houston.*

Th1115 — Discussion. All participants.

Th1150 — Best Paper Awards.

Th1200 — Lunch (Submarine sandwiches) and End of Conference.

INFORMATION ON SAFETY, MAPS, RESTAURANTS, MUSEUMS, AND TRIPS

SAFETY

Scottsdale is in a desert, which means that you will not feel like you are sweating when you are. It is important that you drink plenty of water or liquids.

If you have drunk a lot of alcohol or if you become dizzy, stay out of the sun.

Exercise normal caution swimming and in the hot baths.

Sunny days can pose health problems: wear sunglasses (cataracts), use sunscreen (melanoma).

If you elect to walk over Camelback Mountain on Wednesday morning, be sure your skin is protected from the sun, carry a full water bottle, wear sunglasses, but do not forget your camera and film. You will need shoes with rough soles. For part of the trail (about 50 meters), which is marked by blue dots, you will travel on the seat of your pants. This is a 3-hour hike, and requires good health. If you are very careless, you can fall off this mountain and hurt yourself badly. So be careful. Stay on the trail. Do not hike alone. You should begin at sunrise, and plan for there being no restroom facilities. You will begin at Echo Canyon, and end at J. Dow's house, near the east (tail) end of the Camel. His house is above the two water tanks, is white with a brown tile roof, and is the closest house to the circle in the road above the tanks. (This road does not yet have houses built on it, but the pads are already built.) You may come across some wildlife, such as foxes, coyotes, or snakes (including rattlesnakes), but it is unlikely, especially at this time of day and year. Follow the three basic rules of the desert: (i) never put your hand under a rock; (ii) watch where you place your feet; and (iii) have enough water for a drink every 20 minutes. In all of Arizona, there are about 110 rattlesnake bites per year, and 2/3 of them are people playing with the snakes or reaching under a rock. Most of the rest are in distant mountains (where the snakes lie by the trail and hunt rodents), and in the Spring. The standard treatment is to observe the victim for one day. Rattlesnakes are less dangerous than the average physicist, and if you see one, just back away. I walk part way up Camelback every day, and see about one snake per year, usually a king snake (non-venomous). Should you manage to convince a snake to bite you, stay calm, sit down at least two meters from the snake, rest, and have a friend obtain help. The last thing you want to do is get excited, run down the mountain, and pump the venom into your organs.

MAPS

In your hotel room, you will find "KEY to the Valley," a monthly visitor's guide to the area. Near the center, you will find maps of Metropolitan Phoenix and Scottsdale. Also the TASTE OF PHOENIX in your hotel room has restaurant data and menus, as well as a locator map (back cover).

The Holiday Inn of Old Town Scottsdale is east of Scottsdale Rd. on Indian School at Buckboard. The main north-south road in Scottsdale is Scottsdale Road. The east-west roads north of Main are Avenues; those south are Streets. Of the relevant east-west roads, only Osborn is south of the hotel (about five blocks), then Indian School (=2nd

Ave), Camelback, McDonald, Indian Bend, McCormick, Doubletree Ranch, Shea, and Bell are further north in that order. The north-south streets in Scottsdale are numbered in increasing order to the east, with 70th St being west of Scottsdale Rd.

The (tourist) shopping area of Old Town is due west of the hotel. Scottsdale Fashion Square mall (for residents) and neighboring malls (Neiman-Marcus) are on Camelback, just west of Scottsdale Rd.

The art district is between Indian School and Camelback, centered on Scottsdale Rd.

There are restaurants everywhere, including a good restaurant in the hotel (Bola's Bar and Grill). Some other restaurants you may wish to consider include:

RESTAURANTS

Restaurants at the Scottsdale Mall:

- American: Bola's Bar & Grill, Holiday Inn
- American: Blue Moose, 7373 Scottsdale Civic Center Mall. Burgers, sandwiches.
- American: Arizona 88, 7373 Scottsdale Mall. Sandwiches, salads.
- American: Backstage, 7373 Scottsdale Civic Center Mall.
- American: J. Chew & Co., 7320 Scottsdale Mall. Sandwiches.
- American: Gallery Grill, Scottsdale Mall.
- American: Picnic Company, 7337 2nd St.
- Mexican: Los Olivos, 7328 E. 2nd St.
- Mexican: Mexitali, Scottsdale Mall. Also Pizza, subs.
- Southwest: Z'Tejas Grill, Fashion Square Mall, Camelback and Scottsdale.
- Spanish: Tapas Pepin, 7363 Scottsdale Mall. 2 stars. Spanish guitar in evening.

Some favorites within walking distance, good food, reasonable prices:

***Brown Derby, in Safari Resort, one block north of Camelback on Scottsdale. (Good salad bar, very reasonable prices, I like teriyaki chicken or lobster tails. Try the strawberry blintzes for breakfast.).

**American and European: Impeccable Pig, 7042 Indian School at Marshall Way, west of Scottsdale Rd. (Lamb chops or salmon are usually great. Restaurant prices.)

*Fish: Pacific Fish Company, Scottsdale Rd, one block south of Camelback. Reasonable restaurant prices.

*Irish Pub: Black Rose, 4341 N 75-th, about 4 blocks east of Scottsdale on Sixth Ave. Good Irish food, reasonable prices.

*Mexican: Julio's, Camelback, one block east of Scottsdale. Good food, reasonable prices.

*Sandwiches and Ice Cream: Sugar Bowl, Scottsdale Rd. at 1st Ave. Famous restaurant (in cartoons), reasonable prices.

*Pancakes: Village Inn, Indian School, 2 blocks west of Camelback. Great for breakfast.

*Fast food: A variety of stores at the Fashion Square Mall, Scottsdale and Camelback:

*American: Johnny Rocket's. (Burgers, 1950's style).

*American: Great Steak and Fry.

American: Paradise Bakery.

Chicken and Fish: Gill's Chicken 'n' Sea.
Chinese: Panda Express.
Italian: Italian Express.
Italian: Sbarro.
Japanese: Sakura.
Mexican: La Salsa.
New American: Everything Yogurt & Salad.

Inexpensive restaurants and fast food within walking distance:

Burgers: Jack in the Box: Scottsdale Rd. at 3rd St.
American: Baker's Square, Scottsdale, one block south of Camelback.
American: Denny's, Scottsdale at Osborn.
Italian: Olive Garden, Scottsdale at Osborn (1 block south of 4th St.)
Kosher: Bowman's Kosher Delicatessen: Scottsdale Rd. at 2nd St.
Sandwiches: Schlotzky's Delicatessen, Scottsdale Rd. at 1st Ave.
Steaks: Sizzler, Scottsdale Rd. at 3rd St.

Local restaurants within walking distance, with nearest intersection:

American: Grapevine, 4013 N. Brown.
American: Hops Bistro and Brewery, Fashion Square, Camelback and Scottsdale.
American: T. G. I. Friday's, Scottsdale Rd. at 5th Ave.
American: Pischke's Paradise, 7217 1st St.
American: Summerfield's, Indian School and 68-th.
American: Trapper's, 3815 N. Scottsdale Rd at Main.
BBQ: Tony Roma's, Scottsdale Rd. at 4th Ave.
BBQ, Country: Rockin' Horse, 7000 Indian School at Goldwater.
Burgers: Fuddrucker's, 7145 Indian School, west of Scottsdale Rd.
Cajun: Baby Kay's, 7216 E. Shoeman, one block south of Camelback.
Chicken: Bandera's, 3821 Scottsdale at 1st St.
Chinese: Emperor's Garden, 7228 First Ave.
Chinese: Mr. C's, 4302 N. Scottsdale Rd. at 6th Ave.
Chinese: P. F. Chang's Bistro, Fashion Square Mall, Camelback and Scottsdale Rd.
European: Glass Door, 6939 E. Main.
European: Roland's, 4515 Scottsdale Rd, one block north of Camelback.
French: 6th Avenue Bistrot, 7150 E. 6th Ave.
French: Jean-Claude's Petit Cafe, 7340 Shoeman Ln, 1 block south and 1 block east of Camelback and Scottsdale.
French: Marche Gourmet, Indian School at Marshall Way.
French: Mary Elaine's at the Phoenician (formerly owned by Charles Keating and friends), 6000 Camelback, about 10 blocks west of Scottsdale Rd. Expensive.
Indian: Jewel of the Crown, Scottsdale Rd at Indian School.
Indian: India Palace, Scottsdale Rd at 4th Ave.
Italian: Aldo Baldo, Scottsdale Fashion Mall, Camelback and Scottsdale Rd.
Italian: Italian Grotto, Scottsdale Rd. at Main.

Italian: Marco Polo, Goldwater, 1 block south of Camelback (south of Safeway).

Italian: Oreganos, 3622 Scottsdale Rd.

Italian: Caffe Piccolo, Osborn at Scottsdale.

Italian: The Terrace at the Phoenician (formerly owned by Charles Keating and friends), 6000 Camelback, about 10 blocks west of Scottsdale Rd. Expensive.

Japanese: Mikado, Camelback, one block west of Scottsdale.

Japanese: Kyoto, 7170 Stetson, south of Camelback.

Lamb chops, American, and Baseball: Don and Charlie's, Camelback about 3 block east of Scottsdale Rd.

New American: Arcadia Farms, 7014 E. 1st St.

New American: Moriah at Stouffer's Cottonwood Resort, 6161 N. Scottsdale Rd.

Southwest: Jacqueline's 7303 E. Indian School. Deli and Southwest.

Steaks, American: Pink Pony, 3831 Scottsdale at Main.

Thai: Daa's, 7419 E. Indian Plaza, one block south of Camelback, east of Scottsdale Rd.

Thai: Malee's on Main, 7131 E. Main, 2 blocks south of Indian School, 1 block west of Scottsdale. 2 stars.

Good restaurants that require a car or a long walk:

*American: Quilted Bear, SW corner of Lincoln and Scottsdale. 2 stars. (I recommend fruit salad.)

American: Black Angus, Lincoln and Scottsdale.

American: Other Place, 1 block west of Lincoln and Scottsdale. 2 stars.

Italian: Mancuso's, 6166 Scottsdale, south of Lincoln in Borgata mall. Semi-formal. 3 stars.

Good restaurants that require a car or taxi:

**Steak: Reata Pass, 27500 Alma School. (About 20 mi away. Take Indian School east to Pima. Pima north to Happy Valley Road. Happy Valley east to Alma School. Alma School north 1 mile.) An old stage-coach stop coming over the mountains to Phoenix. Features steaks and rattlesnake. Two live rattlesnakes on display. Good food and authentic. Reasonable prices.

*Steak: Ruth's Chris, Scottsdale at Indian Bend. 3 stars. Moderately expensive. Big servings. Filet mignon and other steaks, together with vegetables, such as spinach.

American: Golden Swan in Hyatt Regency at Gainey Ranch, 7500 Doubletree Rd east of Scottsdale Rd. 3 stars.

Mexican: La Hacienda in the Scottsdale Princess Resort, Princess Dr, north of Bell Rd, off Scottsdale. Semi-formal attire. 4 stars. Expensive.

New American: Remington's, 7200 Scottsdale Rd, near Cheney. 3 stars.

Southwest: Marquesa in the Scottsdale Princess Resort, Princess Dr, north of Bell Rd, off Scottsdale. Formal attire. 5 stars. Expensive.

Southwest: Pinon Grill, 7401 Scottsdale Rd, in Regal McCormick Ranch. 2 stars.

Steak: The Chapparal in Marriot's Camelback Inn, 5402 Lincoln, about 1 mile west of Scottsdale. Semi-formal attire. 4 stars. Expensive.

Steak: Rawhide, 4 miles north of Bell Rd on Scottsdale. Food is only okay, but the restaurant is basically a movie set and entertainment area. Good for kids. 1 star.

Steak: Diamondback Steakhouse, West World, 16601 N. Pima Rd.

Steak: Chart House, 7255 McCormick Pkwy, 1 block east of Scottsdale. 2 stars. A bit expensive.

MUSEUMS, all require a car or taxi

**Heard Museum (Indian and Southwest culture and art), 22 E. Monte Vista

*Desert Botanical Gardens (Gardens), 1202 N. Galvin.

*Champlin Fighter Museum (Combat aircraft), 4636 Fighter Aces Dr. (Falcon Field), Mesa.

*Arizona State Capitol Museum (Territorial capital), Washington and 17 Ave.

Arizona Mining and Minerals Museum (Rocks), 1502 W. Washington.

Taleisin (Frank Lloyd Wright Architecture) 108 St. at Cactus, Scottsdale.

For other museums, see KEY to the Valley, in your room.

TRIPS

Trips of one or more days (for more information, inquire at Conference desk:

Grand Canyon with possible side trips:

**Grand Canyon; for the train ride, telephone 1-800-293 RAIL.

*Montezuma Castle and Wells (Indian ruins), en route to Grand Canyon.

*Tuzigoot National Monument (Indian ruins), en route to Grand Canyon.

Jerome (Mining/ghost town), en route to Grand Canyon.

*Oak Creek Canyon (Rock formations), Sedona, spend a day en route to Grand Canyon.

Northeastern Arizona (Indian reservations):

Globe (Open pit copper mine and Indian ruins).

Mogollon Rim (uplift of Rocky Mountains), Pinetop.

*Petrified Forest National Park and Painted Desert.

*Meteor Crater (Winslow).

**Canyon de Chelly (Indian ruins and scenery), Chinle (Navajo reservation).

*Monument Valley (spectacular rock formations), Kayenta.

*Navajo National Monument (cliff dwellings).

*Wupatki National Monument (Volcanic crater, Indian ruins).

Southeastern Arizona, Tombstone, and Geronimo-Apache territory:

Superstition Mountains, Apache Junction.

**Casa Grande Ruins (Hohokam Indian village of 1400)

*Old Tucson Studios (Movie set), Tucson.

- Titan Missile Museum, Green Valley, near Tucson.
- Pima Air and Space Museum (Old aircraft), Tucson.
- Saguaro National Monument (Cacti), Tucson.
- *Tumacumcori National Historic Park (Mission).
- *Tombstone (O.K. Corral, Boot Hill, Mining and gun-fighting town).
- *Copper Queen Mine, Bisbee.
- *Chiricahua National Monument (Mountains, rock formations, the land of Geronimo and Cochise).
- *Amerind Museum (Indian museum), Dragoon.

Southern Arizona:

- *Organ Pipe Cactus National Monument (Sonoran desert).
- Kitt Peak (Observatory). near Tucson.
- Nogales, Mexico (Mexican border town).

Northern Arizona, Colorado River:

- Glen Canyon National Recreation Area and Lake Powell (Boating, fishing).
- Hoover Dam, Lake Mead.

*Personal favorites.

SIMULATION OF QUANTUM WELL LASERS

Karl Hess
Beckman Institute
University of Illinois at
Urbana-Champaign, Illinois

Simulation of semiconductor laser diodes necessitates a precise knowledge of electron and hole transport in the semiclassical transport regions of p-n junctions as well in a region around the quantum wells (wires or dots) over which the wavefunction exhibits a certain degree of coherence. Carrier transport is coupled to spontaneous and stimulated emission of photons and thus to the optical problem which necessitates the simultaneous solution of Maxwell's equations over a heterojunction region. It is well known that the prime function of the heterolayers in lasers is the confinement of electrons, holes and the electrical field in one and the same region. The use of quantum wells, wires and dots gives in addition a variability on the light frequency and influences the optical matrix element and therefore the all important threshold current of laser diodes.

In this presentation results of the simulator MINILASE will be presented which show that macroscopic laser response depends (with extreme sensitivity) on microscopic and mesoscopic properties of carrier transport and optical transitions. As an example, MINILASE has discovered a very detailed and sensitive connection of the laser modulation response and the electron and hole capture rates in quantum wells (wires, dots). The modulation response depends also on nonequilibrium distributions of carriers around the quantum well, phonons in quantum wells as well as the connection of classical and quantum regions, resonances and dephasing. MINILASE shows that semiconductor lasers would have a poor modulation response without carrier-carrier interactions and dephasing being important.

All of these effects can only be understood in detail if the knowledge of electronic transport and optical processes in heterolayers is considerably increased; particularly for high carrier densities and scattering dynamics in the femtosecond range. This information is needed in addition to improved standard information about heterostructure parameters such as the bandedge discontinuity. While more information on bandstructure and scattering dynamics of high-density charge-carriers in confined geometries is needed foremost, phonons and their confinement also influence laser function.

In summary the simulator MINILASE has reconfirmed and quantified the sensitive influence of the physics and chemistry of interfaces and interface-systems (wells, wires & dots) on semiconductor laser performance and has demonstrated the need of more detailed information on carrier capture and scattering dynamics in the limit of high densities.

Fabrication of Sub - 50 nm Gate Length n-MOSFETs and their Electrical Characteristics

M. Ono, M. Saito, T. Yoshitomi, C. Fiegna*, T. Ohguro, and H. Iwai

Research and Development Center, Toshiba Corporation, * on leave from University of Ferrara, Italy
1, Komukai Toshiba-cho, Saiwai-ku, Kawasaki 210, Japan Tel: +81-44-549-2183 Fax: +81-44-549-2248
E-mail:ono@prd.ull.rdc.toshiba.co.jp

INTRODUCTION

Small geometry MOSFETs have been actively investigated [1-4], and the fabrication and normal operation at room temperature of 40 nm gate length n-MOSFETs were reported in 1993 [5]. There have been many questions related to small size MOSFETs. Of these, two questions are studied using 40 nm gate length n-MOSFETs. One is the question as to whether velocity overshoot can be observed at room temperature. The other is the question as to whether impact ionization rate, which is the ratio of I_{sub} to I_d , decreases or increases with a decrease in gate length in sub - 0.1 μ m region. Using 40 nm MOSFETs, we have succeeded in obtaining the answer to these questions for the first time.

SAMPLE FABRICATION

After a conventional isolation process, 3 nm gate insulator was made and in-situ phosphorus doped polysilicon was deposited. Resist patterning for gate electrode was carried out by excimer lithography, with further thinning by isotropic plasma resist ashing. The length of gate electrode was measured using high-resolution SEM. Following these steps, phosphorus doped silicated glass (PSG) sidewalls were fabricated. After arsenic was implanted outside the PSG sidewalls, rapid thermal annealing was carried out, by which phosphorus was solid phase diffused from PSG sidewalls and implanted arsenic was activated.

EXPERIMENTAL RESULTS

40 nm gate length devices with phosphorus sources and drains operate quite normally at room temperature, even at $V_d = 2$ V. Short channel effects are well suppressed by using solid phase diffusion technique. The V_{th} roll-off of 40 nm gate length devices is only 0.16 V. On the other hand, 40 nm gate length conventional arsenic implanted devices do not operate due to punch-through.

Firstly, in order to investigate the question concerning velocity overshoot, g_m was measured. Although $g_{m,max}$ seems to saturate with a decrease in gate length, it increases by around 30 or 40 % as the channel length decreases from 100 nm to 40 nm. In order to determine whether velocity overshoot can be observed at room temperature, the intrinsic g_m must be compared with the value of C_{ox} times v_{sat} . Since the estimation of parasitic resistance is very difficult, an upper bound of intrinsic g_m was considered. It has been confirmed that the upper bound of intrinsic g_m is smaller than C_{ox} times v_{sat} , so intrinsic g_m cannot be greater than the value of C_{ox} times v_{sat} . Therefore, velocity overshoot cannot be observed at room temperature, at least in 40 nm gate length n-MOSFETs.

Next, the behavior of hot carriers in 40 nm gate length devices was investigated. It has been known that there exists a universal relationship between the impact ionization rate (I_{sub}/I_d) and $V_d - V_{sat}$, where V_{sat} is a function of V_g and L_g [6]. However, this universal relationship has been confirmed only for long channel devices. When the gate length is reduced into 0.1 μ m region, some investigators have reported that impact ionization rate decreases [7], while others have reported that the rate increases [8]. In order to see the dependence of the impact ionization rate on the gate length in the sub - 50 nm region, substrate currents were measured in detail. In the case of the devices of this experiment, the value of the impact ionization rate increased slightly with an increase in channel length until sub-50 nm region.

CONCLUSION

40 nm gate length n-MOSFETs have been fabricated and some questions related to small size MOSFETs have been investigated at room temperature. Firstly, it has been confirmed that velocity overshoot does not occur at room temperature, at least in 40 nm gate length n-MOSFETs. Secondly, it has been confirmed that the universal relationship between the impact ionization rate and $V_d - V_{sat}$ is not valid in the sub-50 nm region. The impact ionization rate increases slightly with an increase in gate length in the sub-50 nm region.

- [1] G. Sai-Halasz et al., IEEE EDL, p.463, 1987
- [3] R. Yan et al., Symp. on VLSI Tech., p.86, 1992
- [5] M. Ono et al., IEDM, p.119, 1993
- [7] G.G. Shahidi et al., IEEE EDL, p.497, 1988

- [2] T. Hashimoto et al., SSDM92, p.490, 1992
- [4] M. Saito et al., IEDM, p.897, 1992
- [6] T.Y. Chan et al., IEEE EDL, p.505, 1984
- [8] T. Mizuno et al., IEDM, p.695, 1992

High Integrity Thin SiO₂ Free from Contamination and Micro-roughness

T. Ohmi, Y. Okada, T. Yabune, and K. Ohmi
Department of Electronics, Tohoku University
Aza-aoba, Aramaki, Aoba-ku, Sendai, 908 Japan
FAX: 81-22-224-2549

Scaling of device dimension progresses aggressively beyond quarter micron regime and recently normal operation of about 0.1 μm CMOS devices has been demonstrated at room temperature. For the realization of 0.1 μm ULSIs where a fundamental variability due to statistical fluctuations play a role, process fluctuations should be minimized. In order to eliminate all possible origins which cause process fluctuations, wafer surface, process environment, and process parameters should be well controlled. This is the target for ultra clean technology developed under the leadership of Tohoku University. Furthermore, it is well proved that ultra clean technology can improve device performance and reliability.

Popularization of portable electronic equipment requires low voltage and low power devices. Especially, for floating gate memories which rely on Fowler-Nordheim tunneling for programming under a high electric field, scaling of tunnel oxide will be further accelerated in order to realize low voltage and low power operation. In this paper we present an advanced oxidation process based on ultra clean technology, which provides excellent oxide thickness control and gate oxide integrity.

First of all, a ramp-up process should be carried out in inert gas to avoid oxide growth at low temperatures, resulting in poor oxide quality and poor thickness control. Therefore the wafer surface should be passivated prior to a ramp-up to an oxidation temperature to suppress micro-roughness. We evaluated pre-oxides grown in various chemical solutions as a passivation layer. It will be shown that chemical oxide grown in ozonized ultra-pure water provides excellent gate integrity. Furthermore, self-limited oxide growth due to diffusion of chemicals to the Si/SiO₂ interface can guarantee oxide thickness uniformity. Also, this approach can be easily integrated into pre-gate oxidation clean processes. A newly developed technique for the evaluation of organic contamination on the wafer surface will be described. We found that the quality of pre-oxide is closely related to organic contamination levels on its surface.

Second, wafers passivated with chemical oxide grown in ozonized ultra-pure water are loaded into an ultra-clean oxidation furnace free from contamination. Therefore, wafers passivated with the chemical oxide can be ramped up to an oxidation temperature of 900°C in a pure Ar ambient without oxidation and pit formation.

Third, wafers are oxidized at 900°C in a reductive ambient with H radicals. The idea of adding hydrogen radicals is to reduce weak Si-O bonds immediately when they are formed during the oxidation process. Then only strong Si-O bonds survive and highly reliable thin oxide films can be grown.

This approach with chemical pre-oxide growth in ozonized ultra-pure water, ramp-up in an Ar ambient with a negligible amount of residual water, and formation of high quality oxide in a reductive ambient with H radicals can completely eliminate uncontrolled oxide growth and provide high quality thin gate oxide.

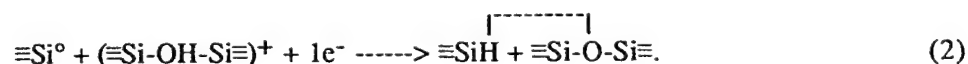
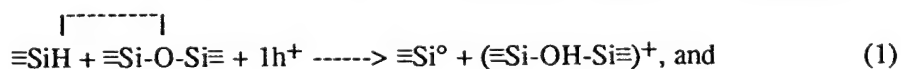
Si/SiO₂ INTERFACE ROUGHNESS MEASURED WITH X-RAY DIFFRACTION

K.W. Evans-Lutterodt, Mau-Tsu Tang, M.L.Green, D. Brasen, K.Krisch, L.Manchanda, G.S. Higashi and T. Boone AT&T Bell Laboratories Murray Hill, New Jersey 07974

The roughness of Si(001)/SiO₂ interfaces is of increasing interest, and has been related to device performance and reliability. We have previously reported a non-destructive, quantitative technique for the measurement of the interface width of crystalline/amorphous Si(001)/SiO₂ interfaces, using both synchrotron and in-house x-ray sources. First we summarize our experimental results. We find that the roughness of the interface depends on the growth variables. The interface width decreases with increasing growth temperature. We also measure the interface width as a function of oxide thickness and find that there is a rapid smoothening with increasing thickness for oxides with thicknesses between 3nm and 20nm, and a more gentle reduction in interface width for oxide thicknesses greater than 20nm. Second, we present a framework within which we can compare the different roughness measurement techniques, by introducing the height-height correlation function $\langle h(r)h(0) \rangle$, and the spectral distribution of roughness. We discuss the relative sensitivities of the x-ray diffraction and AFM (atomic force microscopy) techniques to the spectral distribution of interface fluctuations, and show how the different techniques can extract a different root mean square deviation from flatness, or interface width, from the same distribution spectrum. We also point out how different physical properties of the interface, such as the electron mobility, may depend on different parts of the spectral distribution of roughness.

Hydrogen Bonding Arrangements at Si-SiO₂ Interfaces, Z. Jing, G. Lucovsky, and J.L. Whitten,
 Departments of Physics, and Chemistry, NC State University, Raleigh, NC 27695-8202.

Hydrogen is incorporated intentionally at Si-SiO₂ interfaces during the processing of MOSFET devices to reduce initial defect concentrations, as for example in post-metallization-anneals (PMAs). It is believed that H-atoms compensate what otherwise would be Si-atom dangling bond defects, and thereby contribute to decreased levels of interface trapping states denoted as D_{it}. What has not been recognized to date is that H-atoms bonded directly to Si-atoms at the Si-SiO₂ interface can form weaker hydrogen-bonds with oxygen atoms of the SiO₂ network and possibly reduce reliability. This paper explores the properties of these H-bonds, and focuses on their metastability with respect to charge capture which can occur during device operation. Since other types of atoms have been incorporated intentionally into Si-SiO₂ interfaces to improve initial performance, or operational reliability, we also explore the effects of bonded nitrogen atoms, fluorine atoms and nitrogen-hydrogen (N-H) groups at the Si-SiO₂ interface. The H-bonds that couple interfacial Si-H groups to highly electronegative atoms or groups in the dielectric in the immediate vicinity of that interface are shown to be integral components of a precursor site for charge trapping reactions that can lead to defect generation. Model calculations have shown that trapping a hole at an O-atom site that is H-bonded to an Si-H group can lead to the formation of a three-fold coordinated positively-charged oxonium center in the dielectric and a neutral dangling bond at the Si-SiO₂ interface. Similarly, trapping of a hole at an N-H site that is H-bonded to an Si-H group, can lead to the formation of a four-fold coordinated ammonium center and a Si-atom dangling bond. The stabilities of these over-coordinated and positively charged sites have been studied by ab-initio quantum chemistry calculations which demonstrate that they are stable with O-H and N-H bond energies in excess of 4.5 eV. On the other hand, the same type of calculations indicates that trapping of an electron at the over-coordinated positively-charged sites is destabilizing in the sense that the H-atom is displaced back to the Si-atom, returning the local arrangement to its original configuration with a Si-H bond which is once more coupled to the O-atom or N-H group through a H-bonding interaction. The effects of sequential hole and electron trapping establishes these bonding environments as metastable, with generation/neutralization reactions, respectively, at an H-bonded, O-atom site being given by:



The symbol $| \text{-----} |$ represents a H-bond. Paired-defect states, in the form of a neutral Si dangling ($\equiv\text{Si}^\bullet$) bond that contributes to D_{it}, and a positively charged $(\equiv\text{Si-OH-Si}\equiv)^+$ center that contributes to the fixed oxide charge (Q_f⁺) are created by hole trapping, and relaxed by electron trapping. The H-atom motion associated with these reactions is *displacive*, so that the defect generation/neutralization cycle does not require H-atom diffusion, or any other H-atom transport process. Reaction equations and ab-initio calculations for other bonding configurations, will be discussed, in particular identifying the conditions under which H-bonds can form, and equally important what types of local bonding inhibit H-bond formation and thereby potentially promote increased stability under current stress. Experiments to date by our research group have shown that the controlled incorporation of N-atoms bonded only to Si-atoms, which then do not participate in H-bond formation generally decreases D_{it} and does not contribute to fixed charge in the dielectric near the Si-SiO₂ interface, whereas the incorporation of N-H groups, which can participate in H-bonding interactions leads to simultaneous increases in both D_{it} and Q_f.

Mailing Address: G. Lucovsky, NC State University, Dept. of Physics, Box 8202
 Raleigh, NC 27695-8202 PHONE: (919) 515 3301/3468; FAX: (919) 515 7331

The Initial Oxidation of Silicon(100):

A Unified, Chemical Model for Thin and Thick Oxide Growth Rates and Interfacial Structure*

T. K. Whidden, P. Thanikasalam, M. J. Rack⁺ and D. K. Ferry

Nanostructures Research Group, Center for Solid State Electronics Research, Arizona State University, Tempe, Arizona, 85287-5706

The formation, materials properties and interfacial characteristics of silicon dioxide on silicon have been the subject of intense interest for a number of years^{1,2}. The continued reduction in device size and the advent of realizable fabrication schemes for mesoscopic devices has only intensified the need for a more complete understanding of the mechanism of formation of the oxide and the effects of parametric variations in this mechanism on oxide properties and on interfacial states. The dominant model of oxidation is the Deal-Grove model³ which is inadequate for thin oxides. In order to further our understanding in this area, we have recently undertaken a re-examination of the chemical mechanism of silicon oxidation. In this work, we present a conceptual and mathematical model for the thermal oxidation of silicon based on the initial dissociative chemisorption of molecular oxygen on the 2×1 silicon (100) surface and on subsequent dissociative reactions of molecular oxygen at the Si/SiO₂ interface. The proposed mechanism successfully accounts for current experimental observations on the structural modifications of the reconstructed surface to a 1×1 superlattice on initial exposure to molecular oxygen⁴ and provides a mechanistic rationale for the fact that the initial, low temperature oxidation process apparently self-limits at ca. 0.6 nm. thickness. More detailed examinations of the model have also suggested an internally consistent mechanism for the formation of an inherent Si/SiO₂ interfacial roughness of the order of one silicon atomic diameter. Using the model, we develop rate equations consistent with the molecular reactions occurring at the Si/SiO₂ interface and diffusion limitations in the thick oxide limit. The rate equations predict the kinetics of oxide growth from the initiation of oxidation of the clean silicon surface, through the very thin oxide regime in which the growth rate is proportional to $[O_2]^{1/2}$ to the thick oxide regime in which Deal-Grove behaviour³ dominates. We predict a transitional growth regime in which the molecular dissociative adsorption kinetics at the interface compete with the process of diffusion of molecular oxygen through the oxide film. Auger electron spectroscopy data of the Si LVV transition acquired during and after oxide growth is interpreted in terms of the proposed model. This transition reflects the self convolution of valence band density of states and is most expressive of the chemical bonds present and the general structure in which they exist.

* Work supported by Advanced Research Projects Agency

+ NSF MEADE Doctoral Fellow

1. T. Kunjunny and D. K. Ferry, Phys. Rev. B, **24**, 4593 (1981).
2. G. Lucovsky, S. S. Kim and J. T. Fitch, J. Vac. Sci. Technol., **B8**, 822 (1990).
3. B. E. Deal and A. S. Grove, J. Appl. Phys., **36**, 3770 (1965).
4. E. G. Keim, L. Wolterbeek and A. Silfhout, Surf. Sci., **180**, 565 (1987).

Reliability of Nitrided Si-SiO₂ Interfaces formed by a New, Low-Temperature, Remote-Plasma Process

David R. Lee and Gerald Lucovsky

Departments of Physics, and Materials Science and Engineering
North Carolina State University, Raleigh, NC 27695-8202

Incorporation of nitrogen near the Si-SiO₂ interface has been reported to result in increased immunity to interface trap generation after electrical stressing. Thus, nitrided SiO₂ has been said to be a more reliable dielectric than conventional thermally-grown SiO₂ and therefore may be better suited for deep sub-micron MOS devices that require ultra-thin (< 5 nm) gate dielectric layers. However, the techniques, such as annealing in NH₃ and oxidation in N₂O, that are commonly used to incorporate N in gate oxides are high-temperature processes and may have limited application for small device geometries where thermal budget becomes important.

We have recently developed a new, low-temperature method for incorporating controlled amounts of N at the Si-SiO₂ interface. This technique involves exposing a hydrogen-terminated Si (100) surface to species extracted from a remote plasma of mixtures of O₂ and N₂O as a pre-deposition, surface treatment step prior to gate dielectric deposition by Remote Plasma Enhanced Chemical Vapor Deposition. By controlling the ratio of O₂ to N₂O during this pre-deposition exposure, the amount of N incorporated at the Si-SiO₂ interface can be controlled between 10¹⁴ and 10¹⁵ N-atoms / cm², according to AES and SIMS measurements. Additionally, this pre-deposition remote plasma exposure 1) removes C from the Si surface down to ~ 2x10¹² C-atoms / cm² and 2) results in the plasma-assisted growth of a thin, 5-6 Å, SiO₂ layer. Thus, the Si-SiO₂ interface is *grown* during this pre-deposition exposure step, while the bulk SiO₂ is *deposited* afterwards by Remote PECVD using SiH₄ and N₂O source gases. These steps take place sequentially in the same vacuum chamber at 300 °C. Remote Plasma processing, using this concept of separating the interface and bulk formation has been successfully used to deposit device-quality (as studied in MOS capacitors and FETs) SiO₂ at 300 °C.

In this study, we review the development of this new, low-temperature technique for incorporating N at the Si-SiO₂ interface and report on the interface quality and reliability as a function of the concentration of N. MOS capacitors were fabricated on p-type Si (100) wafers using gate dielectrics deposited as described above and with n⁺ poly-Si gate electrodes in a one-mask process. The Si-SiO₂ interface was characterized using high-frequency and quasi-static C-V techniques. It was found that the initial quality of the interface, as defined by the midgap D_{it}, was not affected by different concentrations of N introduced by the remote-plasma, pre-deposition exposure (midgap D_{it} ~ 1x10¹⁰ cm⁻² eV⁻¹ regardless). Reliability of the plasma nitrided Si-SiO₂ interfaces has been characterized by increases in midgap D_{it} after constant-field and constant-current stressing. Changes in the D_{it} spectrum for different stress conditions and different interfacial N concentrations will be discussed.

David R. Lee
Box 8202
North Carolina State University
Raleigh, NC 27695-8202
Phone: (919) 515-7531
Fax: (919) 515-7331
email: drlee@eos.ncsu.edu

Gerald Lucovsky
Box 8202
North Carolina State University
Raleigh, NC 27695-8202
Phone: (919) 515-3301
Fax: (919) 515-7331

Characterizing wearout and breakdown in thin silicon oxide*

D. J. Dumin, J. R. Maddux**, R. Subramoniam, R. S. Scott, S. Vanchinathan***, N. A. Dumin****, K. J. Dickerson****, S. Mopuri***, and S. M. Gladstone

Center for Semiconductor Device Reliability Research
Department of Electrical and Computer Engineering

Clemson University
Clemson, South Carolina 29634-0915

Abstract

There are several models of how high-voltage induced wearout and breakdown occur in thin silicon oxides. Breakdown initiated by impact ionization processes seems to apply to oxides thicker than 20nm [1]. A somewhat different model based on trap generation caused by high-field emission processes accompanied by atomic motion of the atoms has been developed to describe breakdown in oxides thinner than 20nm.[2]. The uniform trap generation is modulated by local high-field generation regions, particularly near the cathode or at asperities inside the oxide. The thickness and field dependences of time-to-breakdown data for oxides less than 7.6nm thick [3], the temperature and field dependences of time-dependent-dielectric-breakdown distributions [4], the breakdown distributions on oxides as thick as 22nm [5], and the polarity dependence of constant-current, charge-to-breakdown data measured on oxides with different gate materials [6] have all been analyzed using this model. The presence of anomalous positive charge, the ability to change the charge states of the traps, the generation of negative charges inside of the tunneling barrier, the transient shifts in flat-band voltages following high-voltage stress, and the increases in the low-level leakage currents have all be analyzed in terms of the high-field emission model.

In this paper the trap generation process occurring during wearout will be coupled to the statistics of breakdown and will be used to generate and analyze TDDB distributions. It will be shown that the high field trap emission model of wearout and breakdown can be coupled to existing oxide breakdown data to predict safe operating voltages for oxides as thick as 22nm, including the effects of field and temperature on oxide reliability. It will be shown that neither constant-current nor constant-voltage stress testing very accurately corresponds to constant-field testing. It will be shown how this model of wearout and breakdown can be used to explain most existing thin oxide breakdown data in a unified manner. The difficulties associated with measuring wearout in oxides thinner than 6nm will be discussed in terms of trap discharging via tunneling to the two interfaces.

1. D. Arnold, et al, Phys. Rev. **49**, 10278, 1994.
2. D. J. Dumin, et al, Proc. IRPS, 143, 1994.
3. K. F. Schuegraf and C. Hu, Proc. IRPS, 7, 1993.
4. N. Shiono, et al, Proc. IRPS, 1, 1993.
5. J. S. Suehle, et al, Proc. IRPS, 120, 1994.
6. X. Gao, . 136, Extended Abs. Spring Electrochem. Soc. Meeting, 209, 1994.

* Supported by the Semiconductor Research Corporation

** Present address, University of Virginia, Charlottesville, VA

*** Present address, National Semiconductor Corp., Santa Clara, CA 95052

**** Present address, Texas Instruments, Inc., Dallas, Texas 75265

Corresponding author: D. J. Dumin. Phone: 803-656-5919, fax: 803-656-5910, e-mail: dave.dumin@eng.clemson.edu

Process Dependence of the SiO₂/Si(100) Interface Structure

Z.H. Lu and M.J. Graham

Institute for Microstructural Sciences
National Research Council of Canada
Montreal Rd., Ottawa, Ont., Canada, K1A 0R6

S.P. Tay

Telecom Microelectronic Centre
Northern Telecom Limited
185 Corkstown Rd., Nepean, Ont., Canada K2H 8V4

T. Miller and T.-C. Chiang

Department of Physics and Materials Research Laboratory
University of Illinois at Urbana-Champaign
1110 W. Green Street, Urbana, Illinois 61801, USA

Synchrotron radiation photoemission spectroscopy has been used to study thermal SiO₂/Si(100) interfaces. Oxides were grown at 700 °C and were then post-annealed at higher temperatures. Various Si oxidation states Si^x (x represents the oxidation state) at the interface were detected from Si 2p core level measurements. The results show in Figure 1 that the amount of both Si⁺³ and Si⁺² increases while that of Si⁺¹ remains constant as a function of anneal temperature. It is also found that the peak-width of the substrate Si 2p increases with increasing anneal temperature. This is attributed to the disordering of substrate Si atoms adjacent to the interface. The above results are interpreted in terms of anneal-induced structural relaxation to reduce the long-range strain on both sides of the interface.

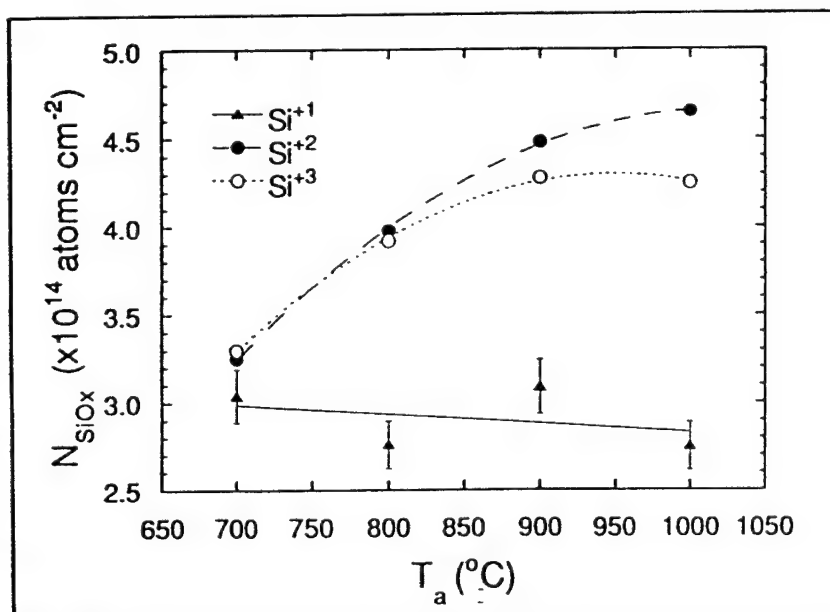


Figure 1

Z.H. Lu

Institute for Microstructural Sciences,
National Research Council of Canada
Montreal Rd., Ottawa, Ont., Canada, K1A 0R6
Phone: 613-991-4714; FAX: 613-952-6337; LU@SG1.CHEM.NRC.CA

Scaling of Si/SiO₂ Interface Roughness

Hiroshi Iwasaki

The Institute of Scientific and Industrial Research, Osaka University

Roughness of materials surface and interface shows, in general, self-affine nature; scale invariant for anisotropic rescaling. The scaling behavior is best seen in a log-log plot of the interface width (rms height) vs. linear size of the area as a straight line. The slope of the line (α) is related with local fractal dimension and is less than 1 for self-affine interface: the interface looks flat when it is seen macroscopically. For a film with finite thickness, the increase of the width with linear size saturate at a correlation length L_c : L_c represents the size of the largest bump of the interface which could grow during the film growth. In the case of polished Si and SiC wafers, saturated regions could be observed after finest polishing. Thus, in general, materials interface roughness can be characterized by the three parameters; α , L_c and the saturated interface width Δ .

Study of scaling of Si/SiO₂ interface roughness is important because it affects inversion layer carrier mobility through roughness scattering. Goodnick et al. have studied interface roughness statistically by TEM. As indicated by them, TEM gives roughness averaged over the thickness of the specimen along the electron beam. AFM is suited for studying scaling behavior of interfaces as it is capable of measuring 2D topographs with wide dynamic range ($\sim 10^6$).

We measured Si/SiO₂ interface roughness by AFM after removing thermal oxides by HF chemical etching. The Δ values are 0.20nm (Si surface before oxidation), 0.27 (Si/dry oxide of 16nm thickness), 0.29 (Si roughened by SC1 etching for 180 min) and 0.30 (Si/dry oxide for roughened substrate), while α and L_c are ~ 0.35 and 100nm, respectively, for the all interfaces. Roughening caused by oxidation may be described by an equation similar to the Langevin equation proposed by KPZ. From such measurements, we can estimate relative magnitudes of the coefficients of the roughening and smoothing terms in the equation.

In the earlier calculations of the carrier mobility, Gaussian autocorrelation functions (ACF) of interface roughness had been assumed. Goodnick et al., however, reported that the ACF is exponential function. Our results also indicate exponential like ACFs: an exponential (Gaussian) ACF corresponds to the above mentioned truncated self-affine relations with $\alpha = 0.5$ (1.0). Our results are also in agreement with large L_c which is needed to explain recent carrier mobility measurement (Kruithof et al.).

Defect Production, Degradation, and Breakdown of Silicon Dioxide Films.

D. J. DiMaria

*IBM Research Division, T.J. Watson Research Center,
Yorktown Heights, New York 10598*

Abstract

The degradation and eventual destructive breakdown of silicon dioxide films on silicon will be reviewed. The relationship of the generation of hot electrons in the oxide layer due to the applied field and the defects subsequently produced will be discussed and related to breakdown. Continuous trap and interface-state production by both free-electron/trapped-hole recombination and the "trap creation" phenomenon will be considered as the dominant mechanisms for this defect generation [1,2].

Free holes have been shown to be produced primarily through bandgap impact-ionization by hot electrons with energies exceeding 9 eV with respect to the bottom of the oxide conduction band [1]. On oxides of thickness less than 13 nm, a smaller amount of hole injection from the anode can occur for applied voltages greater than 8 V (5 eV for the electron energy). Defect production by trap creation has been demonstrated to occur when hot electron energies exceed 2 eV [2]. This latter mode dominates defect production for films less than 13 nm in thickness at any field. For oxide films with thickness below 4.5 nm, electron energies do not exceed 2 eV and interface-state and trap generation are suppressed.

In this review, special emphasis will be given to oxide films with thickness less than 13 nm which are currently technically relevant. Silicon-substrate current on stressed n-channel FETs and oxide stress-induced-leakage current (SILC), occurring prior to destructive breakdown, will be related to defects produced primarily by trap creation. Other explanations for thin-film degradation and breakdown, particularly those involving anode hole injection, will also be reviewed and discussed.

- [1] D. J. DiMaria, E. Cartier and D. Arnold, *J. Appl. Phys.* 73, 3367 (1993).
- [2] D. J. DiMaria and J. W. Stasiak, *J. Appl. Phys.* 65, 2342 (1989).

Oxygen-Associated Defects near Si-SiO₂ Interfaces in Porous Si and their Role in Photoluminescence

W.E. Carlos and S.M. Prokes
Naval Research Laboratory
Washington, D.C. 20375

Porous Si is comprised of nanometer-scale crystallites of Si which are inevitably surrounded by thin oxide layers. It has been proposed that the red room temperature luminescence in this material is primarily due to defects at or near the interface between the crystallites and the thin oxide. We report here the observation of two ESR active oxygen-centric defects; one in nominally unoxidized porous Si and the second in material which has been oxidized for a very short period of time (~1 min.). The first is a variant of the thermal donors observed in crystalline Si and the second is the EX center observed by Stesmans and Scheerlinck in thin layers of SiO₂ on crystalline Si. These two centers are thought to have similar cores, a Si vacancy surrounded by four Si-O linkages, with the primary difference not in the central core but rather in the surrounding lattice (Si vs. SiO₂). Both must be located very near the Si-SiO₂ interfaces of the Si particles within the porous Si layer because of the short diffusion length of O in Si at room temperature and because of the short oxidation times. The donor is rendered paramagnetic by light ($\geq 1\text{eV}$) and remains in that metastable state at low temperatures. Its resonance is anisotropic, reflecting the crystal structure of the Si crystallites. The intensity of this resonance correlates with the intensity of the photoluminescence; however we do not believe it is directly involved in the luminescence process. The EX center has a very sharp resonance indicating that the electronic spin is delocalized over several sites. The relative intensity of the ²⁹Si hyperfine structure is consistent with delocalization. The resonance line narrows with increasing temperature suggesting a dynamic Jahn-Teller distortion. The ESR intensity of this center is also related to the photoluminescence intensity and we believe it may be more directly related to the luminescence process. Details of the models of the relationship of these defects and the luminescence processes in porous Si will be discussed. We will also consider the relationship of porous Si with other similar materials such as Si-rich oxide films.

W.E. Carlos
Code 6863
Naval Research Laboratory
Washington, D.C. 20375
Phone: 202-767-3896 FAX: 202-767-4290
E-Mail: Carlos@ESTD.NRL.Navy.Mil

Silicon Interlayer Based Surface Passivation of Near-Surface Quantum Wells

Satoshi Kodama, Satoshi Koyanagi and Hideki Hasegawa

Research Center for Interface Quantum Electronics and Department of Electrical Engineering,
Hokkaido University, Sapporo 060, Japan, TEL: +81-11-706-6509, Fax: +81-11-706-7890

Recent study[1-3] has shown that the photoluminescence (PL) efficiency of the quantum well(QW) is drastically reduced exponentially, as the QW is placed nearer to the surface, due to interaction between QW states and surface states. Thus, surface passivation is vitally important for planar integration of quantum structures formed near surface region of semiconductor.

The purpose of this paper is to show that our novel silicon interlayer based surface passivation scheme is extremely powerful in passivating surface states and enhancing the PL intensity of the AlGaAs/GaAs near surface QWs. Recovery of PL efficiency of as large as 10^3 times has been demonstrated. The main points are as follows:

(1) The structure of the QW sample passivated by the novel scheme is shown in Fig.1. An ultrathin silicon interface control layer (Si ICL) by MBE and an ultrathin silicon nitride layer by photo-CVD are inserted between the near surface QW (QW1) and the thick SiO₂ layer by photo-CVD. A second QW(QW2) is formed far from the surface as the reference. Passivation was done *in-situ* after the MBE growth of QW structures, using an UHV-based system where MBE, ArF laser based photo-CVD, XPS and other chambers are connected by UHV-transfer chamber.

(2) In our original passivation structure without ultrathin silicon nitride [4], photo-excited oxygen radicals penetrated through Si ICL and oxidized the semiconductor during photo-CVD deposition of SiO₂. The addition of an ultrathin Si₃N₄ barrier has solved this problem. The novel scheme has achieved a minimum interface state density of as low as $2 \times 10^{10} \text{ cm}^{-2} \text{ eV}^{-1}$ on In_{0.53}Ga_{0.47}As MIS test structures.

(3) The observed variation of the PL intensity from the near-surface QW (QW1) normalized by that from the reference QW (QW2) is shown Fig. 2 for unpassivated samples as a function of the thickness t_B of the top AlGaAs barrier layer. When t_B is large, the normalized intensity is nearly equal to unity, but when t_B becomes less than about 100Å, the intensity is reduced exponentially and becomes about 10^{-3} for $t_B = 50\text{Å}$.

(4) As also shown in Fig.2, the PL intensity of the passivated samples is, on the other hand, kept remarkably near unity for the barrier thicknesses of $t_B = 50\text{Å}$ -500Å, demonstrating an observed maximum PL enhancement factor of 10^3 . No such enhancement was obtained when only SiO₂ was deposited without Si ICL.

(6) A careful successive chemical etching study of the passivated structure, using the buffered HF solution and an AFM thickness calibration, has revealed a sudden dramatic reduction of PL intensity on removal of the ultrathin Si ICL, showing directly the essential importance of the Si ICL in the present passivation scheme.

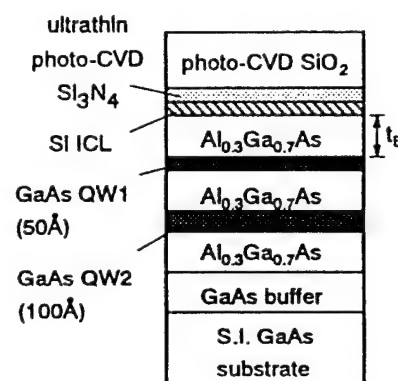


Fig.1 Sample structure

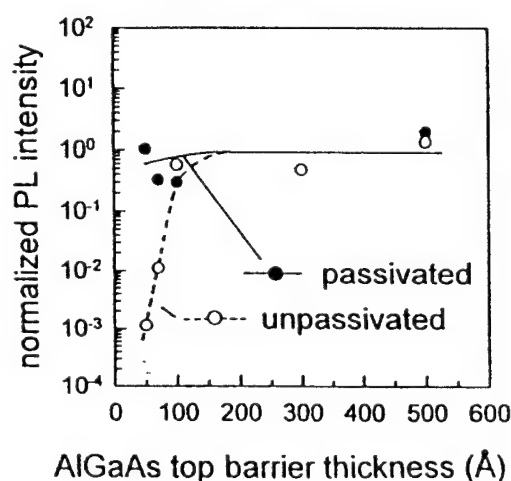


Fig.2 Dependence of PL intensity on t_B

- [1] J. Moisson et al.: Phys. Rev. B **41** (1990) 12945.
- [2] Z. Sobiesiersky, T. Fukui and H. Hasegawa: 1993 PCSI; J. Vac. Sci. Technol. **B11** (1993) 1723.
- [3] Y.-L. Chang et al.: 1994 PCSI; J. Vac. Sci. Technol. **B12** (1994) 2605.
- [4] H. Hasegawa et al.: 1990 PCSI; J. Vac. Sci. Technol. **B8** (1990) 867.

Corresponding Author: Hideki Hasegawa, Research Center for Interface Quantum Electronics, Hokkaido Univ., N13, W8, Sapporo 060, Japan, TEL: +81-11-757-1163, FAX: +81-11-757-1165.

Quasi-epitaxy of the organic semiconductor PTCDA on Se-passivated GaAs(100)

Y. Hirose, S.R. Forrest and A. Kahn

Dept. of Electrical Engineering, Princeton University, Princeton, N.J. 08544, USA

Quasi-epitaxy in highly mismatched systems is of fundamental importance, in particular for crystalline organic-organic and organic-inorganic (OI) heterojunctions. At OI heterojunctions the nature of the substrate surface has a profound impact on the crystallinity of the organic film. Chemically active defects such as dangling bonds, vacancies or steps pin molecules in random positions and prevent molecular ordering at the interface with, and in the films grown on, surfaces of inorganic semiconductors. In that regard, the *chemical passivation* of inorganic substrates helps by smoothing the surface and by reducing the strength of interface interaction [1].

Films of organic semiconductor 3,4,9,10 perylenetetracarboxylic dianhydride (PTCDA) are grown by molecular beam evaporation in UHV on GaAs(100). PTCDA is deposited on three different types of surfaces prepared by MBE: the As-rich c(4x4) GaAs(100), the As-terminated (2x4)-c(2x8) GaAs(100) and the (2x1) Se-passivated GaAs(100). The Se-passivation of GaAs is performed in-situ by supplying an overpressure of Se for two minutes at 450°C, followed by a 5 minute anneal at 510°C. The PTCDA film thickness ranges between 3Å (~1ML) and 2000Å. We use X-ray and electron diffraction, and Auger electron and ultra-violet photoemission spectroscopies to characterize the film composition, growth mode and electronic properties.

The molecular spacing in the direction perpendicular to the substrate is found in all films to be consistent with the 3.21Å value of bulk PTCDA. Films grown on the (2x4)-c(2x8) surface consist of small domains randomly oriented in the plane parallel to the substrate, leading to LEED patterns consisting mainly of a specular beam and very diffuse rings. Increasing molecular order is observed in films grown on highly ordered c(4x4) GaAs surfaces. A drastic improvement in crystallinity is observed in films grown on highly ordered Se-passivated surfaces. These films produce very sharp LEED patterns resulting from a net azimuthal orientation of the molecules with respect to the substrate Se-dimers. The diffraction pattern is interpreted in terms of several domains of PTCDA with 12Åx19.4Å rectangular unit cell compatible with that of the PTCDA (102) plane. In addition, the molecular arrangements at the PTCDA/GaAs interface and at the surface of 2000Å thick films are found to be identical, suggesting that the film grows at the onset with the bulk PTCDA structure. The drastic improvement in crystallinity with Se-passivation is attributed to improved substrate smoothness and to the termination of chemically active defects by Se which results in a reduced energy of interaction between the inorganic surface and the adlayer (interlayer interaction << intralayer interaction). Our results demonstrate the quasi-epitaxial growth of a van der Waals bonded film on a highly lattice mismatched substrate surface. The ability to *engineer* such structures without regard to lattice matching constraints common to conventional epitaxy of inorganic compounds has profound implications for producing a wide range of materials for many optoelectronic device applications.

1. T. Kawaguchi, H. Tada, and A. Koma, J. Appl. Phys. 75, 1486 (1994) ; H. Yamamoto, T. Kawaguchi, and A. Koma, Appl. Phys. Lett. 64, 2099 (1994)

Hydrogen induced modification of the optical properties of the GaAs(100) surface

N. Esser^a, P.V. Santos^a, M. Kuball^a, M. Cardona^a, M. Arens^b, W. Richter^b, F. Stietz^c,
J.A. Schaefer^c and B. O. Fimland^d

^aMax-Planck-Institut, FKF, Heisenbergstr. 1, D-70569 Stuttgart, Germany

^bInstitut für Festkörperphysik, TU Berlin, Hardenbergstr. 36, D-10623 Berlin, Germany

^cFachbereich Physik, Universität Kassel, D-34132 Kassel, Germany

^dDepartment of Physical Electronics, NIT, N-7034 Trondheim, Norway

We investigated the influence of hydrogen adsorption on the surface order, the dielectric function, and its anisotropy of the main reconstructions ($c(4 \times 4)$, (2×4) , $c(8 \times 2)$) of GaAs(100)-surfaces by combining LEED, spectroscopic ellipsometry, and reflectance difference spectroscopy (RDS), respectively. We find a layer-by-layer removal of the As surface atoms which converts into an inhomogeneous surface etching as soon as the first Ga layer is exposed. This is most pronounced for the $c(4 \times 4)$ -surface, where the first two atomic layers consist of As. At low exposures the optical anisotropy of the $c(4 \times 4)$ surface is removed almost completely by hydrogen adsorption due to removal of the As-dimers in the outermost As-layer while the LEED pattern changes from $c(4 \times 4)$ to (1×1) . We conclude that at this stage the surface is terminated by one complete As layer where the dangling bonds are saturated with H, thus preventing a new dimerization at the surface. At intermediate hydrogen exposures, the RDS spectra show the signature of Ga dimers while LEED indicates a mixed (1×2) and $(\sqrt{2} \times \sqrt{2})$ -reconstruction. This result is due to the removal of the second As layer, but the corresponding Ga terminated surface is not as effectively saturated with H as the As terminated one, thus giving rise to a new dimerization of the Ga atoms. Finally, at even higher dosages the Ga dimers are broken by hydrogenation and the LEED pattern shows a weak (1×1) symmetry. At this stage an onset of surface roughening occurs leading to a disordered surface. For H adsorbed on the clean (2×4) -surface, the As dimers are broken in the low exposure regime, while the LEED pattern is changed to (1×4) -symmetry. Consequently, the dimer related features disappear in the RDS spectra. At larger exposures the As is removed and a (1×1) LEED pattern appears. A dimerization of Ga is not observed, neither by LEED nor by RDS, which demonstrates that the surface is not well ordered. At large exposure again surface roughening occurs. For the Ga rich $c(8 \times 2)$ surface a very similar development upon hydrogen adsorption is found, namely breaking of the dimers at low exposures, removal of the outermost Ga layer at intermediate and surface roughening at large coverages.

Surface ordering on GaAs(100) by Indium-termination

U. Resch-Esser^a, C. Springer^a, W. Richter^a, N. Esser^b, J. Zegenhagen^b, P.V. Santos^b,
M. Cardona^b, and B. O. Finland^c

^aInstitut für Festkörperphysik, TU Berlin, Hardenbergstr. 36, D-10623 Berlin, Germany

^bMax-Planck-Institut für Festkörperforschung, Heisenbergstr. 1, D-70569 Stuttgart, Germany

^cDepartment of Physical Electronics, NIT, N-7034 Trondheim, Norway

The growth of a well ordered Indium-layer on GaAs(100) surfaces of different reconstructions has been investigated by STM, LEED, AES, and reflectance anisotropy spectroscopy (RAS). As substrates MBE-grown GaAs(100) of a doping concentration of $n = 1 \times 10^{18} \text{ cm}^{-3}$ (Si) was used. Clean surfaces were prepared in UHV by thermal desorption of a protective Arsenic layer. By annealing, the $c(4 \times 4)$, (2×4) , and $(4 \times 2)/c(8 \times 2)$ surface reconstructions are formed with increasing temperature. For the (2×4) reconstruction, the STM results show fairly well ordered surfaces. Besides a large number of dislocations, which has been previously explained by Pashley et al. [1] as source of surface acceptor states, a surface roughness of around three double-steps height is observed. Indium subsequently deposited on this surfaces at room temperature exhibits a laminar, disordered growth, followed by island formation for higher coverages. By annealing of around one monolayer of Indium to approximately 450 °C a well ordered Indium-layer is established on top of the GaAs surface. The LEED pattern reveals a $(4 \times 2)/c(8 \times 2)$ symmetry for this Indium-terminated surface. In contrast to the clean surface prepared by decapping, the STM results now show a highly ordered Indium-terminated surface, where the number of dislocations as well as the surface roughness is drastically reduced. The Indium is arranged in an anisotropic surface structure which appears as a ladder-type pattern consisting of alternating straight and broken rows orientated along the $[0\bar{1}1]$ -direction. Even in atomically resolved STM pictures no corrugation appears along the straight rows.

[1] M.D.Pashley, K.W.Haberern, R.M.Feenstra, J.Vac.Sci.Technol. B 10, 1874 (1992)

U.Resch-Esser

e-mail: USCHI@MARIE.PHYSIK.TU-BERLIN.DE

Interactions between vacancies on InP(110) surfaces

M. Heinrich ^a, Ph. Ebert ^{a,b}, Xun Chen ^b, M. Simon ^a, K. Urban ^a, and M.G. Lagally ^b

^a*Institut für Festkörperforschung, Forschungszentrum Jülich GmbH, D-52425 Jülich, Germany*

^b*University of Wisconsin, Madison WI 53706, USA*

The electronic properties of compound semiconductors are to a significant part determined by defects. Point defects in the bulk, such as vacancies or impurity atoms, can cause deep-level trap states that shift the Fermi energy and thus also influence electronic and optical properties of the crystals. Similarly defects at the surface can lead to localized states and charges that bend bands and influence the electrical properties of a structure. For example the importance of surface defects in the formation of electrical contacts to compound semiconductors has long been recognized. However, individual defects could not be identified. Scanning tunneling microscopy makes such identification possible, leading to the opportunity to explore the influence of individual surface defect types on electronic and optical properties.

We have determined directly the charge localized at a phosphorous vacancy on p-doped InP(110) surfaces from the interaction between the vacancies. The interaction potential is deduced from scanning tunneling microscopy images using statistical mechanics. We took the coordinates of the vacancies from the images and determined the correlation function. The interaction potential calculated from the correlation function was found to have a functional form of a screened Coulomb potential. The charge of the vacancies is +1. The screening length is (1.15 ± 0.1) nm. The charge deduced is used to determine the position of the charge transition levels in relation to the Fermi energy. It is found that the charge transition levels from the single to double and double to triple positively charged vacancy are both below the valence band maximum. Deviations from the screened Coulomb potential occur for separations smaller than 1.2 to 1.5 nm. These deviations have the same spatial extent as changes of the surface buckling around the vacancies and thus are attributed to lattice relaxations.

Ph. E. thanks the Alexander von Humboldt-Foundation for a Feodor Lynen Research Fellowship. This work was partially supported by ONR.

Communications information

Philipp Ebert, 1500 Johnson Dr., ERB 1107, University of Wisconsin, Madison, WI 53706

Phone: (608) 265 4119

Fax: (608) 265 4118

Structure and Dynamics of Anion and Cation Vacancies at III-V (110) Surfaces

G. Lengel and M. Weimer

Department of Physics, Texas A&M University
College Station, Texas 77843

J. Gryko and R.E. Allen

Center for Theoretical Physics, Texas A&M University
College Station, Texas 77843

Scanning tunneling microscopy and spectroscopy, in conjunction with tight-binding molecular dynamics simulations, now permit the microscopic characterization of point defects at semiconductor surfaces. We have focused on the simplest defects at one of the best-studied semiconductor surfaces: As and Ga vacancies on GaAs(110) [1, 2]. When an As vacancy is created, each of the neighboring Ga surface atoms is left with only two bonds of the original four in a bulk tetrahedral environment. Rather than rebonding, however, they relax upward by several tenths of an Angstrom. This vacancy relaxation is driven by a lowering of the occupied dangling-bond vacancy states. It is therefore analogous to the original GaAs(110) *surface* relaxation, which is driven by a lowering of the occupied dangling-bond *surface* states. A similar upward relaxation is observed for the two surface As atoms neighboring a Ga vacancy, although the STM tip voltage appears to be playing a role in this case. The As vacancy is observed on degenerate *p*-type GaAs, and not on degenerate *n*-type, whereas the opposite is true for the Ga vacancy. This observation is explained by the calculated dangling-bond levels: The occupied levels are higher for the As vacancy, and the unoccupied levels lower for the Ga vacancy. The As vacancy is positively charged (probably in a +2 state) and the Ga vacancy negatively charged (probably -2). The spectroscopy shows a local Fermi level for the As vacancy that is very near the valence band edge, in agreement with the calculations.

Several hundred vacancy migration events have been observed. These events are induced by the STM tip, and they exhibit very striking spatial and bias asymmetries: (1) Contrary to naive expectations, most events are *across* the GaAs(110) surface zigzag chains, rather than along them. (2) Of the two directions across the chains (left and right in our convention), all of the events for the As vacancy are to the left and *none* to the right. (3) The As vacancy migrates only when electrons are tunneling *into* the surface, out of the STM tip. (4) The Ga vacancy migrates only when electrons are tunneling *out of* the surface. A fifth key signature is the strong *locality* of the effect: A scatter plot reveals that the tip is always very near the vacancy when the migrations occur. These experimental signatures, together with tight-binding molecular dynamics simulations, indicate that the mechanism involves nonradiative capture of minority carriers into dangling-bond trap states, releasing ~ 1.5 eV of energy to promote vacancy migration.

Our most recent STM observations, on GaSb (110), show significant differences in vacancy concentrations, which are interpreted as arising from (a) the smaller band gap and (b) the lighter doping employed. Theoretical simulations for GaSb, and for GaP and InP [3], are currently in progress.

- [1] G. Lengel et al., Phys. Rev. Lett. **72**, 836 (1994).
- [2] G. Lengel et al., Proceedings of the 22nd International Conference on the Physics of Semiconductors (Vancouver, August, 1994).
- [3] P. Ebert et al., Phys. Rev. Lett. **72**, 840 (1994).

This work was supported by the U.S. Office of Naval Research and the Robert A. Welch Foundation.

Scanning Tunneling Microscopy and Spectroscopy of the Reaction of NH₃ with GaAs (110)

G. Brown and M. Weimer

Department of Physics, Texas A&M University, College Station, TX 77843-4242

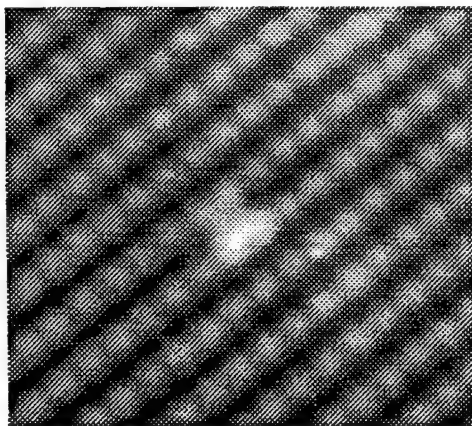
It is known that the reaction of gaseous ammonia with the (110) surfaces of GaAs and InP results in non-dissociative chemisorption, but important details concerning the adsorption geometry and local electronic structure, as well as the extent of surface etching, are not well understood. These issues are relevant to such complex processes as the Atomic Layer Epitaxy of nitride compounds (e.g., GaN), and to continuing efforts to grow suitable insulating nitride layers for compound semiconductor device applications.

We have examined the adsorption of submonolayer amounts of ammonia on the (110) surface of *p*-type GaAs with scanning tunneling microscopy (STM) and spectroscopy (STS). We find two chemisorption-related features that are attributed to perturbations in dangling bonds of the substrate, and not to molecular orbitals of the adsorbate.

A filled-state STM image of the first, and most common, structure is shown below. The associated empty-state images reveal that the in-chain gallium neighbor shared by the enhanced arsenic atoms is usually depressed, but sometimes shifted, depending on the nature of the probe tip. The symmetry and appearance of these structures, as well as their associated screening, imply that ammonia is bonded to surface gallium atoms. The band-bending observed in the vicinity of the adsorbates is consistent with the screening of a surface dipole. The orientation and sign of this screening suggest the molecules are tilted with their lone pair directed toward the surface as expected from Lewis acid-base chemistry and inferred in prior electron spectroscopic studies. This is the first direct visualization of a *single* adsorbate's dipole moment by STM, and it suggests new methods that may provide more detailed information about adsorption sites and molecular orientations. STM-induced migration of individual ammonia molecules across the surface has also been observed.

The second structure, found on high coverage samples, appears to be an arsenic vacancy with ammonia bonded to one or both of the adjoining gallium atoms. Since these features are found with greater frequency than the native vacancies on GaAs (110), they imply that etching of surface arsenic atoms also occurs.

Finally, we will present preliminary STS results and discuss their relation to possible adsorbate-induced surface states. This work was supported by the Office of Naval Research and the Robert A. Welch Foundation.



Hot electron transport through Metal-Oxide-Semiconductor structures studied by Ballistic Electron Emission Spectroscopy

R. Ludeke, A. Bauer^{a)} and E. Cartier

IBM T.J. Watson Research Center, P.O. Box 218, Yorktown Heights NY, 10598

We report the first hot electron studies through metal/SiO₂/Si(100) structures achieved with Ballistic Electron Emission Microscopy (BEEM), and demonstrate BEEM to be a powerful tool to study oxide properties on a microscopic scale. The SiO₂ layers are device quality oxides thermally grown at a Si IC processing facility. Their thickness for the studies reported here ranged from 27 to 68 Å, i.e. a range contemplated for future device applications. Platinum dots, ~30 Å in thickness, were evaporated onto the SiO₂ in UHV. The completed MOS structure was then transferred to the UHV STM chamber, where individual Pt dots could be contacted in order to apply the STM tip voltage ($1 \leq V_T \leq 10$ V), as well as a gate bias ($-3 \leq V_b \leq +2$ V) across the oxide. For all but the thinnest SiO₂ samples, a collector current I_c from the Si substrate was observed only if the kinetic energy of the electrons ($\equiv eV_T$) injected into the Pt by the STM tip exceeded ~4 eV. This value corresponds to the barrier height eV_o between the Pt Fermi level and the bottom of the SiO₂ conduction band, and indicates that transmission through the SiO₂ occurs by electron transport in its conduction band. By applying a gate bias $V_b \lesssim -0.5$ V, a value that corresponds to the built-in oxide potential, the threshold could be moved to higher energies as the effective barrier height is increased by the oxide potential V_{ox} . A positive V_b , on the other hand, accelerates the electrons toward the Si and does not affect the threshold value, which remains at V_o .

Detailed analysis reveals that the collector current, or more specifically the transmission probability through the SiO₂, is quite sensitive near threshold for $0.5 \lesssim V_{ox} \lesssim 0.5$ V. This is a consequence of the strong electron-phonon (mostly LO) scattering in the SiO₂, which increases the probability that injected electrons backscatter to the metal for small oxide fields. Current transport was modeled in a three-band approximation, with transverse momentum not conserved. From fits to the data, which yielded the threshold $V_o = 3.90 \pm 0.05$ V, the energy dependent transmission probability $T_{ox}(E)$ was determined for various values of V_b for oxide layers of 38 and 62 Å. $T_{ox}(E)$ was also obtained from semi-classical Monte Carlo simulations that included energy dependent phonon scattering rates and an energy dependent effective mass. Agreement with T_{ox} derived from experiment was quite good when injection into the SiO₂ layer was assumed to be isotropic.

Evidence for charged centers and defects in the oxide were also observed. BEEM images for a 27 Å SiO₂ layer revealed the presence of regions of ~30 Å in size that showed anomalously high transmission. Spectra taken at these areas revealed thresholds as low as 1 eV, compared to the normal 3.9 eV measured on 94% of the surface. Thresholds larger than 3.9 eV were also frequently observed on isolated points over the MOS sample surfaces. The magnitude of the shifts are consistent with threshold shifts arising from isolated, negatively charged centers (traps) near the SiO₂-Si interface.

^{a)} Present address: Institut für Experimentalphysik, Freie Universität Berlin, D-14195 Berlin, Germany.

Interface Characterization by Scanning Tunneling Microscopy

S.L. Skala, W. Wu, K.-Y. Cheng, J.R. Tucker, J.W. Lyding

Department of Electrical and Computer Engineering, Beckman Institute, and Microelectronics
Laboratory, University of Illinois at Urbana-Champaign, Urbana, IL 61801

A. Seabaugh, E.A. Beam III, and D. Jovanovic

Texas Instruments Incorporated, Central Research Laboratories, M/S 147, Dallas, TX 75265.

A lattice-matched InP/InGaAs resonant tunneling diode is studied by scanning tunneling microscopy and spectroscopy. The interfaces of the double barrier structure have been mapped with atomic resolution for a length over 4000 Å. STM images show the roughness to be very asymmetric with the inverted (InP on InGaAs) interface being considerably rougher than the normal interface. Roughness wavevectors determined from Fourier analysis are well fit by a Lorentzian and allow determination of roughness amplitudes and correlation lengths for the different interfaces. A chemical asymmetry between the interfaces is also observed in certain images which exhibit an enhanced and reduced state densities at the normal and inverted interfaces respectively. Termination of the growth surface by differing Col. V species during interface formation most likely affects the local state density. Spectroscopic observations of evanescent valence band states tailing into the InP barrier allow for direct measurement of the valence band offset. Additionally, evidence has been obtained of direct observation of the 2-D electron gas envelope function within the channel of a MODFET by STM.

Correspondence:

Joseph Lyding
Beckman Inst.
405 N. Mathews
Urbana, IL 61801

ph# (217) 333-8371 fax# (217) 244-8371 e-mail: lyding@assistant.beckman.uiuc.edu

Photomodulation Raman Scattering Spectroscopy of ZnSe/GaAs(001) Heterostructures Interface

H. Talaat, L. Elissa and S. Negm

Department of Physics, Faculty of Science, Ain Shams University, Cairo, Egypt.

E. Burstein

Department of Physics, University of Pennsylvania, Philadelphia, Pennsylvania 19104.

The interfacial band profile of the heterostructures ZnSe/GaAs continues to attract intense interest due to the material's important optoelectronic applications. Recently, we have reported our Raman studies using LO Fröhlich interaction as a probe to study the band bending at the buried interface. Photoexcited plasmon-LO phonon modes were also used to characterize the interface quality of the ZnSe/GaAs heterostructure [1].

In this work, we employ photomodulation Raman studies to affect and measure the band bending at the interface. Our samples are pseudomorphic layer of undoped ZnSe (001) grown by MBE on an undoped GaAs (001) film terminated with a 2x4 surface reconstruction. The interdiffusion of Zn (Ga) into GaAs (ZnSe) during growth produces an intrinsic band bending at the interface.

The ZnSe overlayer offers a transparent window both for the photomodulating pumping beam creating electron-hole pairs either in the GaAs or in both GaAs and ZnSe side as well as for the Raman incident frequencies used. The photomodulating beam with energy ≤ 2.67 eV introduces a negative interfacial charge while the one with energy > 2.67 eV, introduces both positive and negative interfacial charge into the system, resulting in the observed change in the band profile and the measured *forbidden* LO intensity. In the first case, electrons in GaAs move towards the interface whereas holes move away from it. Hence, the positive charges at the interface are partially neutralized which explain the drop obtained in the LO_{GaAs} intensity and the increase in the LO_{ZnSe} intensity. In the second case, both electrons in GaAs and holes in ZnSe move towards the interface which tends to flatten the band bending, however we have obtained a drop in the LO_{ZnSe} intensity with an increase in the LO_{GaAs} intensity. This last observation suggests that the interface traps are mainly hole traps and that the 2x4 interfaces are initially negatively charged. This is in agreement with the prediction of the negative interface charge in the 2x4 samples[2] and with photomodulation second-harmonic generation results [3]. Photomodulating Raman spectroscopy proves to be not only a sensitive technique to characterize the interface, but also enables one to identify the interfacial charge traps.

References:

1. A. Krost, W. Richter and D.R.T. Zahn; Appl. Surf. Sci. 56-58, 691 (1992).
2. H.H. Farrell, M.C. Tamargo and J.L. de Miguel; Appl. Phys. Lett. 58, 355 (1991).
3. M.S. Yeganeh, J. Qi, A.G. Yodh and M.C. Tamargo; Phys. Rev. Lett. 69, 3579 (1992).

Surface roughness and pattern formation during homoepitaxial growth of Ge(001) at low temperatures, Joseph E. Van Nostrand, S. Jay Chey. and David G. Cahill, Department of Materials Science, University of Illinois, Urbana, IL.

Reducing the growth temperature for molecular beam epitaxy reduces intermixing of layers and dopant segregation but a low growth temperature also leads to multilayer growth with an inherent increase in interface roughness. Using *in-situ* scanning tunneling microscopy (STM), we have quantified the surface morphology of Ge(001) during multilayer growth as a function of film thickness, growth temperature, and miscut angle of the substrate. We observe that given a sufficiently thick film, a regular pattern of growth mounds develops over a wide range of growth temperatures, 60-230°C. At 60°C only a 5 nm thick film is needed to observe this pattern formation, while at 230°C, a pattern of nearly pyramidal growth mounds is not fully evolved until the film is nearly 1 micron thick. At 155 and 230°C, the STM images show that the growth mounds are made up of narrow (001) terraces separated by atomic height steps.

At selected temperatures, we track the evolution of this pattern formation as a function of film thickness. The STM images show that the in-plane length scale of the surface roughness evolves directly from the spacing between islands during the first monolayer of growth; this length scale d increases with film thickness t in a manner consistent with a power law, $d \propto t^{0.4}$. In contradiction to theoretical proposals, the slope of the sides of the growth mounds is not a constant of the growth and increases with increasing film thickness. As the film thickness approaches the critical thickness h_{epi} at which the films become amorphous (h_{epi} is larger than the thickness needed to form a pattern of growth mounds), we observe the onset of high-aspect ratio surface roughness that may be responsible for determining h_{epi} .

Growth on a dimpled, concave substrate enables us to characterize the dependence of the pattern formation on the magnitude and direction of miscut angle. Growth mounds prepared at 230°C on nearly singular surfaces are approximately pyramidal with four-fold symmetry. With increasing miscut angle, the mounds elongate and form patterned, ridge-like structures when the miscut angle exceeds $\sim 1^\circ$.

David G. Cahill
University of Illinois, ESB
1101 W. Springfield Ave.
Urbana, IL 61801

Phone: (217) 333-6753
Fax: (217) 244-1631
Email: d-cahill@uiuc.edu

Hydrogen-ion treatment of AlGaAs/GaAs near-surface quantum well: A new approach to surface passivation

Ying-Lan Chang, Sang I. Yi, Song Shi, Evelyn Hu, W. H. Weinberg and James Merz
Center for Quantized Electronic Structures (QUEST)
University of California, Santa Barbara, CA 93106

Surface passivation is a key issue in III-V semiconductor device technology. The high density of midgap states on oxidized, unpassivated surfaces of most III-V compound semiconductors results in high surface recombination velocities that limit device performance. Several techniques have been proposed to improve the electronic properties. Most of them have focused on the removal of the oxide and the prevention of re-oxidation after the passivation treatments. The reproducibility and duration of such treatments have generally been limited. In this work, we propose a new approach to surface passivation, utilizing hydrogen-ion irradiation. Our results demonstrate the effectiveness of hydrogen ion passivation of a native oxide-covered AlGaAs surface. The passivation treatment takes place *in the presence of* a native oxide, which itself may serve as an over-passivation layer. We have measured hydrogen ion-treated samples where the passivation effect remained unchanged for more than two years, which we believe to be a record. Those samples were maintained at room temperature: the goal of these studies is to determine the thermal stability of the treatment, and to gain further insight into the exact mechanism of passivation.

Our assessment of passivation is related to the luminescence efficiency of near-surface quantum wells (QWs)[1]. QWs situated closer to the surface (< 10 nm) show reduced luminescence; that luminescence intensity is increased after treatment with hydrogen ions at an exposure of 10^{16} cm $^{-2}$. *In situ* Auger electron spectroscopy (AES) of the hydrogen-treated surface, carried out in an ultra-high vacuum (UHV) chamber with 5×10^{-11} Torr base pressure, showed a reduction in surface arsenic, without a change in the surface oxygen concentration. This correlation suggests that the passivation mechanism may involve the removal of arsenic, through the reaction between the hydrogen ions and the substrate, yielding volatile arsine (AsH $_3$). Temperature-programmed desorption (TPD) measurements indeed show that AsH $_3$ desorbs at $T > 200$ K, from an oxidized surface hydrogenated at 80K. We postulate that the oxide layer, which appears to remain throughout the hydrogenation treatment, serves as a passivation over-layer for the As-deficient surface/interface, leading to the long-term stability of this process: desorption of Ga $_2$ O $^+$ and As $_2^+$ are not seen until the substrate is heated to ~ 800 K.

Further studies of the temperature stability of the passivation treatment were carried out using a strip annealer with a nitrogen base pressure of 1 Torr. The luminescence efficiency of the QW remains the same after thermal treatment at $T = 473$ K. Increasing degradation of the PL intensity were observed as the temperature was increased to 573K and 673K. No significant desorption of any species had been observed by TPD in this temperature range in the UHV chamber. The reduction in PL intensity may be linked to indiffusion of oxygen or other surface impurities through the oxide layer, with subsequent degradation of the underlying substrate.

The enhancement of luminescence efficiency and long-term stability of the hydrogen ion treatment indicates that this process is effective in achieving both chemical and electrical passivation of the AlGaAs surface. These results offer hope for the improvement of device performance, particularly for those structures having a high surface-to-volume ratio.

¹Ying-Lan Chang, *et al.*, Appl. Phys. Lett. 62, 2697 (1993).

Ying-Lan Chang, Center for Quantized Electronic Structures (QUEST), University of California, Santa Barbara, CA 93106 TEL: (805) 893-8679, FAX: (805) 893-8170, e-mail: crystal@engrhub.ucsb.edu

The microscopic picture of Si(113): a novel surface reconstruction, the origin of defects, and adsorption sites. Theoretical and experimental study.

J. Dąbrowski[†], H.-J. Müssig, and G. Wolff

INSTITUT FÜR HALBLEITERPHYSIK, BOX 409, D-15204 FRANKFURT(ODER),
GERMANY

[†]EMAIL: jarek@th1.lhp-ffo.de, FAX: +(0335) 326 195

Due to technological importance of heterostructures, one of the most important objectives of the contemporary surface science is to improve the quality of heteroepitaxial layers. Si(113) is a potential new substrate which could solve the problems encountered for Si(001). It can be easily prepared¹ and is very promising for heteroepitaxy². Besides, this orientation is of a general interest: e.g., Ge islands on Si(001) and Si(111) have (113) facets, Si(113) is stable despite its high index, and its atomic reconstruction was unknown until recently.

We bring into focus this lately determined³, peculiar atomic structure of Si(113). Guided by STM measurements and ab-initio calculations we discovered³ a novel structural unit which contains a subsurface interstitial atom. Such interstitials may be present also at other surfaces, particularly at steps, and may play an important role in atomic diffusion in the subsurface layer. The interstitials lower the surface energy through relief of tensile strain. Moreover, they induce a metal \rightarrow semiconductor transition of an interesting kind: they behave like double donors and fill the metallic surface band. The interstitials are *sixfold* coordinated; this unexpected result disturbs the simple picture of reconstruction driven by rebonding of dangling bonds. In addition, we show that energy optimization of the atomic positions is required when STM images are used to determine a new atomic structure.

Next, we discuss the microscopic origin of the fundamental surface defects. STM images of Si(113) reveal high density of antiphase boundaries and point defects. We find that these defects are mainly due to misplaced interstitial atoms. Our calculations show that the interstitials are weakly bonded and should be released during (hetero)epitaxial growth. We therefore predict that the defected character of Si(113) surfaces should not influence the quality of the interface.

Finally, the adsorption of Sb₄ has been studied. We discuss different adsorption sites and the role of subsurface interstitials in the initial stage of the adsorption process. We find that at about 500°C Sb atoms kick out individual Si atoms and are incorporated into the surface. Depending on the antimony coverage, two different types of reconstruction are observed. It is plausible that these structures may influence heteroepitaxial growth in a different way.

¹K. Jacobi, M. Gruyters, P. Geng, T. Bitzer, M. Aggour, S. Rauscher, and H.-J. Lewerenz, to be published.

²J. Knull and J. B. Pethica, Surface Science 265, 156 (1992).

³J. Dąbrowski, H.-J. Müssig, and G. Wolff, Physical Review Letters 73, 1660 (1994).

Band discontinuities at heterojunctions between crystalline and amorphous silicon

Chris G. Van de Walle

Xerox PARC, 3333 Coyote Hill Road, Palo Alto, CA 94304

and

L. H. Yang

Lawrence Livermore National Laboratory, P. O. Box 808, Livermore, CA 94550

Heterojunctions between amorphous silicon (*a*-Si) and crystalline silicon (*c*-Si) can be used to improve the performance of solar cells and of heterojunction bipolar transistors. In addition, they enable the study of the amorphous/crystalline interface, and may provide more information about density of states and other electronic or structural properties of *a*-Si. One of the key properties of the heterojunction, namely the band lineup at the *a*-Si/*c*-Si interface, has been a subject of controversy. For interfaces between *c*-Si and hydrogenated *a*-Si (*a*-Si:H) experimental results range from zero offset in the valence band^{1,2} to zero offset in the conduction band.^{3,4}

We have performed a theoretical investigation of this issue, based on first-principles calculations for the electronic structure of *a*-Si and *c*-Si, and the model-solid theory.⁵ The *a*-Si models were generated based on the Stillinger-Weber potential.⁶ The models were initially thermalized at 300 K for 10 picoseconds and then quenched by *ab initio* pseudopotential methods. Fifteen configurations were generated to average the valence-band maximum. For the *a*-Si:H models, we took the initial configurations of Guttman and Fong⁷ and then quenched them by using *ab initio* pseudopotential methods.

For the interface between unhydrogenated *a*-Si and *c*-Si, assuming equal density for both materials, we obtain a valence-band offset of -0.25 eV (higher in *a*-Si). For *a*-Si:H/*c*-Si (for which experimental information is available), we obtain a valence-band offset of 0.20 eV (higher in *c*-Si), assuming equal density and $\sim 11\%$ H concentration. The theoretical approach reveals the fact that, even without invoking interface-specific effects, the value of the offset is sensitive to the hydrogen concentration in *a*-Si:H. Some uncertainty also arises because of the lack of information about the density of *a*-Si(:H). We will discuss experimental determinations of the band discontinuities in light of these findings.

¹ M. Cuniot and Y. Marfaing, J. Non-Cryst. Solids, **77-78**, 987 (1985); Phil. Mag. B **57**, 291 (1988).

² N. Lequeux and M. Cuniot, J. Non-Cryst. Solids, **114**, 555 (1987).

³ J. M. Essick and J. David Cohen, Appl. Phys. Lett. **55**, 1232 (1989).

⁴ H. Mimura and Y. Hatanaka, Appl. Phys. Lett. **50**, 326 (1987).

⁵ C. G. Van de Walle, Phys. Rev. B **39**, 1871 (1989).

⁶ F.H. Stillinger and T.A. Weber, Phys. Rev. B **31**, 5262 (1985).

⁷ L. Guttman and C. Y. Fong, Phys. Rev. B **26**, 6756 (1982).

Chris G. Van de Walle
Xerox PARC
3333 Coyote Hill Road
Palo Alto, CA 94304

Ph. (415) 812-4163
Fax (415) 812-4140
e-mail: vandewalle@parc.xerox.com

ELECTRON ENERGY LOSS INVESTIGATION OF NON-UNIFORM CARRIER DEPTH PROFILES FROM HOLE-PLASMON EXCITATION OF BORON-DOPED Si(111) SURFACES

J. E. Rowe, R. A. Malic, and E. E. Chaban

AT&T Bell Laboratories

Murray Hill, NJ 07974

ABSTRACT

High resolution electron energy loss spectroscopy (HREELS) measurements have been performed on Si(111) surfaces heavily p-doped by the decomposition of adsorbed decaborane with subsequent diffusion more than $\sim 1000\text{\AA}$ below the surface. After thermal decomposition of the decaborane to produce B atoms on the surface the low energy electron diffraction pattern shows a $\sqrt{3} \times \sqrt{3}$ periodicity due to 1/3 monolayer of boron in the second complete layer. The HREELS data have two strong features: (1) the B-Si dipole vibrational mode at 96 meV and a broad electronic surface plasmon mode at ~ 100 meV loss energy due to the free carriers in the region below the B-reconstructed surface layer. We have investigated the energy dependence of the plasmon mode in order to determine the possibility of using HREELS to determine the depth profile of the free carriers due to B diffusion into the region $\sim 50\text{--}500\text{\AA}$ below the surface. Unexpectedly, we find that kinematic factors play an important role in the energy range used, 1.5-28 eV, and thus limit the degree of quantitative information that can be obtained about the carrier depth profile from HREELS data in this low energy range. A non-uniform depth profile is deduced from the well-established three layer model (vacuum-surface-bulk layers) after correcting the plasmon peak position for the kinematic factors. This depth profile has a spatial resolution of $\sim 50\text{\AA}$ and is in very good agreement with independent *ex situ* measurements using secondary ion mass spectrometry (SIMS) over the depth range of 0-1000 \AA . We attribute the non-uniform doping density to a competition between the entropy associated with bulk in-diffusion and the strong tendency for surface segregation to form the low-energy $\sqrt{3} \times \sqrt{3}$, 1/3 monolayer B-induced reconstruction.

Jack E. Rowe
Member of Technical Staff

Room 3L-401
600 Mountain Ave.
Murray Hill, NJ 07974
908 582-5878
FAX 908 582-3901
EMAIL rowe@physics.att.com

Site specific Si 2p core level spectroscopy of Si(111) 7x7: a fundamental assignment

G. Le Lay¹, M. Göthelid², M. Grehk², M. Björkquist²,
V.Yu. Aristov¹ and U. O. Karlsson²

¹CRMC2 - CNRS, Campus de Luminy, Case 913,
F-13288 Marseille Cedex 09, France.

²Department of Physics, Material Physics, Royal Institute of Technology,
S-10044, Stockholm, Sweden.

The Si(111) 7x7 surface exhibits the dimer-adatom-stacking-fault reconstruction; it consists of 7 rest atoms, 12 adatoms, 36 pedestal atoms, 18 dimer atoms and a corner-hole structure in each 7x7 unit cell which is further split into faulted and unfaulted halves. Until now the Si 2p core level line shapes available from this surface have not permitted to identify the different constitutive entities since only one surface component (so-called S2), appearing as a small bump, shifted to lower binding energy as compared to the bulk component (B), was distinctly observed in the spectra. Even its assignment for either rest atom or adatom emission was controversial. We have recently obtained at MAX-Lab, the Swedish Synchrotron Radiation Facility, extremely well-resolved Si 2p core-level spectra from a very well-ordered Si(111)7x7 surface at 100 K, for several photon energies and different take off angles. New surface shifted components are noticed just by visual inspection of the spectra; contributions from the constitutive entities of the complex 7x7 reconstruction, i.e. rest atoms, adatoms, pedestal atoms and dimer atoms are clearly identified.

We are thus in the situation of providing an exact decomposition scheme which gives a new insight into the spectroscopy and physics of the "prototypical" Si(111)7x7 surface and opens up new perspectives on the use of Si 2p synchrotron radiation high resolution core level spectroscopy, typically, for example, to site-specific adsorption studies.

p^+ doping of Si by Al diffusion upon annealing Al/*n*-Si(111)

H.J. Wen, M. Prietsch, A. Bauer, M.T. Cuberes, I. Manke, and G. Kaindl

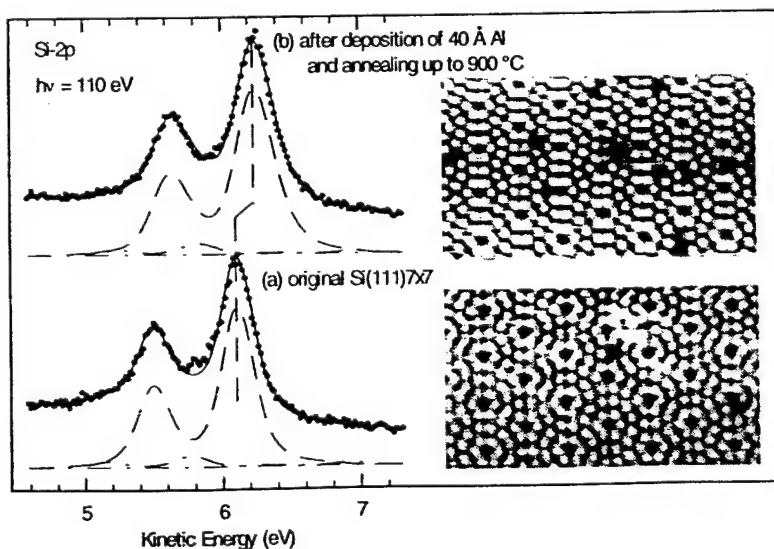
Institut für Experimentalphysik, Freie Universität Berlin, Arnimallee 14, D-14195 Berlin, Germany

Thermal diffusion is one of the key processes used to introduce controlled amounts of dopants into semiconductors. Al as the fastest diffusing dopant in Si is widely used in the semiconductor industry for lightly doped base profiles and heavily doped junction termination systems. Here we demonstrate that a p^+ layer underneath a Si(111)7×7 surface is fabricated by thermal diffusion of Al into Si, using high-resolution photoelectron spectroscopy (PES), scanning-tunneling microscopy (STM), and low-energy electron diffraction (LEED).

Room-temperature deposition of up to 40 Å Al onto *n*-type Si(111)7×7 is characterized by epitaxial growth and a decrease of the Fermi-level position to 0.40 eV above the valence-band maximum (VBM). Annealing around 500 °C leads to the formation of large Al clusters with a flat thin Al-silicide film in between, which exhibits a Fermi-level position at 0.30 eV above VBM.

Further annealing up to 900 °C causes complete Al desorption from the surface, and the original Si(111)7×7 surface structure is recovered, while the bulk-sensitive Si-2p spectrum is shifted to 0.15 eV higher kinetic energies and exhibits a noticeable asymmetrical tail on the high kinetic-energy side of the spectrum (see figure). In addition, a strong potential variation near the surface is observed in Si-2p spectra measured at different probing depths. These effects strongly indicate the formation of an Al-induced p^+ layer upon annealing. By using an appropriate deconvolution of the PES spectra, a doping density of $(4\pm2)\times10^{18}/\text{cm}^3$ in the p^+ region and a

lowering of the surface Fermi-level position by (0.06 ± 0.02) eV are derived. The lowering of the Fermi-level position is mainly due to charge transfer from the Si(111)7×7 surface to the dopant states, while the slight modifications in the structure of the Si(111)7×7 surface observed by STM cannot explain this shift to its full extent.



HOMOEPITAXY AND CONTROLLED OXIDATION OF SILICON AT LOW TEMPERATURES USING LOW-ENERGY ION BEAMS

J. W. Rabalais, A. H. Al-Bayati, S. S. Todorov, K. J. Boyd, and D. Marton

Department of Chemistry, University of Houston

Houston, Texas 77204-5641.

ABSTRACT

Homoepitaxy and controlled oxidation of a silicon surface at low temperatures have been achieved using low-energy, mass-selected, ion beam deposition. The beams were produced by a unique dual-source, UHV, ion beam instrument designed for surface modification and film deposition. For silicon homoepitaxy, $^{28}\text{Si}^+$ ions in the energy range 5 to 30 eV were used to grow films on Si(100) at various temperatures ranging from 50° to 750° C. The films were analyzed by *in situ* reflection high energy electron diffraction (RHEED) and *ex situ* high resolution transmission electron microscopy (TEM), Rutherford backscattering spectrometry (RBS), and atomic force microscopy (AFM). Different RHEED patterns characteristic of 2-D layer-by-layer and 3-D island growth are observed at different temperatures. Cross-sectional TEM images indicate the epitaxial ordering of the films with respect to the substrate. RBS dechanneling results show that the quality of the films is as high as that of the substrate. AFM results for films 20 nm thick show that the surfaces of films deposited at 200° C and below are smooth and featureless. In the range 350°-550° C, the surfaces are characterized by islands of typical height and diameter in the range of 2.5-20 and 100-200 nm, respectively. At 750° C, high density features with smooth surfaces are observed, suggesting ion-enhanced surface annealing and diffusion processes. For silicon oxidation, films of SiO_2 on Si(100) at room temperature were grown by using alternating 25 eV beams of $^{28}\text{Si}^+$ and $^{16}\text{O}^+$. Fast switching of the magnetic sectors allows deposition of these ions in alternating increments. These dose increments were $1 \times 10^{16} \text{ cm}^{-2}$ for Si^+ and $4 \times 10^{16} \text{ cm}^{-2}$ for O^+ . Analysis of the oxide films by *in situ* Auger electron spectroscopy (AES) and *ex situ* x-ray photoelectron spectroscopy (XPS) shows that the films are SiO_2 , that there is no evidence for suboxides of silicon, and that there is no limitation to the thickness of the oxide films that can be grown.

The effects of ion energy and substrate temperature, contamination, and surface damage on the growth mechanism will be discussed. The use of low-energy ion beams for film growth will be compared to molecular beam epitaxy (MBE), which uses thermal energy species, and ion implantation, which uses high energy species. This new pulsed, dual-ion beam deposition technique has the potential of (1) growing unique, previously unknown materials and (2) growing conventional materials under different conditions by judicious manipulation of the ion energy, type, and arrival rate and substrate temperature. The results will enhance our understanding of the fundamental physical and chemical processes involved in low-energy ion-surface interactions. This knowledge will be transferable to those technological processes and procedures involving low-energy ions that are currently used in film deposition and surface modification in fields such as ion beam deposition, plasma and sputter deposition, ion beam assisted and plasma assisted chemical vapor deposition, reactive ion cleaning/etching, etc.

Phone (713) 743-3282 FAX (713) 743-2709

Calculation of the Average Interface Field in Inversion Layers Using Zero-Temperature Green's Function Formalism*

Dragica Vasileska-Kafedziska, Paolo Bordone,[#] Terry Eldridge,[@] and David K. Ferry
*Center for Solid State Electronics Research, Arizona State University
 Tempe, Az, 85287-6206, USA*

Using the variational wave-function, Fang and Howard¹ calculated that the average field seen by the electrons in the silicon inversion layer is proportional to $E_{av} \propto \left(\frac{11}{32}N_s + N_{depl}\right)$. Later, Matsumoto and Uemura² calculated that in the electronic quantum limit $E_{av} \propto \left(\frac{1}{2}N_s + N_{depl}\right)$. This result is extensively used in the literature by many authors. However, recent experimental data suggests that E_{av} does not follow these predicted dependencies. We investigate the dependence of E_{av} on the inversion and depletion charge density by using a zero-temperature Green's function formalism for the evaluation of the broadening of the electronic states. Various models for surface-roughness that exist in the literature are studied in our calculations, including both Gaussian and exponential models for the surface-roughness autocovariance function. Beside surface-roughness scattering, which is the dominant scattering mechanism at high electron densities, we also include charged impurity scattering, interface-trap and oxide charge scattering. The position of the subband minima as well as the electron wave-functions are obtained by the self-consistent solution of the Schrödinger, Poisson and Dyson equations for each value of the inversion charge density. Many-body effects are included by considering the screened matrix elements for the various scattering mechanisms included in the simulation instead of the bare ones and through the inclusion of the exchange-correlation term that gives rise to additional potential-energy term in the Schrödinger equation and contributes towards bigger separation of the electronic subbands. Screening is treated within the mean-field approximation (known as RPA) which includes only the long-range Coulomb interaction in the dielectric response and leaves out all exchange-correlation corrections. We find that the dependence of the mobility and the effective field upon the inversion charge density is sensitive to the model chosen, and discuss the manner in which this may be used to study the interface itself.

* Work supported in part by the ONR.

[#] On leave from: Dipartimento di Fisica ed Istituto Nazionale di Fisica della Materia, Università di Modena, Via Campi 213/A, 41100 Modena, Italy.

[@] McDonnell Douglas Helicopter Systems, 5000 E. McDowell Rd, Mesa, Az, 85215, USA.

¹ F. F. Fang, and W. E. Howard, *Phys. Rev. Lett.* **16**, 797 (1966).

² Y. Matsumoto, and Y. Uemura, *Jpn. J. Appl. Phys. Suppl.* **2**, 367 (1974).

HYDROGEN DIFFUSION AND REACTIONS ON THE Si(100) SURFACE*

A. Selloni

Department of Chemistry, University of Geneva, Switzerland.

The adsorption, diffusion, and desorption of hydrogen from silicon surfaces play an important role in many key technological processes, such as chemical vapor deposition of silicon from silanes, and reactive ion-etching processes. In this talk I shall review some recent theoretical studies of hydrogen diffusion and reactions on Si(110), based on density functional theory and carried out using the Car-Parinello approach in a supercell geometry. The potential energy surface for the diffusion of a single hydrogen atom on Si(100)- 2×1 has been determined, and from this, stable adsorption sites, migration paths, and energy barriers have been obtained. Our results indicate that H diffusion is anisotropic, with the H atoms moving essentially along a dimer row. From the study of H₂ adsorption on and desorption from the monohydride 2×1 and dihydride 1×1 phases of Si(100), likely adsorption/desorption pathways have been identified. For the monohydride surface, we find that a previously proposed mechanism involving the concerted desorption of H₂ from doubly occupied surface dimers yields a barrier in good agreement with experiments. A barrier within the experimental range is found also for a new interdimer pathway corresponding to recombination of two H atoms sitting on adjacent dimers along a row. For the dihydride surface, the preferred pathway involves the desorption of two H atoms belonging to the same SiH₂ unit. Substrate relaxation is found to be very important for the energetics of all these processes.

*Work done in collaboration with A. Vittadini.

Hydrogen desorption from Si: How does this relate to film growth?

C. Michael Greenlief, Department of Chemistry, University of Missouri-Columbia, Columbia, MO 65211.

The desorption of hydrogen from the Si(100) surface is investigated. The hydrogen coverage is generated during silicon epitaxy using silane in a rapid thermal chemical vapor deposition reactor. Temperature programmed desorption studies are then used to help yield information about the hydrogen surface coverage during epitaxy and the desorption kinetics of hydrogen. The desorption of hydrogen was found to be first order, consistent with previously reported single crystal studies. However, the activation energy for desorption is considerably different. The activation energy for hydrogen desorption from these epitaxially grown layers is 49 ± 3 kcal/mol. The presence of monatomic steps on the surface, that are created during the temperature quench, is believed to play a role in this difference of reported activation energies. Single crystal, ultra-high vacuum based studies of silane and disilane adsorption and desorption exhibit similar discrepancies with hydrogen desorption energies.

This talk will focus on the role of hydrogen during silicon chemical vapor deposition. Comparison of studies completed in a cold-wall reactor with ultra-high vacuum based studies will be made in an effort to help clarify several previously published studies examining the desorption of hydrogen from silicon.

C. Michael Greenlief
University of Missouri-Columbia
123 Chemistry Bldg.
Columbia, MO 65211

Phone: 314-882-3288
FAX: 314-882-2754
E-mail: chemcmg@mizzou1.missouri.edu

Cross-sectional Scanning Tunneling Microscopy of AlGaAs/GaAs Heterojunctions: Interfacial Roughness and Alloying Effects

A. R. Smith¹, K.-J. Chao¹, C. K. Shih¹, Y.C. Shih,² A. Srinivasan,² and B. G. Streetman²

¹Department of Physics and ²Department of Electrical and Computer Engineering
The University of Texas at Austin, Austin, Texas 78712

Cross-sectional scanning tunneling microscopy was used to study the AlGaAs/GaAs heterojunction systems. Our studies focus on two subjects: (1) The influence of the growth interrupt on the abruptness of interface, and (2) The bonding configurations of substitutional isovalent impurities and their atomic motions within the alloy regions. In addressing the first subject, we have studied short period superlattice of AlAs/GaAs. Superlattices with two different periodicities, 4/2 (4 lattice constants of GaAs and 2 lattice constants of AlAs) and 2/1, were grown with two different durations of growth interrupt time, 30 sec and 5 sec. The 4/2 superlattices grown using the 30 second growth interrupt time are observed atom by atom, while those grown with the 5 second growth interrupt time are not. However, we have not observed the 2/1 superlattices regardless of the growth interrupts. In addition, in the 4/2 superlattices, intermixing of AlAs and GaAs within one lattice constant is also evident.

In addressing the second subject, we have studied $\text{Al}_x\text{Ga}_{1-x}\text{As}$ alloys with x varying from 0.05 to 0.5. For the dilute alloy ($x = 0.05$), we have identified the bonding configuration of Al for the surface and subsurface layers. High resolution STM images suggest that in dilute alloys, Al-atoms are mostly located at isolated substitutional sites. Namely, we have observed very little clustering effect. We have also discovered that Al-atoms on the surface layer move under the influence of STM operation while subsurface Al-atoms do not. Although most likely a tip-induced effect, the motion of surface Al-atoms presents an intriguing phenomenon: these atomic motions occur in a region of perfect lattice and in the absence of vacancies, implying a direct atomic exchange mechanism. For alloys with larger Al-concentration ($x > 0.2$), composition fluctuations are also observed (as reported by Johnson et al.). However, we found that a clear identification of the local bonding is highly non-trivial due to the large number of possible configurations. More work is underway to clarify this issue.

This work was supported by NSF Grant No. DMR-94-02938.

Dr. Chih-Kang Shih
Department of Physics, The University of Texas at Austin
26th & Speedway RLM Hall/5.208
Austin, TX 78712
Phone: (512) 471-6603 Fax: (512) 471-1005

Lourdes Salamanca-Riba
Materials and Nuclear Engineering Department
University of Maryland
College Park, MD 20742-2115
phone (301) 405-5220
FAX (301)314-9467
e-mail: riba@eng.umd.edu

Misfit Dislocations in ZnSe-based Films Grown on (001) GaAs Substrates.-- L. Salamanca-Riba, and L.H. Kuo, University of Maryland, College Park, MD.

We have observed the formation of misfit dislocations by the dissociation and interaction of partial dislocations bounding stacking faults in-situ using transmission electron microscopy. Frank partial dislocations dissociate to form a 60° mixed dislocation and a Shockley partial dislocation. The Shockley partial glides on the (111) plane of the stacking fault and interacts with the other Frank partial of the fault. This interaction gives rise to another 60° mixed dislocation. The two 60° mixed dislocations glide on different (111) planes until they reach the interface. At this point, they become misfit dislocations. This mechanism produces a regular array of interfacial misfit dislocations along the [110] and $\bar{[110]}$ directions. The Frank partial dislocations bound stacking faults that usually occur in pairs at the film substrate interface forming a bow tie-shape defect. The density of these faults depends on the doping concentration and the stoichiometry of the substrate surface. Shockley partial dislocations are also observed in films grown by the island growth mode. These dislocations also bound stacking faults and under certain conditions dissociate to produce interfacial dislocations of the screw type. The mechanisms for the generation of the dislocations will be discussed.

Na/Carbon-Rich β -SiC(100) Surface: Initial Interface Formation and Metallization

F. Semond,¹ P.S. Mangat,² V. Yu. Aristov² and P. Soukiassian^{1,2}

[1] Commissariat à l'Energie Atomique, DSM-DRECAM-SRSIM, Bâtiment 462,
Centre d'Etudes de Saclay, 91191 Gif sur Yvette Cedex, France

and

Département de Physique, Université de Paris-Sud, 91405 Orsay Cedex, France

[2] Department of Physics, Northern Illinois University, DeKalb, Illinois 60115-2854


Silicon carbide is an interesting "refractory" IV-IV compound semiconductor which could potentially provide high temperature ($\approx 600^\circ\text{C}$) and high power devices. Surface metallization and passivation are among the main issues to address. However, silicon carbide have received much less attention than silicon and other compound semiconductors. Recently, we have shown that alkali metal (Rb) could promote $\text{SiO}_2/\beta\text{-SiC}(100)$ interface formation (by 4 orders of magnitude) with removal of the catalyst by thermal desorption at moderate temperatures [1]. In this work, we investigate the initial steps of interface formation for the Na/carbon-rich cubic $\beta\text{-SiC}(100)$ surface by core level and valence band photoemission spectroscopy using synchrotron radiation. The deposition of a Na monolayer results in surface metallization as evident from the presence of plasmon loss features at Si 2p and Na 2p core levels, and from Fermi level building-up in the valence band. Furthermore, large chemical shifts at both C 1s and Si 2p core level indicate reactive interface formation and surface disruption with the Na atom bridge-bonded between C and Si atoms. This situation apparently differs somewhat from the behavior of stoichiometric $\beta\text{-SiC}(100)$ surfaces. Exposition to small amount of oxygen results in the removal of surface metallization. with oxygen atoms bonding to both C and Si atoms forming a carbonate-like oxide product.

[1] M. Richl-Chudoba, P. Soukiassian and C. Jaussaud, J. of Appl. Phys. 76, 1332 (1994).

Work supported by the U.S. National Science Foundation

Corresponding Author:

Patrick Soukiassian
Commissariat à l'Energie Atomique
DSM-DRECAM-SRSIM, Bât. 462
Centre d'Etudes de Saclay
91191 Gif sur Yvette Cedex, France

 (33) 1 69 08 31 62
Fax: (33) 1 69 08 84 46

High-Brightness Light-Emitting Diodes Grown by MBE on ZnSe Substrates

D.B. Eason, Z. Yu, W.C. Hughes, C. Boney, J.W. Cook, Jr., and J.F. Schetzina
Department of Physics, North Carolina State University, Raleigh, NC 27695-8202
PH: (919) 515-3314; FAX: (919) 515-7667; E-MAIL: JAN_SCHETZINA@NCSU.EDU

Gene Cantwell and William C. Harsch
Eagle-Picher Laboratory, Miami, OK 74354
PH: (918) 542-1801; FAX: (918) 542-3223

High-brightness blue and green light-emitting diodes (LEDs) operating at peak wavelengths in the range 489 -514 nm have been successfully synthesized, processed, and tested. The high-brightness LEDs are II-VI heterostructures grown by molecular beam epitaxy (MBE) at NCSU using (100) ZnSe substrates produced at Eagle-Picher Laboratory by the Seeded Physical Vapor Transport (SPVTTM) process. The double-heterostructure (DH) LED devices consist of a ~1.8 μm thick layer of n-type ZnSe:Cl, a ~0.1 μm thick active region consisting either of a ZnCdSe MQW (blue) or a ZnTeSe layer (green), and a ~1.8 μm thick p-type ZnSe:N layer deposited using a nitrogen plasma source. Thin (~100 Å) epitaxial surface layers of HgSe/ZnTeSe were deposited by MBE to obtain excellent ohmic contact to the top p-type ZnSe layer. Standard photolithographic techniques were used to fabricate 250 μm x 250 μm mesa diode structures. Gold was used as a metal contact to the top HgSe layer of each device; indium was used to contact the n-type ZnSe layer. Direct contact to the n-type ZnSe epilayer was necessitated because of the insulating nature of current ZnSe substrates. The devices were packaged in a standard T-13/4 clear-epoxy lamp configuration for testing. The blue LEDs produce 327 μW @ 10 mA with external quantum efficiency of 1.3%. If one compares the ZnCdSe LED with the Nichia Chemical InGa_N blue LED characteristics one finds that the Nichia device is about three times brighter but displays a much broader spectral output. In contrast, the ZnCdSe DH blue LED output is sharply peaked at 489 nm with a spectral purity of 96%. In terms of photometric units, the luminous performance of the ZnCdSe LED is 1.6 lumens/watt at 10 mA. The brightest ZnTeSe green LEDs tested to date produce 1.3 mW at 10 mA peaked at 512 nm with an external quantum efficiency of 5.3%. These are the brightest pure green LEDs ever produced in the history of semiconductors. The luminous performance of the green LED is 17 lumens/watt at 10 mA. This exceeds the luminous performance of super-bright red LEDs (650 nm) based on AlGaAs DHs and greenish-yellow (570 nm) AlGaInP DH devices; it also exceeds the luminous performance of the super-bright Nichia blue LEDs based on GaN/InGa_N DHs (3.6 lumens/watt). The green LEDs which we are reporting are more than fifty times brighter than commercial GaP LEDs which produce outputs peaked in the yellow-green at 555 nm. At NCSU, our best green LEDs presently have useful lifetimes (40% degraded) of more than 750 hr when operated at 15 A/cm². Several LEDs have been operational for more than 4000 hrs. The degradation process involves the generation of dark line defects. For a given initial dislocation density, the degradation process appears to depend on the total charge/unit area flowing through the device. Detailed studies of degraded devices, based on optical microscopy and TEM/SEM experiments, will be reported.

This work was supported by Eagle-Picher internal funds and by NIST ATP contract 70NANB3H1374. At NCSU, additional support was provided by ONR grant N00014-92-J-1644 and ARPA grants N00014-92-J-1893 and DAAL03-91-G-0131.

Deep Level Formation at ZnSe/GaAs(100) Interfaces

A. D. Raisanen and L. J. Brillson

Xerox Wilson Center for Research & Technology, Webster, NY 14580

A. Franciosi, L. Vanzetti, and L. Sorba

Laboratorio TASC-INFM, Trieste, Italy and Dept. of Chem. Eng. & Mater. Sci., Univ. Minnesota, Minneapolis, MN 55455

We have used low energy cathodo- and photoluminescence spectroscopies (CLS and PLS, respectively) to characterize the formation of charge states deep within the ZnSe band gap and localized near the ZnSe/GaAs interface. These deep levels are a common feature of the ZnSe/GaAs heterostructure and depend sensitively on growth conditions¹ and post-growth annealing. The formation of charge states near the heterointerface and their changes with growth conditions are consistent with the variation of interface dipole and heterojunction band offset observed via photoemission spectroscopy.² Here we report in-situ measurements of deep level formation near the ZnSe/GaAs interface during post - growth annealing and their dramatic dependence on the initial epitaxial growth conditions.

CLS and PLS changes in emission intensity with excitation depth provide a means to identify deep levels associated with the heterointerface. We used 1-2 keV electron beam energies in tandem with HeCd and HeNe excitation to obtain emission spectra characteristic of the free ZnSe surface, the ZnSe bulk, and the ZnSe/ GaAs(100) interface. Epitaxial ZnSe films ranging in thickness from 5 to 500 nm, nominally undoped ($n \sim 1-2 \times 10^{15} \text{cm}^{-3}$) were grown by solid source molecular beam epitaxy at 290°C on GaAs(100)(2x4) epilayers on GaAs(001) wafers and capped with a protective Se layer. After decapping in UHV, the ZnSe epilayers exhibit CLS emission peaks at 0.8, 0.9, 1.0, 1.14, and 1.3 eV, related to native defects and defect complexes,¹ whose relative intensities depend systematically on Zn- versus Se-rich growth conditions.

Annealing in UHV in the 400 to 500°C range produces dramatic changes in the emission spectra of these heterojunction structures. We obtained 90 K spectra before and after each 5 minute thermal anneal for each of three ZnSe growth conditions: Zn to Se beam pressure ratio (BPR) = 0.1, 1, and 10. Specimens grown with similar BPR were found earlier² to control interface composition, with high (low) valence band offsets associated with Zn (Se)-rich configurations. For all three growth conditions, HeCd PLS of ZnSe/GaAs(100) heterostructures reveals a new emission feature at ~ 1.9 eV, previously identified as a "self-activated" (SA) emission associated with V_{Zn} or $V_{\text{Zn}}/\text{Ga}_{\text{Zn}}$ defects³. Combined CLS and PLS spectra show the deep centers associated with this feature to be localized primarily at the ZnSe interface. The corresponding emission grows with increasing temperature, exhibiting a threshold at 400°C independent of BPR, and eventually dominating all lower energy features. However, its intensity relative to both low energy and near band edge emission (NBE) depends dramatically on BPR, increasing nearly two orders of magnitude with increasing Se overpressure for 450°C anneals. Thus annealing causes pronounced defect formation which is enhanced (suppressed) by Se (Zn) -rich growth, consistent with a dependence primarily on Zn vacancies and/or Ga indiffusion. These results emphasize the importance of local composition in the formation of interface deep level defects and their subsequent effects on luminescence efficiency and heterojunction stability. In addition, they illustrate potential tradeoffs between growth methods to control heterojunction band offsets and actual device performance.

1. A. D. Raisanen et al., J. Electron. Mater., submitted.

2. R. Nicolini et al., Phys. Rev. Lett. 72, 294 (1994).

3. J. Gutowski, N. Presser, and G. Kudlek, Phys. Stat. Sol. (a) 120, 11 (1990).

Study of Reconstruction at Interfaces of CdSe/ZnTe Superlattices by Total Energy Calculation*

S.-F. REN, Illinois State University,

Z.-Q. GU, Institute of Semiconductors, Chinese Academy of Science
and Y.-C. CHANG, University of Illinois at Urbana-Champaign

CdSe/ZnTe superlattices have been grown successfully in recent years. One important feature of such superlattices is that it is lattice matched. The lattice constants of CdSe and ZnTe are 6.077 Å and 6.099 Å respectively, so the mismatch is less than 0.3 %. Because of the closely matched lattice constants, one expects negligible strain at interfaces, thus allowing high quality superlattices with ideal and sharp interfaces to be grown. However, close examination of high resolution Transmission Electronic Microscopic (TEM) spectra showed the existence of two to three layers of reconstruction at interfaces in such superlattices[1]. Extended x-ray absorption fine structure (EXAFS) studies of such interfaces indicate the existence of interchange of atoms across the interfaces in spite of the large resulting strain[2]. By using a first-principles pseudopotential method we have calculated the total energy of CdSe/ZnTe interfaces with different configurations. Our calculations confirm the existence of exchange of atomic layers across interfaces observed by above experiments, and the calculated band offsets are consistent with experimental data when the interfacial exchange is taken into account.

* Work supported by ONR N00014-90-J-1267.

1. H. Luo, N. Samarth, F. C. Zhang, A. Pareek, M. Dobrowolska, J. K. Furdyna, K. Mahalingam, N. Otsuka, W. C. Chou, A. Petrou, and S. B. Qadri, Appl. Phys. Lett. 58 (16), 1783 (1991).

2. K. M. Kemner, B. A. Bunker, H. Luo, N. Samarth, J. K. Furdyna, M. R. Weidmann, and K. E. Newman. Phys. Rev. B 46 (11), 7272 (1992).

Corresponding author: Shang-Fen Ren, 4560 Physics, Illinois State Univ. Normal, IL 61790-4560. Phone: (309) 438-8756, Fax; (309) 438- 5413. Email: ren@phy.ilstu.edu

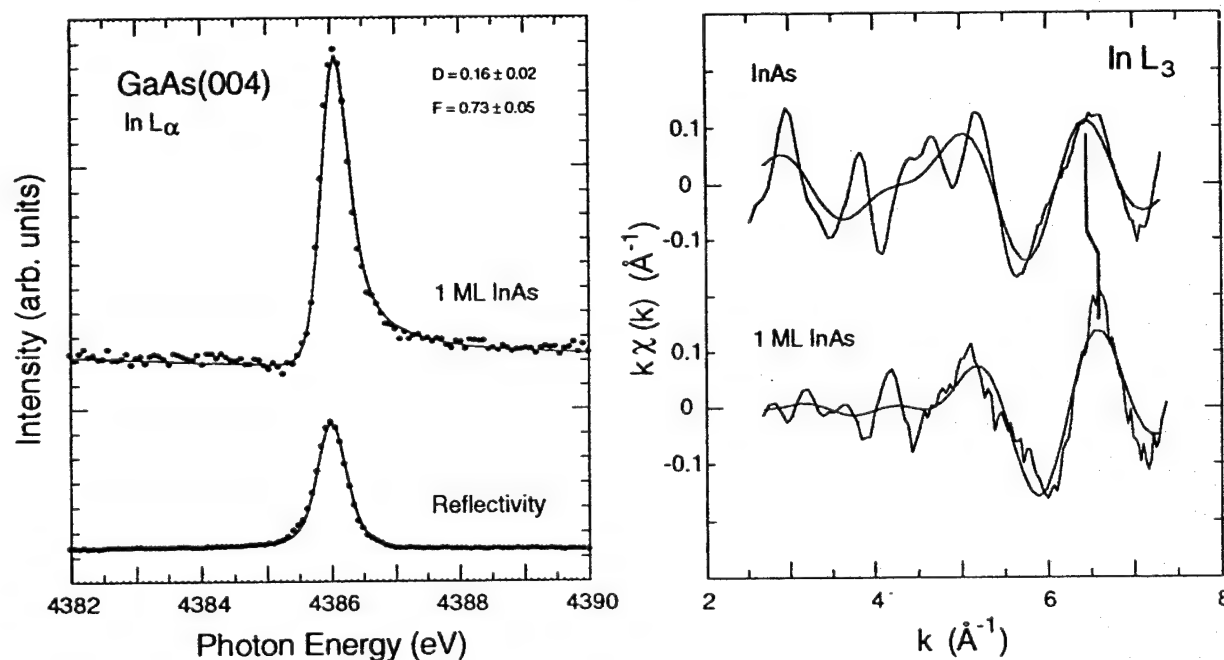
Accommodation of strain in ultra-thin InAs/GaAs films

J.C. Woicik, J.G. Pellegrino, S.H. Southworth, P.S. Shaw, and B.A. Karlin

National Institute of Standards and Technology, Gaithersburg, MD 20899

K.E. Miyano, Department of Physics, Brooklyn College, Brooklyn, NY 11210

The geometric consequences of strain in a buried ultra-thin (1 monolayer) InAs film grown on GaAs(001) by molecular beam epitaxy have been studied with the x-ray standing wave and extended x-ray absorption fine structure techniques. The perpendicular distance of the In layer from the first GaAs plane is found to be 0.16 ± 0.02 d_{004} GaAs lattice units. As the natural lattice constant of InAs is 7 % larger than GaAs, this corresponds to a 9 % expansion of the In position along the [001] direction due to the compression in the (001) plane imposed by the substrate. Surprisingly, this expansion agrees nearly exactly with the prediction of macroscopic elastic theory, but falls short of the prediction of a simple bond angle distortion. This deviation is directly observed as a small, but measurable, compression of 0.04 ± 0.02 Å in the In-As near neighbor bond length. A microscopic model is presented which accounts for these as well as distortions in other epitaxial semiconductor systems.



Joseph C. Woicik
Bldg. 510E, NIST PRT
Brookhaven National Laboratory
Upton, NY 11973

First principles studies of MBE growth, band offsets at heterojunctions,
and surface oxidations using Gaussian dual-space density functional theory

X. J. Chen, J. Hu, B. Tsai, A. Mintz and W. A. Goddard III

Materials and Molecular Simulation Center, Beckman Institute (139-74),
Caltech, Pasadena, CA 91125

We have recently developed the dual space approach for first principles density functional calculations using Gaussian basis functions (GDS-DFT). This method treats two- and three- dimensional periodic systems and is suitable for describing localized states and chemical processes involving any element of the periodic table (with or without pseudopotentials). Transferable separable pseudopotentials are constructed including scalar relativistic effects. The dual space approach augmented with an accurate numerical grid makes Fock matrix calculations scale linearly with the size of the basis set, making possible studies of large systems.

We illustrate the accuracy and general applicability of the method by applying it to the properties of surfaces and heterojunctions, including

1. **MBE and MOMBE growth of HgCdTe:** we report the surface reconstructions of CdTe and HgTe (100) and (211) surfaces. These results are used to discuss the mechanism of MBE growth of HgCdTe. We also report studies on candidate metalorganic compounds for MOMBE growth.
2. **MBE growth of GaN/AlGaIn:** we report the surface reconstruction of cubic GaN and AlN and discuss the MBE growth mechanism (given a source of N atoms).
3. **Oxidation of H-terminated Si surface:** we report the reconstruction of (2×1-H) and (1×1-2H) Si (100) surfaces and compare the mechanism of oxidation of clean Si (100) surface with that of H-terminated surfaces.
4. **Band offsets, superlattice band structures, quantum wells:** we report the band properties of HgTe/HgCdTe, GaN/GaInN, and GaAs/GaAlAs heterojunctions and superlattices.

Author to whom correspondences should be addressed:

Dr. Xiaojie Chen

Materials and Molecular Simulation Center, Beckman Institute (139-74),
Caltech, Pasadena, CA 91125

Phone: (818)-395-2729; Fax: (818)-585-0918; Email: xec@wag.caltech.edu

Explanation of the origin of electrons in the unintentionally doped InAs/AlSb system

Jun Shen and Herb Goronkin

Motorola Inc., Phoenix Corporate Research Laboratories

2100 E. Elliot Rd., Tempe, AZ 85284, U.S.A. (602)-413-5949, email: shen@pcrl.sps.mot.com

The InAs/AlSb heterojunction system is attractive for future-generation ultra-fast electronic device applications because of its high mobility and large conduction-band offset. The unique band alignment (type-II staggered) and the interface atomic arrangements (AlAs or InSb) in the system lead to some interesting doping properties, viz., large electron populations in the unintentionally doped samples. Here we provide explanation of the origin of these electrons in InAs/AlSb heterojunction systems.

Experimentally, the large electron population ($\sim 10^{12} \text{ cm}^{-2}$) is consistently observed in unintentionally doped samples with an InAs quantum well of width $\sim 100 \text{ \AA}$ sandwiched by AlSb barriers [1]. The electron population has been traced to three sources: (i) the sample's free surface, (ii) bulk AlSb, and (iii) the hetero-interfaces between InAs and AlSb. The surface contribution decreases with the distance of the InAs quantum well from the surface and becomes negligible for a well a few hundred Angstroms below the surface. The bulk and interface contributions have been attributed to various origins (bulk and interface donors, Tamm states, etc.) and have not been conclusively determined. Our calculations focused on the deep levels produced by various native defects and revealed the relationships between these deep levels and the electron concentrations.

A native anion-site anti-site defect, Al_{Sb} , is shown to be responsible for the bulk AlSb contribution to the InAs electron concentrations. This defect produces a deep level about 0.45 eV above the valence-band edge of bulk AlSb and is responsible for its semi-insulating behavior. When an InAs quantum well is grown in between AlSb barriers, the quantum well ground state can be below the Al_{Sb} level. The electrons in the neutral Al_{Sb} deep level become unstable and fall into the InAs quantum well, doping the well n-type. We call this type of impurity a "remote false-valence donor" because it would have been classified as an acceptor according to effective mass theory. Our calculations also predict that the counterpart Ga_{Sb} anti-site level is in the valence band of GaSb, consistent with the fact that unintentionally doped bulk GaSb is p-type.

Our results also support the existence of Tamm states induced by the interfacial In-Sb bonds between InAs and AlSb at the InAs/AlSb interface [2]. The calculated energies of the Tamm states, however, are too low to account for the observed carrier concentrations in the InAs quantum wells. We then analyzed several other possible candidates and concluded that the As_{Al} native defect at an AlAs-like interface is responsible for the high values of electron concentration in the wells. The decrease of electron concentration with temperature can be attributed to partial freezing of electrons into the shallow levels associated with ionized donors.

Acknowledgment: This work was partially performed under the management of FED (the R&D Association for Future Electron Devices) as a part of the R&D of Basic Technology for Future Industries supported by NEDO (New Energy and Industrial Technology Development Organization, Japan).

- [1] G. Tuttle, H. Kroemer, and J. H. English, J. Appl. Phys. **67**, 3032 (1990).
- [2] H. Kroemer, and Q.-G. Zhu, J. Vac. Sci. Technol. **19**, 143 (1982); Q.-G. Zhu and H. Kroemer, Phys. Rev. B **27**, 3519 (1983).

Study of Abruptness and Band Alignments at InAs-GaSb Interfaces.

M.W. Wang^a, D.A. Collins^a, R.W. Grant^b, R.M. Feenstra^c, and T.C. McGill^a

^a T. J. Watson, Sr., Laboratory of Applied Physics California Institute of Technology, Pasadena, CA 91125, USA

^b Rockwell International Science Center, Thousand Oaks, CA 91360, USA

^c IBM Research Division, T.J. Watson Research Center, Yorktown Heights, NY 10598

We present the results of X-ray photoelectron spectroscopy (XPS), reflection high energy electron diffraction (RHEED), secondary ion mass spectroscopy (SIMS) and cross sectional scanning tunneling microscopy (STM) studies of the abruptness of InAs-GaSb interfaces. We find that the interface abruptness depends on growth order, with GaSb-grown-on-InAs (GaSb/InAs) being abrupt, while InAs-grown-on-GaSb (InAs/GaSb) is extended. We also present XPS measurements of the dependence of the InAs/GaSb valence band offset on both interface composition and growth order.

XPS studies have been performed on several InAs-GaSb structures grown by molecular beam epitaxy (MBE) in both the InAs/GaSb and GaSb/InAs geometries under a variety of growth conditions and interface shuttering schemes. We find that the GaSb/InAs structures are consistent with abrupt interfaces while the InAs/GaSb structures have extended anion sublattices. The XPS data also suggests that both Sb incorporation into the InAs overlayer and As exchange for Sb in the GaSb underlayer can occur.

Time resolved RHEED studies of InAs/GaSb interface formation further indicate Sb incorporation into the InAs overlayer and As exchange for Sb in the GaSb underlayer. Data is presented for a number different structures which indicates that the amount and type of anion intermixing can be modified by the growth conditions and interface formation scheme.

Sb incorporation in InAs epilayers grown on GaSb is seen directly in both SIMS data and by cross-sectional STM. Both techniques further show that the amount of Sb incorporation in the InAs overlayer is a strong function of growth temperature.

Changes in the InAs/GaSb valence band offset were determined by monitoring the core level binding energy separations across the junction. Since core level to valence band edge separations are constant, changes in the cross-junction core level binding energy separations reflect changes in the InAs/GaSb valence band offset. Results from this analysis showed no dependence of the valence band offset on interface composition; however, a 90 meV increase in the valence band offset was observed for InAs grown on GaSb compared to GaSb grown on InAs. This difference is attributed to the more extended nature of the InAs/GaSb interface compared to the GaSb/InAs interface as described above.

Ballistic Electron Emission Microscopy of strained and relaxed $\text{In}_{0.35}\text{Ga}_{0.65}\text{As}/\text{AlAs}$ interfaces

Mao-long Ke, D. I. Westwood, S. Wilks, S. Heghoyan, A. Kestle, C. C. Matthai, B. E. Richardson, R. H. Williams

Department of Physics and Astronomy, UWCC, Cardiff, CF2, 3YB, UK

Although the effects of strain and misfit dislocations upon band alignment at semiconductor heterojunctions are of crucial importance both in basic physics and in device applications, they are very poorly understood at the present stage. Ballistic Electron Emission Microscopy (BEEM) is a technique that affords a way of investigating barriers to electrical conduction at interfaces. Because of possible nanometer lateral resolution, the variation of the band offsets near dislocation cores may be investigated.

The band discontinuities of $\text{In}_{0.35}\text{Ga}_{0.65}\text{As}/\text{AlAs}$ heterojunctions grown by molecular beam epitaxy (MBE) have been studied with BEEM. The thickness of the $\text{In}_{0.35}\text{Ga}_{0.65}\text{As}$ overlayer has been varied from 70Å to 200Å in order to cover a range from pseudomorphic, to partially relaxed and to completely dislocated interfaces. The BEEM current threshold has been found to vary between the pseudomorphic and completely relaxed cases, suggesting that the band alignment has been altered due to the presence of misfit dislocations. The lateral variations of the conduction band discontinuity have been successfully probed with BEEM in view of establishing the influence of misfit dislocations on the local barrier height. A drastical decrease of collector current has been observed in the case of completely relaxed system, which is an indication of increased hot carrier scattering due to the misfit dislocation. Monte-Carlo simulation has been used to quantify the extent of hot carrier scattering at each case. Also, in strained pseudomorphic layers increasing doping might be expected to result in a reduction of measured effective barrier, however in relaxed overlayers Fermi level pinning would suggest little or no variations on the effective barrier with doping. We have therefore done extensive measurement of band offsets for different doping density and those results are presented.

Strain dependence of the valence-band offset in arsenide compound heterojunctions determined by photoelectron spectroscopy

C. Ohler, J. Moers, A. Förster, and H. Lüth

*Institut für Schicht- und Ionentechnik, Forschungszentrum Jülich GmbH,
D-52425 Jülich, Germany*

We have used ultraviolet and x-ray photoelectron spectroscopy to study the strain dependence of the valence-band offset (VBO) *in situ* for binary arsenide compound semiconductor heterojunctions grown by molecular beam epitaxy; i. e., we have measured the VBO of InAs/GaAs, InAs/AlAs and AlAs/GaAs(100) heterojunctions as it changes when these heterojunctions are pseudomorphically strained to lattice constants ranging from 5.653 Å (GaAs) to 6.058 Å (InAs). Intermediate lattice constants have been realized by using fully relaxed $\text{In}_x\text{Ga}_{1-x}\text{As}$ buffer layers as virtual substrates.

The spectrum of two distinct core-levels, one from either side of the coherently strained junction, monitors the energetic alignment across the junction. To establish the band offset, one has to know in addition the binding-energy separation of the core-level to the respective valence-band maximum (VBM) for each of the junction's two components and corresponding to their correct bulk strain state. Here, we have recorded valence-band and core-level spectra of strained 'bulk' samples to determine this energy difference experimentally. The key issue is then the precise determination of the VBM. We have accounted for the true shape of the density of states near the VBM by using results of k-p theory, thus avoiding a full pseudopotential calculation.

InAs/GaAs and InAs/AlAs heterojunction VBOs are heavily strain dependent. E. g., one can alter the InAs/GaAs VBO by 530 meV on going from the GaAs to the InAs lattice constant, the InAs VBM being 0.04 ± 0.10 eV *lower* than the GaAs VBM when InAs is strained to the GaAs lattice constant and 0.57 ± 0.10 eV *lower* when the strain is vice versa. The AlAs/GaAs heterojunction VBO is independent of strain within our limits of accuracy.

The results will be compared with recent theoretical data, both model theories and *ab initio* calculations, shedding some light on the features that are important for the band alignment at polar heterojunctions. The results can be interpolated in a straightforward manner to estimate the VBO for the more realistic case of heterojunctions built up of *any* two *ternary* arsenide compounds strained to *any* reasonable lattice constant. This allows for a comparison with the few special cases that have been experimentally investigated before. The availability of such data could add some flexibility to the design of novel heterojunction devices.

C. Ohler

ISI

Forschungszentrum Jülich GmbH

D - 52425 Jülich

Germany

Phone: +49-2461-615119 or 612392

FAX: +49-2461-612940

Email: asi604@zam001.zam.kfa-juelich.de

Optoelectronic Devices Based on GaN/AlGa N Heterojunctions

M. Asif Khan

APA Optics, 2950 N. E. 84-th Lane, Blaine, MN 55449

Phone: (612)784-4995; FAX: (612)784-2038; Email: 70702.2032@compuserve.com

Due to its direct bandgap over the entire alloy composition, the AlGa N material system is ideally suited for devices in the ultraviolet and visible parts of the spectrum. Excellent progress has been made towards fabricating high brightness LED's, high responsivity visible blind UV detectors and high frequency transistors for high temperature applications. We will review the current status of these developments. Emphasis will be placed on the heterojunction devices. We will also describe our preliminary work aimed at depositing and characterizing short-period superlattices based on the AlGa N material system.

ELECTRON MICROSCOPY CHARACTERIZATION OF GaN AND AlN FILMS GROWN BY MBE ON DIFFERENT SUBSTRATES

Zuzanna Liliental-Weber and Hyunchul Sohn

Materials Science Division, Lawrence Berkeley Laboratory 62/203, Berkeley CA 94720

Gallium nitride is the one of the promising semiconductors for a light emitting diodes that can fill the blue and UV wavelength region. Even though recent progress has improved drastically the crystal quality of GaN films grown on various substrates, its practical application is still hampered by the high defect density and difficulty in p-type doping. In order to control the defect formation, it is essential to understand their nature.

The microstructure of GaN grown by molecular beam epitaxy on (0001) sapphire and SiC as well as AlN layers grown on (001) GaAs was characterized by transmission electron microscopy in plan-view and cross-section samples. All studied layers crystallized in wurtzite structure. Two types of extended defects on the planes perpendicular and parallel to the interface were found for the GaN layers grown on sapphire. Layers grown on SiC showed drastic reduction of these defects. The defects perpendicular to the substrate surface were formed at the interface and typically extended through the thickness of the film. They appear to be twins. Models explaining these defects will be presented with extended image simulation. Nonstoichiometry within the defects needs to be considered in order to explain the TEM image contrast. Defects parallel to the substrate are stacking faults often with fcc stacking order and their density is decreasing with the increasing distance from the interface. This observation can account for the RBS data which showed significantly smaller dechannelling in the subsurface area of the layer.

Thin layers of AlN layers grown on the GaAs substrate show polycrystalline growth with small angle boundaries, therefore, electron diffraction patterns show only slight elongation. Outdiffusion of Ga and the formation of the protrusions in the GaAs substrate with embedded As was detected by high resolution TEM studies. Columnar growth is observed for increased layer thickness and formation of larger As rich protrusions in the substrate.

Relation between the structural quality of these films and photoluminescence will be presented.

Dr. Zuzanna Liliental-Weber
Lawrence Berkeley Laboratory 62/203
Berkeley, CA 94720
PHONE: (510) 486-6276
FAX: (510) 486-4995
e-mail: zlw@ux5.lbl.gov

MBE Growth and Properties of GaN Films on GaN/SiC Substrates

W. C. Hughes, W.H. Roland, M.A.L Johnson, J.W. Cook, Jr., and J. F. Schetzina
Department of Physics, North Carolina State University, Raleigh, NC 27695-8202
PH: (919) 515-3314; FAX: (919) 515-7667; E-MAIL: JAN_SCHETZINA@NCSU.EDU

J. Ren and J. A. Edmond
Cree Research, Inc., 2810 Meridian Parkway, Durham, NC 27713
PH: (919) 361-5709 ; FAX: (919) 361-2358

High-brightness blue and green LEDs based on III-N heterostructures have recently been demonstrated by Nichia Chemical (Japan) using sapphire substrates. However, many potential applications of III-N materials will require the use of conducting, more closely lattice-matched substrates such as SiC or GaN. At NCSU, a homoepitaxial approach to MBE growth of GaN on GaN/SiC substrates is being studied. The GaN/SiC substrates consist of 3-4 μm thick GaN epitaxial layers grown at Cree Research on SiC substrates. The GaN layers on these SiC substrates exhibit double-crystal x-ray rocking curves as narrow as 85 arc sec FWHM and photoluminescence at 300K which is dominated by strong band-edge emission at 3.4 eV. After standard chemical cleaning, Auger spectroscopy studies showed that the GaN/SiC substrate surface was contaminated with large amounts of oxygen and carbon. Dry-etching and thermal annealing techniques were employed which reduced the carbon and oxygen surface contamination to below the Auger detection limit. RHEED patterns from these cleaned GaN/SiC substrates exhibit Kikuchi lines and streaks along the principal axis directions. Upon initiation of GaN film growth by MBE, several different surface reconstructions, which were dependent on growth conditions, were observed by means of RHEED studies. To our knowledge, this is the first observation of surface reconstructions for GaN. At NCSU, MBE growth of GaN is being investigated using an elemental Ga source and two different nitrogen plasma sources: an ASTeX compact ECR source and an Oxford MPD21 rf source. Optical emission spectra from the ECR plasma source, operated at powers ≤ 100 W, are dominated by large peaks in the 350-450 nm spectral region (UV-violet) indicative of the presence of N_2^+ ions and highly-excited 2nd positive series N_2 molecules. In contrast, emission spectra from the Oxford rf source, operated at the same power and pressure, displayed more intense emissions in the orange and near-IR spectral regions which are associated with 1st positive series N_2 molecular transitions and transitions associated with atomic nitrogen. The growth rate and surface morphology of GaN films grown with both types of plasma sources were studied for a variety of nitrogen-plasma-source operating parameters including plasma powers ranging from 20-250 W and nitrogen pressures from 5×10^{-6} Torr to 4×10^{-4} Torr in the MBE chamber. Films grown using the Oxford rf plasma source tend to have smoother, clearer surfaces due, perhaps, to the "softer" N_2 molecules and the high concentration of atomic nitrogen emitted from this type of source, which improved the overall film quality. The best MBE-grown GaN films that have been prepared to date exhibit 300 K PL spectra dominated by band-edge emission at 3.4 eV, double-crystal x-ray rocking curves as narrow as 156 arc sec FWHM, and sharp electron channeling patterns.

This work was supported by ARPA and by Cree Research internal funds.

The Barrier Height at the Valence Band Discontinuity in GaAs/GaN Heterostructures

X Huang, T S Cheng, S E Hooper, T J Foster, L C Jenkins, **C T Foxon**, J W Orton*, P C Main and L Eaves

Department of Physics, University of Nottingham, Nottingham, NG7 2RD, UK

* Department of Electronic and Electrical Engineering

Tel: 44-602-515138 Fax: 44-602-515184 e-mail: ppzctf@ppn1.nott.ac.uk

The growth of III-V heterostructures incorporating nitrides is currently the subject of intense investigation due to the promise of this material system for opto-electronic applications at the blue end of the spectrum [1]. Recently, GaAs/GaN heterostructures have been successfully grown and some electrical properties have been investigated [2]. Despite the large lattice mis-match and associated defect states, *over the barrier* thermionic experiments on n-GaAs/GaN/GaAs, single barrier diodes have indicated the presence of a well defined GaN barrier with a conduction band offset at this interface of approximately 1.0 eV [2]. Recently, however, it has been suggested that there is a large electro-negativity difference between GaAs and GaN with the result that the bandgap of Ga(AsN) alloys decreases rapidly with increasing N content [3]. The proposed large difference in electro-negativity is inconsistent with the above observation.

In this paper we investigate the properties of the corresponding valence band interface in p-GaAs/GaN/GaAs diodes. These single barrier heterostructures were grown by a modified Molecular Beam Epitaxy method using an atomic nitrogen source.

At temperatures below $\sim 200\text{K}$ the hole tunnel current through the GaN barrier dominates the conduction process. However, at higher temperatures hole conduction due to thermionic *over the barrier* conduction increasingly dominates and can be used to measure the size of the valence band discontinuity. A series of Arrhenius plots (Fig.1) provides values of the barrier heights as a function of applied bias as shown in Fig.2 below. By extrapolating the data to zero bias we estimate the valence band discontinuity to be $0.48 \pm 0.02\text{eV}$. We have also carried out similar measurements on n-doped samples and obtained broad agreement with previously reported data [2]. The sum of the conduction and valence band discontinuities is approximately consistent with the difference in band-gap of bulk GaAs and GaN. Sakai et al [3] have suggested that the large electro-negativity difference between GaAs and GaN result in a type II band alignment. Our experimental results, however, indicate a type I band alignment which in turns casts doubt upon their conclusions concerning the band gap of Ga(AsN) alloy films. The results of measurements on similar double barrier structures will also be described.

References

- 1) S Nakamura, T Mukai and M Sench, Appl. Phys. Lett., 64 (1994) 1687
- 2) G Martin, S Strite, J Thornton and H Morkoc, Appl. Phys. Lett., 58 (1991) 2375
- 3) S Sakai, Y Ueta and Y Terauchi, Jap. J. Appl. Phys., 32 (1993) 4413

Auger Electron Spectroscopy, X-ray Diffraction and Scanning Electron Microscopy of InN, GaN and GaAsN films on GaP and GaAs(001) substrates.

L.C.Jenkins, T.S.Cheng, C.T.Foxon, J.W.Orton, S.E.Hooper,
S.V.Novikov*, and D.E.Lacklison†.

*Department of Physics, University of Nottingham,
University Park, Nottingham NG7 2RD, England.
Telephone (44 602) 515151 EXT 8332. Facsimile (44 602) 515180.
Email ppzlcj@ppnl.physics.nottingham.ac.uk.*

*†Department of Electrical and Electronic Engineering, University of Nottingham.
AF Ioffe Physical-Technical Institute, St Petersburg, Russia.

Abstract

In recent years there has been an ever increasing demand for the fabrication of short wavelength light emitting semiconductor diodes and lasers. Such new devices require the controlled growth of high quality, epitaxial, wide bandgap semiconductor films. The group III nitrides are promising candidates for such applications as they have bandgaps in the range of (1.9 to 6.2)eV. However single crystal epilayers of the nitrides have proven difficult to grow due to the lack of an appropriately lattice matched substrate material with a reasonably close thermal expansion coefficient. Further complications arise as GaN exists naturally in a hexagonal structure, but can also exhibit a metastable zinc blende phase.

A modified molecular beam epitaxy technique has been used to grow InN and GaN layers on both GaP and GaAs(001) substrates. In addition, attempts have been made to grow the ternary alloy GaAsN lattice matched to GaP (and potentially to Si). In-situ Auger Electron Spectroscopy and Electron Probe Microanalysis measurements have provided information on the nitrogen content of the overlayers, and any intermixing at the heteroepilyer-substrate interface. It has also been established using X-ray diffraction that the structure of the GaN overlayers on both GaP and GaAs can be controlled by tailoring the MBE growth conditions such that mixed phases, or exclusively hexagonal or zinc blende GaN can be acheived. GaAsN layers grown so far exhibit phase separation into GaAs and GaN rich regions. Complementary scanning electron micrographs have provided further information on the morphological relationship between the substrate and overlayer on samples received immediately after growth and also after an ex-situ anneal.

UHV-TEM study of the growth and relaxation of SiGe on Si(001)

F.K. LeGoues

IBM Research Division, P.O. Box 218, Yorktown Heights, NY 10598

Transmission Electron Microscopy (TEM) has been the technique of choice to determine the structure, nature and location of dislocation networks at interfaces, in part because it can probe the microstructure of an interface through a thick overlayer with high spatial resolution. However, most TEM experiments are limited to a "post mortem" analysis, wherein the sample is removed and observed at different stages of growth. Here, we study the growth of Ge islands and SiGe layers on Si(001) in-situ in a new UHV-TEM. We can thus follow the evolution of the microstructure and the formation of strain relieving dislocations in real time. I will present video tapes of the growth, which show that new insight is gained by being able to follow this process in-situ.

MBE grown SiGe and devices

Ulf König

Daimler-Benz AG, Research Center Ulm

Wilhelm-Runge-Str. 11, 89081 Ulm

Phone(+49)731-505-2050; FAX (+49)731-505-4102

Future communication systems need extremely fast devices with frequencies up to 100 GHz, with switching times below 10 ps and furthermore with noise below 1 dB. In former days those data could be fulfilled only by III-V hetero-structures. But recent exciting results and estimations for the novel Si/SiGe hetero-system, with performances just in the aspired area, are regarded as a ray of hope for the Si-establishment. Of course, the cheapest way to manufacture outstanding devices is to use one of the numerous existing Si-production lines and to apply well known Si-processes. Only with the Si/SiGe system multifunctional one-chip solutions can be envisaged taking profit from highly complex Si-ICs.

A brief review is given on the status of the present outstanding SiGe devices, *i.e.*, the SiGe hetero-bipolar transistor (SiGe HBT), the SiGe hetero-field-effect transistor (SiGe HFET or MODFET), and the SiGe optoelectronic devices (SiGe PIN, SiGe LED). SiGe HBTs are just going to be produced. Other SiGe devices are from long-term interest. However, already now the results are encouraging, *e.g.*, concerned to transconductances around 400 mS/mm for SiGe HFETs or to the first observation of RT-luminescence in SiGe superlattices, pointing to a direct band gap transition.

The breakthrough in device performance came with increasing know-how in growing superior layer structures. The most flexible growth system is the molecular beam epitaxy (Si-MBE). Layers with a precision down to the atomic level, and with n- and p-doping between 10^{14} and $5 \times 10^{20} \text{ cm}^{-3}$ can be produced. Researchers found out the critical SiGe layer thickness, they learned to use Ge-grade buffers, both essential steps to overcome the Si-Ge misfit. Many open questions remain, concerned, *e.g.*, to the choice of the buffer, to the buffer resistance, to the individual layer thicknesses and dopings, and last but not least to proper semiconductor interfaces. All these tasks will target to optimized mobilities, saturation velocities and sheet carrier concentrations. I will discuss Si/SiGe layer aspects in more detail and relate to device results.

Measurements of Local Strain Variation in $\text{Si}_{1-x}\text{Ge}_x/\text{Si}$ Heterostructures*

L. D. Bell, A. M. Milliken, S. J. Manion, W. J. Kaiser, R. W. Fathauer, and W. T. Pike

Center for Space Microelectronics Technology

Jet Propulsion Laboratory

California Institute of Technology

Pasadena, CA 91109

Strained-layer $\text{Si}_{1-x}\text{Ge}_x$ continues to play a major role in Si-based heteroepitaxy. Devices based on the $\text{Si}_{1-x}\text{Ge}_x/\text{Si}$ system, such as heterojunction bipolar transistors and long-wavelength infrared detectors, have recently been demonstrated. Direct measurement of fundamental aspects of strained $\text{Si}_{1-x}\text{Ge}_x$ electronic structure is important to ongoing progress in this area. In addition, well-characterized contact technology is vital to the development of these devices.

This talk will describe the application of ballistic-electron-emission microscopy (BEEM) to the local measurement of strain-induced band structure modifications in $\text{Si}_{1-x}\text{Ge}_x$ and Si. Lifting of the degeneracy of the conduction-band minimum of $\text{Si}_{1-x}\text{Ge}_x$ due to lattice deformation has been directly measured by BEEM in $\text{Ag}/\text{Si}_{1-x}\text{Ge}_x/\text{Si}$ structures. Results for the conduction-band splitting agree well with calculations. For the case of $\text{Au}/\text{Si}_{1-x}\text{Ge}_x/\text{Si}$, an unexpected heterogeneity in the strain is introduced. This characteristic strain heterogeneity also appears in the case of strained Si grown on relaxed $\text{Si}_{1-x}\text{Ge}_x$ layers. The effect is not observed with Ag. Several possibilities for the variation were evaluated and will be discussed. High-resolution transmission electron microscopy results indicate a dramatic roughening of the $\text{Au}/\text{Si}_{1-x}\text{Ge}_x$ interface. The roughening is attributed to interdiffusion between the Au and the $\text{Si}_{1-x}\text{Ge}_x$.

The roughness produced at the $\text{Au}/\text{Si}_{1-x}\text{Ge}_x$ interface has an average amplitude of 3 nm and a characteristic period of about 200 nm. It is suggested that spatially non-uniform interdiffusion of the Au and $\text{Si}_{1-x}\text{Ge}_x$ produces the non-planar interface. The non-uniform nature is perhaps due to trace contamination remaining at the interface, or to Au crystallite orientation.

Roughness of the $\text{Si}_{1-x}\text{Ge}_x$ surface will produce a non-uniform modification in the strain of the layer, resulting in a corresponding variation in the conduction-band splitting. For the simple case of a sinusoidal surface profile, strain is reduced near the peaks and is enhanced in the troughs. In order to correlate the observed roughness with BEEM measurements of strain variation, a finite-element implementation of elasticity theory has been used to calculate the strain non-uniformity in the $\text{Si}_{1-x}\text{Ge}_x$ layer produced by the roughened interface. Preliminary results of these calculations will be presented.

* Research supported by ONR and BMDO/IST

L. D. Bell, M/S 302-231
Jet Propulsion Laboratory
4800 Oak Grove Drive
Pasadena, CA 91109
Tel: 818-354-4761

Fax: 818-393-4540

email: dbell@vaxeb.pl.nasa.gov

Surface and interface roughness anisotropy of $\text{Si}_{1-x}\text{Ge}_x/\text{Si}$ superlattices*

C. Teichert, Y. H. Phang, L. J. Peticolas¹, J. C. Bean¹, M. G. Lagally. University of Wisconsin-Madison, Madison, WI 53706, ¹AT&T Bell Laboratories, Murray Hill, NJ 079974.

The surface and interface roughness of $\text{Si}_{1-x}\text{Ge}_x/\text{Si}$ superlattices grown by molecular-beam epitaxy on vicinal $\text{Si}(001)$ surfaces has been characterized by *ex situ* atomic-force microscopy and x-ray diffraction diffuse-intensity measurements as a function of Ge concentration, the substrate miscut, the individual layer thicknesses, and the number of bilayers. At high Ge concentration ($x > 0.35$) in the alloy layers the surface as well as the interfacial roughness exhibit a one-dimensional waviness with an orientation of the resulting ripples always parallel to the substrate steps. The mean ripple spacing varies between 400 nm (0.4° miscut) and 900 nm (0.16° miscut), many times greater than the average separation of the substrate steps. The amplitude of the ripples is in the range of 0.6 nm to 1.5 nm. From the measured cross sections of the ripples it can be excluded that they are due to the formation of low-index facets. Using AFM we show that the waviness forms already in the first alloy layer. With increasing number of bilayers the ripple amplitude increases while its wavelength remains nearly the same. Furthermore, for small Si layer thicknesses the x-ray measurements reveal vertical correlation of the interfacial roughness. On the basis of these morphological data a model based on stress accommodation by step bunching is developed for the origin of this roughness anisotropy and its spatial evolution.

* Research supported by NSF Grant No. DMR 92-01856. One of us (C. T.) acknowledges support by the German Academic Exchange Service.

Communications information:

Christian Teichert, University of Wisconsin-Madison, Engineering Research Building, 1500 Johnson Dr., Madison, WI 53706. Phone: (608)-263-0831, Fax: (608)-265-4118.

Ge/Si Superlattices Grown by Sn Surfactant-Mediated Molecular Beam Epitaxy

X.W. Lin^{a)}, Z. Liliental-Weber, J. Washburn, E.R. Weber,
A. Sasaki*, A. Wakahara*, and T. Hasegawa*

Materials Science Division, Lawrence Berkeley Laboratory,
MS 62-209, Berkeley, CA 94720

*Department of Electrical Engineering, Kyoto University, Kyoto 606, Japan

The growth of Ge/Si superlattices (SLs) has been a subject of intensive study in recent years, because of its promising applications in high-mobility and optoelectronic device fabrication. In order to produce Ge/Si heterostructures of high interface quality, surfactant-mediated epitaxy has recently been developed, which makes the use of such surface-active species as Sb and As to promote two-dimensional heteroepitaxy. In this work, we used Sn as the surfactant to grow Ge/Si SLs. Tin was chosen as a surfactant, because it belongs to group IV elements and is neither donor nor acceptor in Si or Ge. When incorporated, it presumably will not affect the electrical properties of the Ge/Si SLs, as opposed to Sb and As. It was found that, as long as the Ge layer is ≤ 3 ML thick (the critical thickness for Ge islanding), Sn-mediated epitaxy produces Ge/Si SLs with superior interface qualities to those grown using Sb and As as surfactants.

Ge/Si SLs with each period consisting of 3 ML Ge and 25 ML Si were grown by molecular beam epitaxy on Si (001) at 450 - 500°C. Prior to the SL growth, a layer of Sn was deposited on the Si (001) to a coverage of 0.5 ML. Using high-resolution electron microscopy, it was found that the interface flatness is significantly improved over SLs grown without Sn. Moreover, secondary ion-mass spectrometry showed that Sn-mediated epitaxy results in compositionally sharper interfaces than growth without Sn, due to suppression of Ge surface segregation. These two results were further confirmed by x-ray diffraction, whose peak profiles were consistent with an ideal SL structure. The improvement in interface flatness can be accounted for, in terms of Sn-induced enhancement in surface mobility. This is in contrast with heterostructures grown using surfactants like As and Sb, which usually exhibit a high density of interface steps, due to drastic reduction of surface mobility by As or Sb.

It is concluded that Sn is a superior surfactant over As and Sb, when used to grow Ge/Si SLs with the Ge layers not exceeding the critical thickness for island formation. Not only is Sn a nondopant in Ge/Si SLs, but also it can improve both the structural and chemical abruptness of the Ge/Si interfaces.

a) phone: (510) 486-6254 fax: (510) 486 - 4995 email: xwlin@ux5.lbl.gov

Effect of Interface Roughness on Mobility of Si/SiGe Heterostructures

R.M. Feenstra, M.A. Lutz, Frank Stern*, K. Ismail**, J.O. Chu,
and B.S. Meyerson

IBM Research Division, T. J. Watson Research Center
P.O. Box 218, Yorktown Heights, NY 10598

Atomic force microscopy (AFM) and scanning tunneling microscopy (STM) are used to measure surface roughness of $\text{Si}_{1-x}\text{Ge}_x$ strain relaxed layers, and computed mobility limits of heterostructures due to this roughness are found to correlate with observed device mobilities. Layers are grown by ultra-high-vacuum chemical vapor deposition, at temperatures in the range 500–560°C. Step graded $\text{Si}_{1-x}\text{Ge}_x$ buffer layers are grown, reaching 30–40% Ge composition, on top of which are grown strained Si channels with thickness of 10 nm. A 15 nm thick spacer layer, n-type supply layer, and 4 nm thick cap layer complete the growth. Measured electron mobilities, at 0.4 K, are in the range 100,000–600,000 cm^2/Vs , depending on the details of the buffer layer growth. AFM/STM measurements are performed on the top surface of the structure, as well as on the surface of the channel using structures where the growth is terminated there. Roughness is quantitatively measured over lateral length scales of 20 Å–10 μm , and analyzed using Fourier spectra.

Three distinct components are found in the roughness spectra: At the μm -scale, undulations in the surface topography ("cross-hatch") give rise to a large spectral peak. At the 50–100 Å scale, atomic roughness on the surface is seen in the spectra, with amplitude which does not vary from film to film. Finally, at the 500 Å scale, a roughness feature associated with apparent islanding of the films is seen. This roughness shows amplitude variations of 0–15 Å from film to film. Detailed mobility computations have been performed, using the roughness spectra as input. The resulting low temperature mobilities show a sample to sample variation which correlates well with the measured mobilities, although the absolute magnitudes of the computed mobilities are about a factor of 3 too large. The 500 Å scale roughness, which provides the mobility limit in the films, is believed to represent the onset of 3-dimensional growth in the strain-relaxed buffer layers. Further studies on the physical origin of this significant roughness feature are in progress.

*Research Staff Member Emeritus

**permanent address: Dept. of Electronics, Cairo University, Giza, Egypt

contact author:	R. M. Feenstra
email:	feenstra @ watson.ibm.com
phone:	914-945-2492
FAX:	914-945-2141

In situ ballistic-carrier spectroscopy on epitaxial CoSi_2 / Si(111) and (100)

H. Sirringhaus, E. Y. Lee, and H. von Känel

Laboratorium für Festkörperphysik, ETH Hönggerberg, 8093 Zürich, Switzerland
Tel.: ++41'1'6332278; Fax: ++41'1'6331072

At an epitaxial metal-semiconductor interface ballistic-electron-emission microscopy (BEEM) is expected to be very sensitive to the interface band structure [1]. A powerful experimental method to obtain information about the fundamental concepts governing the interface transmission, such as k_{\parallel} -conservation, as well as about the BEEM process itself, is to compare electron and hole BEEM spectra for the same metal, but for different faces of the semiconductor. We have performed *in situ* BEEM at low temperature (77K) on CoSi_2 /Si films grown by molecular beam epitaxy (MBE), both on p- and n-type Si as well as Si(111) and Si(100).

A direct comparison between different interfaces is complicated by the observation that the BEEM current depends on the atomic surface structure, i.e. the details of the injection process at the surface (see BEEM contrast between the 2×1 and 1×1 surface region on CoSi_2 / p-Si(111), Fig.1). Based on this surface effect, periodic surface structures could be imaged at atomic resolution by BEEM for the first time. The comparison of the surface contrast on p- and n-Si suggests an explanation in terms of the energy distribution of the tunneling electrons.

On CoSi_2 / Si(100) there exist two epitaxial orientations ($\text{CoSi}_2(100) \parallel \text{Si}(100)$ and $\text{CoSi}_2(011) \parallel \text{Si}(100)$). The BEEM current differs by up to a factor of 5 between the two orientations.

Hot carrier scattering at individual interface dislocations gives rise to a sharply localized *increase* of the BEEM current on *n-Si(111)* [2] and a *decrease* on *p-Si(111)* (see Fig.1). This effect is interpreted as a local violation of k_{\parallel} -conservation, which implies that a significant fraction of the carriers crosses the interface ballistically. However, this does not exclude a certain, spatially uniform contribution to the BEEM current from k_{\parallel} -non-conserving processes, e.g. scattering at interfacial point defects, even in the dislocation-free regions. This issue will be discussed on the basis of a comparison between Si(111) and Si(100).

[1] W. J. Kaiser et al., Phys. Rev. B 44, 6546 (1991)

[2] H. Sirringhaus, et al., Phys. Rev. Lett. 73, 577 (1994); J. Vac. Sci. Technol. B 13, 2629 (1994); E. Y. Lee et al., Surf. Sci. Lett. 314, L823, (1994)

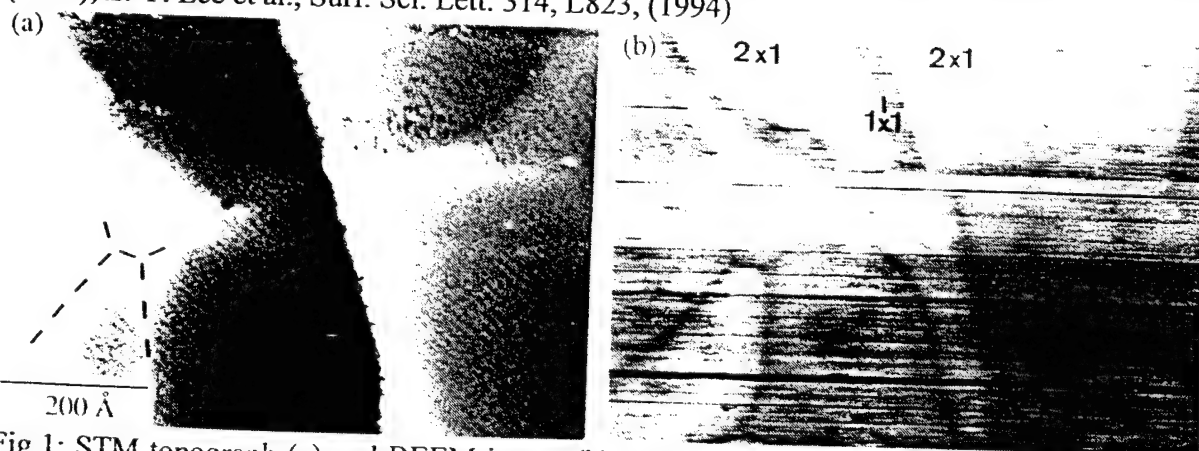


Fig.1: STM topograph (a) and BEEM image (b) obtained with a tip voltage of 1.3V on a 30 Å CoSi_2 / p-Si(111) film. The image contains a crescent-shaped, 2×1 reconstructed surface region (with a small 1×1 stripe parallel to the step edge) at the top and several interface dislocations (indicated by dashed lines) in the unreconstructed, lower part.

Formation of the Ce/Si(111) and Ce/CaF₂/Si(111) interfaces

H.J. Wen, I. Manke, A. Höhr, A. Bauer, M. Prietsch, and G. Kaindl

Institut für Experimentalphysik, Freie Universität Berlin, Arnimallee 14, D-14195 Berlin, Germany

Interfaces of rare earths with Si have recently attracted attention because of the formation of epitaxial silicides on Si(111) and their low Schottky-barrier heights on *n*-type Si of 0.2 - 0.3 eV [1]. In order to investigate the chemical processes occurring during interface formation, we studied the growth of the rare-earth metal cerium on Si(111)7×7 and the behavior upon annealing using high-resolution photoemission (PES), low-energy electron diffraction (LEED), and scanning-tunneling microscopy (STM). While room-temperature deposition of Ce on Si(111)7×7 results in rather unordered films and a slight diffusion of Si to the surface, annealing above the eutectic temperature of 650 °C leads to at least four different chemical species resolved in the Si-2p PES spectra. These can be assigned to a mixture of various compounds ranging from Ce₅Si₃ to CeSi₂ and of Si dissolved in elemental Ce. The chemical shift varies linearly with the Si content, and the average Si content increases with annealing temperature. The corresponding LEED pattern consists of a superposition of 2×2 and $\sqrt{3}\times\sqrt{3}$ superstructures, and the STM images show regions with different surface roughness. These data indicate a multi-phase formation above the eutectic temperature. Even after annealing at 1050 °C, at least two chemical species are present. For this case, a Schottky-barrier height of 0.23 eV on *n*-type Si is derived, which agrees nicely with values observed for other rare-earth silicides.

Metal/insulator/semiconductor (MIS) systems based on rare-earth metals have been investigated only scarcely up to now [2]. Here we present a PES study on the formation of the Ce/CaF₂/Si(111) MIS structure, performing CaF₂ epitaxy at 750 °C and Ce deposition at room temperature. The growth is characterized by an absence of intermixing between Si and Ce, in contrast to the Ce/Si interface, demonstrating that CaF₂ layers even as thin as two monolayers are able to form effective diffusion barriers. PES intensities and spectral shapes indicate a formation of Ce clusters on top of the CaF₂ surface. Furthermore, Ce deposition leads to a homogenization of the Fermi-level position at the CaF₂/Si(111) interface close to midgap. Upon annealing up to 500 °C, a coalescence of the Ce clusters occurs, while no indications for chemical interactions are observed.

- [1] Tu et al., Appl. Phys. Lett. **38**, 626 (1981); Baptist et al., Phys. Rev. Lett. **64**, 311 (1990)
- [2] R. Hofmann et al., Phys. Rev. B **47**, 10407 (1993)

INTERFACE ROUGHNESS IN GaAs-AlAs HETEROSTRUCTURES: THE ROLE OF Ga SURFACE SEGREGATION

G.S. Spencer,[†] J. Menéndez,^{1,†} L.N. Pfeiffer,[‡] K.W. West[‡]

[†]Arizona State University

[‡]AT&T Bell Laboratories

The GaAs-AlAs interface has been the subject of controversy in recent years due to the contradictory interpretation of photoluminescence and electron-microscopy results. The observation of closely spaced emission lines in the photoluminescence spectra of GaAs-AlGaAs quantum wells was explained in terms of large, flat islands with heights of a few monolayers. The existence of the flat islands could not be confirmed by electron microscopy, which consistently reveals the presence of considerable cation intermixing in the layers closest to the interface. The present consensus is that the roughness at GaAs-AlAs interfaces is bimodal: it has a long range component, which produces island-like features and explains the photoluminescence results, and a short range component which is responsible for the significant degree of intermixing within "islands" observed in microscopy experiments.

Ga surface segregation has been proposed as the microscopic mechanism that leads to the observed roughness at the GaAs-AlAs interface. Several surface-sensitive experimental techniques have been used to confirm the existence of Ga segregation during the growth of AlGaAs on GaAs. In this paper, we assess the validity of surface segregation models as a description of the GaAs-AlAs interface disorder. We take advantage of the extraordinary sensitivity of phonon Raman scattering to compositional fluctuations at the GaAs-AlAs interface. We combine our Raman experiments with full three-dimensional calculations of phonons in disordered structures, using models fit to first-principles calculations of the phonon dispersion relations. This makes it possible to predict with high accuracy the Raman spectrum expected for a given surface segregation profile.

Our results for a series of (GaAs)₆(AlAs)₆ superlattices, grown by MBE at different temperatures ranging from 350 °C to 650 °C, show that current surface segregation models do not accurately reproduce the features found in the Raman spectra. Specifically, samples grown at the lowest temperatures show GaAs layers which deviate very little from the profile of a perfect GaAs layer, whereas the AlAs layers always display some degree of Ga intermixing. At the highest growth temperatures, the spectra deviate drastically from the predictions of surface segregation models indicating that, at these temperatures, other mechanisms play an important role in determining the interfacial composition.

¹Department of Physics and Astronomy, Arizona State University, Box 871504, Tempe, AZ 85287-1504; Phone: (602) 965-4817; Fax: (602) 965-7954; Internet: menendez@phyast.la.asu.edu

Optical Study of Heterointerfacial Growth Interrupts in Type-II GaAs/AlAs Superlattices by Time-Resolved PL-Imaging

T. Chang, L.P. Fu, F.T. Bacalzo, G.D. Gilliland, K.K. Bajaj, A. Antonelli, R. Chen
Emory University, Physics Dept., Atlanta, GA 30322

D.J. Wolford

Iowa State University, Physics Dept., Ames, Iowa 50011

J. Klem and M. Hafich

Sandia National Laboratories, Albuquerque, NM 87185

The quest to grow high quality interfaces in semiconductor heterostructures is scientifically interesting and technologically relevant. Heterostructures are now widely employed in the design of semiconductor devices. The carrier kinetics in these structures often involve interaction between the heterointerface and the carriers, thus interface quality may have a profound effect on device performance. One method to control interface quality is through the use of growth interrupts during epitaxial fabrication of the heterostructure. In particular, the quality of the two types of interfaces in a superlattice (inverted or normal) may be affected differently by the use of growth interrupts. In this study we employ a time-resolved photoluminescence imaging technique, essentially using excitons to probe heterointerfacial quality, as a method of determining the effect of growth interrupts on the inverted and normal interfaces in type-II GaAs/AlAs superlattices.

In $(\text{GaAs})_m/(\text{AlAs})_n$ system, a type-II structure may be achieved for GaAs-layer thicknesses $< 35 \text{ \AA}$ ($m < 13$) and AlAs-layer thicknesses $> 15 \text{ \AA}$ ($n > 6$). In these structures, type-II excitons manifests itself with the holes residing at the Γ point of the GaAs layers, and the electrons residing at the X conduction band edges of the AlAs layers. Excitons in these type-II systems are thus indirect in both real- and momentum-space. Since these type-II excitons actually straddle the heterointerfaces, in contrast to their behavior in type-I heterostructures, the excitonic decay kinetics and transport along the heterointerfaces are very sensitive to the presence of defects or roughness at the interfaces.

We have performed all-optical time-resolved photoluminescence imaging measurements to characterize the heterointerfaces in a variety of MBE-prepared GaAs/AlAs superlattices with different types of growth interrupts (at either normal, inverted, none, or both interfaces). We have observed systematic differences in these samples grown with different interrupts. PL was carried out from 1.8 to 50K, with $3 \mu\text{m}$ spatial resolution, 0.1 \AA spectral resolution and 500 ps time resolution. The measured diffusivities varied systematically from $10^{-3} \text{ cm}^2/\text{s}$ at 1.8K to $100 \text{ cm}^2/\text{s}$ at 30K. Additionally, we have measured PL time decays in these structures and find very different decay kinetics, indicative of different quality of the heterostructures. The measured lifetimes at 30K ranges from 10 to 100 ns. Further, the measured lifetimes at 1.8K were used to estimate the strength of Γ -X mixing potentials in these samples: the interface mixing potential obtained is 0.19meV, whereas the superlattice mixing potential is 1.27 meV. Employing a quantitative model that relates the measured lifetimes to diffusivities, we have characterized the various heterointerfaces in terms of the density of nonradiative defects. And the defect sheet densities determined are on the order of 10^7 cm^{-2} . Our model verifies the existence of these heterointerfacial nonradiative defects, and allows the quantification of Γ -X band mixing due to both the superlattice potential and interfacial disorder.

Supported, in part, by AFOSR under grant No. AFOSR-91-0056, and the U.S. DOE under contract DE-AC04-94AL85000.

Corresponding Author: G.D. Gilliland, Emory Univ., Physics Dept., 1510 Clifton Rd., Atlanta, GA 30322, (404) 727-2978, FAX (404) 727-0873, E-mail: GGILLIL@EMORYU1.CC.EMORY.EDU.

XPS study of the MnS/ZnSe valence band discontinuity

L. Wang and S. Sivananthan

Microphysics Laboratory, Physics Department (m/c 273), University of Illinois at Chicago,
845 W. Taylor Street (Room SES 2236), Chicago, IL 60607-7059

R. Sporken and R. Caudano

Laboratoire Interdisciplinaire de Spectroscopie Electronique,
Facultes Universitaires Notre-Dame de la Paix, Rue de Bruxelles 61, 5000 Namur (Belgium)

Lattice-matched quantum well structures based on the quaternary alloy $\text{Zn}_{1-x}\text{Mn}_x\text{Se}_y\text{S}_{1-y}$ are an attractive alternative to the Mg-based materials for Laser or LED applications in the blue-green region of the visible spectrum. In such heterostructures, the electronic transport properties are determined, to a large extent, by the way in which the valence and conduction bands line up at the interfaces.

We present the growth and characterization of binary zinc-blende MnS/ZnSe heterostructures on GaAs(100). The valence band discontinuity was measured by x-ray induced photoelectron spectroscopy (XPS), using an SSX-100 spectrometer with a spot size of 300 μm . Samples for this study were grown by molecular beam epitaxy on GaAs(100) substrates. Since the GaAs surface reacts with elemental sulfur, exposing it to a flux of sulfur would make it rough. Therefore, a thin ZnSe buffer layer was deposited before the growth of MnS. With the appropriate growth conditions, we were able to grow β -MnS with the metastable zinc-blende structure, rather than the stable rock-salt structure (α -MnS). This compound (β -MnS) is one of the end points of the quaternary alloy $\text{Zn}_{1-x}\text{Mn}_x\text{Se}_y\text{S}_{1-y}$. The β -MnS and ZnSe layers have been extensively characterized with RHEED, photoluminescence, x-ray diffraction, to name only a few techniques. We then grew several heterostructures with either a β -MnS or a ZnSe layer on top. The topmost layer was thinner than the sampling depth of XPS (about 5 nm). This is necessary to obtain a contribution from both sides of the interface. Core-level spectra indicated the absence of new compounds at the interface, suggesting that the interface is sharp. Furthermore, the layers do not contain any of the four elements (Mn, S, Se, Zn) in non-reacted form, indicating that they are of the proper stoichiometry.

We are not aware of any theoretical calculations of the VB discontinuity at the β -MnS/ZnSe interface. This can be attributed to the lack of knowledge of the electronic structure of β -MnS, and to the complication arising from the shallow d-levels in ZnSe. This VB discontinuity is also difficult to measure experimentally. Indeed, it is not resolved in valence band spectra from the interface, thereby suggesting that the discontinuity is rather small. We therefore determined the discontinuity from the separation of the core levels at the interface and in reference samples of ZnSe and β -MnS. Ideally, this should be done using as many combinations of core levels as possible in order to improve the accuracy, but overlapping core levels and the rather complex line shape of the Mn core levels restricted the possible combinations. Nevertheless, most of the information was obtained from the Se 3p and S 2p core levels. The results suggest that the valence band discontinuity at the zinc-blende MnS/ZnSe interface is small (on the order of 150 meV) and that the band alignment is of type II.

Corresponding Author: S.Sivananthan, Phone- (312) 996 5092, Fax - (312) 996 9016,
e-mail: U41400@UICVM.UIC.EDU

PCSI-22 (1994)

SPATIALLY RESOLVED INTERNAL PHOTOEMISSION
by NEAR FIELD OPTICS

Th0815

J. Almeida, Tiziana dell'Orto, C. Coluzza and G. Margaritondo

Ecole Polytechnique Fédérale

PH-Ecublens, CH-1015 Lausanne, Switzerland.

O. Bergossi, M. Spajer and D. Courjon

Laboratoire D'Optique, P. M. Duffieux, Université de Franche-Comté,

25030 Besançon, France.

We present the first to our knowledge, spatially resolved internal photoemission (IPE) measurements using a near field optics scanning microscope. Shear-force and photocurrent X-Y images at different photon energies enable us to map the topography and the Schottky barrier height on the same surface. The measurements revealed strong differences in the photocurrent mappings within a spatial resolution of 100 nm.

We performed IPE measurements on Pt/GaP Schottky barriers. The heterostructures were obtained by Pt electron gun evaporation on n-type chemical etched GaP substrates.

Piezoelectric feedback-controlled oscillators provided the vertical approach up to the near field condition as well as the X-Y scanning over an area ranging from 8-30 μm . Pulled and aluminum coated optical fibers were utilized to concentrate the light on an open edge aperture of 50 nm. A Titanium-Sapphire pumped laser was tuned between 1.35 and 1.5 eV and the light was injected through the tip into the 10 nm semitransparent Pt metallic layer. The light beam was modulated before entering the fiber and the photocurrent was detected by a standard lock-in technique. On the same samples we performed also spatially integrated IPE.

The topography's images, compared with the IPE images, revealed zones where the morphology of the metallic layer was homogeneous whereas, the photocurrent was varying from place to place. The spatially resolved IPE measurements revealed local Schottky barrier differences of about 20 meV in the Fowler plots.

These results give additional evidence of the microscopically inhomogeneous character of the Schottky barrier and demonstrate the feasibility of this new and powerful analysis technique, based on the collimated light beam of the near field optics.

Near-field Optical Characterization of Quantum Wells and Nanostructures

Harald F. Hess

AT&T Bell Laboratories

A spatial distribution of luminescent centers with sharp ($<0.1\text{ meV}$), spectrally distinct emission lines are revealed in a GaAs/AlGaAs quantum wells[1] using low temperature near-field scanning optical microscopy[2], a technique where a subwavelength source and /or detector of light in close proximity ($< 40\text{ nm}$) to the sample is used to probe with a resolution beyond the diffraction limit. These centers are the energy eigenstate components that comprise the inhomogeneously broadened line shape observed in standard far-field photoluminescence. Measurements as a function of temperature, magnetic field, and well width establish that these centers arise from excitons localized by quantum well thickness fluctuations. For sufficiently narrow wells, virtually all emission originates from such centers. Quantities such as diffusion (both thermal and tunneling), lateral confinement energies, lifetimes, g-factors from magnetic field induced spin splittings, diamagnetic energy coefficients of the luminescent states can now be measured at a site-by-site individual quantum level rather than averaged over a statistical distribution. This information can be used in turn to provide a direct local picture of the interface fluctuations and how they vary under different MBE growth conditions. Near-field microscopy /spectroscopy provides a means to access energies and homogeneous line widths for the individual eigenstates of these centers, and thus allows the luminescent components to be identified and characterized with the extraordinary detail previously limited to the realm of atomic physics.

1. H. F. Hess, E. Betzig, T.D.Harris, L.N. Pfeiffer, and K. W. West, Science 264, 1740 (1994).

2. E. Betzig and J. K. Trautman, Science 257, 189 (1992).

Doping and Composition Fluctuation in Epitaxial Semiconductors

H. W. N. Salemink*, M. B. Johnson*, P. M. Koenraad†, M. Pfister*, and S. F. Alvarado*

*IBM Research Division, Zurich Research Laboratory, CH-8803 Rüschlikon, Switzerland

†Physics Department, Eindhoven University of Technology,
NL-5600 Eindhoven, The Netherlands

For semiconductor structures with critical dimensions on the nanometer scale, the atomic alloy composition and the distribution of dopant impurities are critical issues. Our experiments on UHV-cleaved cross sections of MBE-grown multilayers demonstrate the unique use of an STM to study these two topics. Our work in this field is reviewed with emphasis on (i) atomic-scale composition fluctuations in ternary III-V alloys and (ii) the effects of active dopant impurities in III-V materials.

Atomic-scale composition fluctuations: In the AlGaAs alloy, the chemical identification within the group III sites allows us to delineate the epitaxial interfaces on the atomic scale. In the majority of our MBE material we find clustering of the Al sites on the scale of 3-5 nm alternating with Al-depleted areas. These findings demonstrate that the size of the Al cluster is important for the interface smoothness on the atomic scale (*e.g.*, in quantum wells)[1].

Effects of active dopant impurities: Doping effects appear on the UHV-cleaved III-V (110) surfaces in two ways: via the tunneling spectra or in the slight perturbations of the local charge density [2]. In the present work, we concentrate on the the second mode. For epitaxially MBE-grown GaAs doped with Be impurities, we observe the electronic signature from individual dopant sites. Both the magnitude and the density of these features suggest that the active impurities are detected with a Bohr-type radius below the surface. The conclusions are supported by STM work on modulation-doped superlattices [3] and SIMS [4] as well as by recent experiments on delta-doped multilayers. In the present work, we analyzed sets of delta-doped Be:GaAs layers separated by undoped spacers having several Be (sheet) concentrations by studying the delta layer width and dopant statistics in real space. At a nominal density of more than 10^{13} cm^{-2} , the width of the Be layer increases sharply. This spreading as well as the appearance of structure within the Be layer is attributed to Coulombic repulsion between the ionized dopants.

The reported experiments indicate a way to analyze doping and composition profiles at the nanometer scale in realistic quantum [5] and delta-doped semiconductor structures. This technique is important as a complement to such existing techniques as photoluminescence, HRTEM and SIMS since it delivers data from the real-space domain at an atomic to nanometer scale.

[1] H. W. M. Salemink and O. Albrechtsen, Phys. Rev. B **47**, 16044 (1993).

[2] M. B. Johnson *et al.*, Appl. Phys. Lett. **63**, 2923 (1993).

[3] M. B. Johnson *et al.*, Appl. Phys. Lett. **63**, 3636 (1993).

[4] The SIMS work was performed by F. Cardone, IBM Yorktown.

[5] M. Pfister *et al.*, Appl. Phys. Lett. **65**, 1168 (1994).

Direct Sublattice Imaging in Compound Semiconductor Heterostructures

A J McGibbon*, S J Pennycook and D E Jesson

Oak Ridge National Laboratories, Solid State Division, Oak Ridge, TN 37831-6031

*Tel: 615-574-6286 Fax: 615-574-4143 Email: ak4@solid.ssd.ornl.gov

The structural and electronic properties of many heteroepitaxial semiconductor materials rely strongly on the precise atomic arrangement at interfaces and dislocations. The ultimate aim therefore of microstructural characterization of these systems is to provide direct and unambiguous information on atomic structure on a column-by-column scale. In this paper, we introduce an important step towards this goal by using atomic resolution Z-contrast imaging at 1.3Å resolution in conjunction with maximum entropy image analysis to provide direct, compositionally sensitive images of the sub-lattice in both III-V and II-VI heteroepitaxial systems.

Z-contrast imaging in a scanning transmission electron microscope (STEM) is an incoherent imaging technique which, when used to observe crystalline specimens oriented along a zone axis, provides a direct, Z-sensitive map of the atomic column arrangements, the resolution of which is limited primarily by the size of the electron probe. When carried out using a newly developed 300kV STEM the image resolution is 1.3Å, enabling the observation of all zinc blende-type semiconductor structures (including GaAs) in the <110> orientation. Furthermore, image incoherence enables the application of maximum entropy image analysis, moving beyond the probe-limited resolution limit to retrieve accurate information on column position and composition below the 1Å level.

We will concentrate on the analysis of two MBE-grown multilayer systems, CdTe/GaAs(001) and InGaAs/GaAs. In the former, we have probed the precise nature of interface structure in both (001) and (111) oriented CdTe. In these materials we can determine, for example, the direction of structural polarity across an interface, the terminating atomic species at the substrate, the precise point at which dislocations nucleate and their core structure. In the InGaAs/GaAs system, emphasis is given to the relation between interface abruptness and material growth conditions. Using Z-contrast, it is possible to observe interfacial imperfections of the order of one monolayer.

This research was sponsored by the Division of Materials Sciences, U.S. Department of Energy, under contract DE-AC05-84OR21400 with Martin Marietta Energy Systems, Inc.

PHOTON CHANNELING IN THE VACUUM ULTRAVIOLET WAVELENGTH RANGE

J. E. ROWE, R. A. MALIC, E. E. CHABAN, R. J. CHICHESTER, C.-M. CHIANG and N. V. SMITH^(a)

AT&T Bell Laboratories, Murray Hill, NJ 07974.

ABSTRACT

Experimental measurements in our laboratory have shown a new type of focusing of far ultraviolet light, $\lambda < 1000\text{\AA}$, using tapered capillary tubes similar to those first developed for the near-field scanning optical microscope (NSOM) which we call photon channeling. We have tested silica tubes with taper-half-angles of -0.5° to 6° .

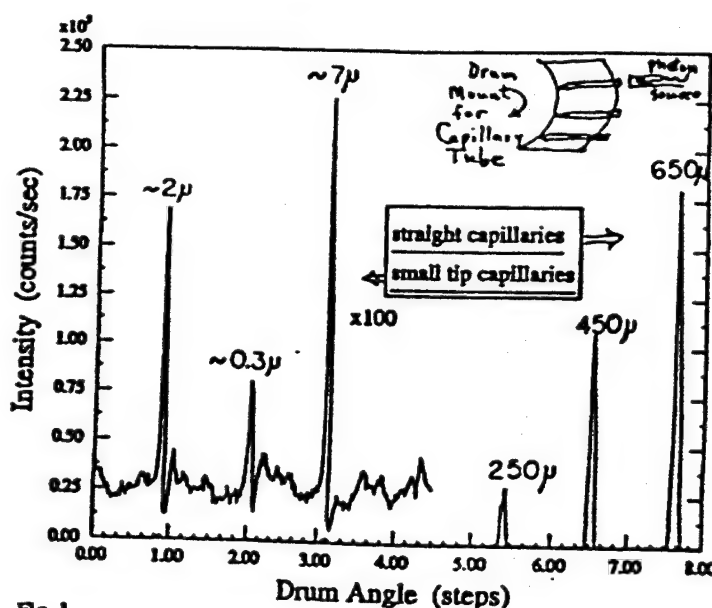


Fig. 1

Figure 1 shows the schematic idea of an array of capillaries mounted on a rotatable drum placed in front of a collimated photon source obtained from a rare-gas discharge lamp. By rotation of the drum, successive capillaries can be brought into alignment, and the photoemission detected by a channeltron-grid detector. The straight capillary intensity (shown on the right as dotted lines) shows no significant light guide effect; it simply decreases as the area of the capillary.

However, the tapered capillaries show an enhanced transmission (or photon channeling effect). In quantitative agreement with simple numerical estimates [1] we find that the transmission enhancement factor varies from ~ 10 -500 times the collimated transmission of a pinhole aperture of the same dimensions with an approximately linear dependence of channeling factor on inverse of the half angle. Useful intensity suitable for photoelectron energy analysis with capillary openings of $\sim 0.7\mu$ has been demonstrated. The expected spatial resolution is comparable to that obtained with more complex lithographically formed Fresnel zone plates and has the important advantage that the image probe size is independent of photon wavelength. A scanning stage has been developed to form spectral energy-resolved images and requires a tip approach feedback control different from that of NSOM to operate in high vacuum. Preliminary calibration measurements and scanning tests will be presented.

(a) Present address: Advanced Light Source, Lawrence Berkeley Laboratory, Berkeley, CA 94720

[1] N. V. Smith, W. A. Royer and J. E. Rowe, Rev. Sci. Instr. 65, (1994) in press.

Jack E. Rowe
Member of Technical Staff

Room 31-401
600 Mountain Ave.
Murray Hill, NJ 07974
908 582-5878
FAX 908 582-3901
EMAIL rowe@physics.att.com

A METHOD FOR THE EXPERIMENTAL DETERMINATION OF THE TENSORIAL COMPONENT OF STRESS IN Si-BASED STRUCTURES AND DEVICES

G.S. Loechele[†], N. Cave[‡], J. Menéndez^{†,1}

[†]Arizona State University

[‡]Materials Characterization Laboratory, Motorola Inc.

A critical structural consideration for the design of semiconductor devices is the development of significant fabrication stresses. A particularly important case is the SiO₂-Si interface. The small-size requirement of state-of-the-art devices implies that the active regions are in many cases under the influence of stress fields generated at nearby Si-SiO₂ interfaces. The measurement of these fields is a challenging task. Methods that allow the direct observation of a distorted lattice parameter, such as X-ray or electron diffraction, frequently lack the desired spatial resolution of about 1 μ or require the destruction of the device. On the other hand, Raman spectroscopy has been shown to be a technique with the required spatial resolution and sensitivity to determine the strain fields of interest to the semiconductor industry. A major shortcoming of the Raman approach, however, is the fact that all experiments so far focus on the observation of the stress-induced shift in the energy of a *single* phonon line. This single experimental datum does not allow the determination of the stress-strain-*tensors*. The tensorial nature of the strain is usually deduced from theoretical models developed to explain the shift of the single phonon line.

In this paper, we demonstrate the use of Raman scattering for a direct experimental determination of the strain-stress tensors in semiconductor devices. No theoretical modelling of the stress-strain fields is in principle necessary. Our method is based on the observation of *several* Raman peaks corresponding to stress-split degenerate phonon levels in cubic Si. This is a very challenging experiment due to the selection rules for Raman scattering at the (001) crystal face of Si, which overwhelmingly favor the observation of the single Raman line reported in conventional experiments. However, by carefully selecting the scattering geometry and using high-quality optics, we demonstrate that it is possible to detect other phonon lines and *fit* the strain-stress tensors to the experimental data.

To demonstrate the validity of the approach, we designed and built several apparatuses that allow the application of a known stress to a standard Si wafer. We will discuss the applicability of our approach to the case of real device structures with unknown stress fields.

¹Department of Physics and Astronomy, Arizona State University, Box 871504, Tempe, AZ 85287-1504; Phone: (602) 965-4817; Fax: (602) 965-7954; Internet: menendez@phyast.la.asu.edu

Fabrication of In-Plane Gate Quantum Structures through Direct Schottky Interface Formation by In-situ Selective Electrochemical Process

Th1030

T. Hashizume, H. Okada, K. Jinushi and H. Hasegawa

Department of Electrical Engineering and Research Center for Interface Quantum Electronics, Hokkaido University, Sapporo 060, Japan, TEL:+81-11-706-6509, Fax:+81-11-706-7890

Fine quantum structures are attracting attention for application to future electronic devices. Particularly, the so-called in-plane gate structure is attractive since it realizes electric fields that are almost perpendicular to the edge of two-dimensional electron gas (2DEG), and thus it produces a strong and efficient potential confinement of carriers into a quantum wire or dot. Previously, such structures were produced by using focused ion beam and reactive ion etching where resultant material damage may be a critical issue.

The purpose of this paper is to demonstrate that our novel technique[1] of direct Schottky contact formation to the quantum well (QW) edges by a in-situ selective electrochemical process can be successfully applied for fabrication of a new class of in-plane gate quantum structures. The main points are as follows:

(1) The electrochemical process consists of controlled anodic etching of semiconductors and cathodic deposition of metals, both of which were done *in-situ* in the same electrolyte. Selective contact formation at the QW edge becomes possible by utilizing the fact that both etching and metal plating take place selectively at the place with the lowest surface potential[1].

(2) Figure 1 shows the in-plane gate wire transistor structure formed in this study. AlGaAs/GaAs double-hetero QW structure was grown by standard MBE and a wall-like structure was formed by EB lithography and wet chemical etching. After formation of ohmic contacts, the Schottky in-plane gates were fabricated by the selective plating of Pt.

(3) The depletion characteristic were characterized by electron beam induced current (EBIC) technique. As shown in Fig.2, the EBIC images clearly gave the potential peaks at QW edges, indicating formation of Schottky/QW contact. Depletion widths from the EBIC signals depended linearly on the applied reverse voltage, being in agreement with theory.

(4) The I-V characteristics of the fabricated in-plane gate transistor exhibited field-effect behavior with excellent gate control and pinch-off at room temperature, as shown in the inset of Fig.3, whose behavior is in excellent agreement with the quasi-planar depletion characteristics of the Schottky/QW contact. At low temperature (2K), clear conductance steps were seen near pinch-off as shown in Fig.3. This can be explained in terms of formation of multiple quantum point contacts.

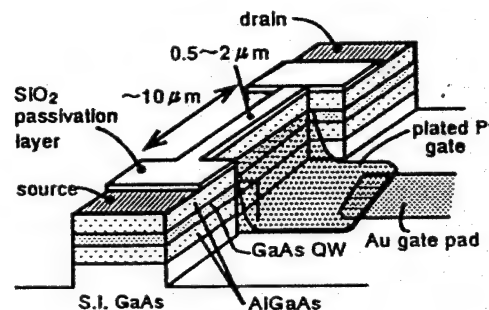


Fig.1

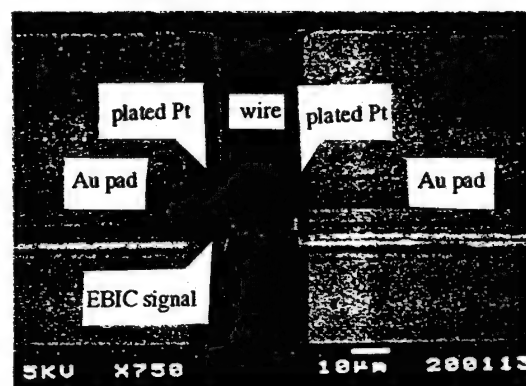


Fig.2

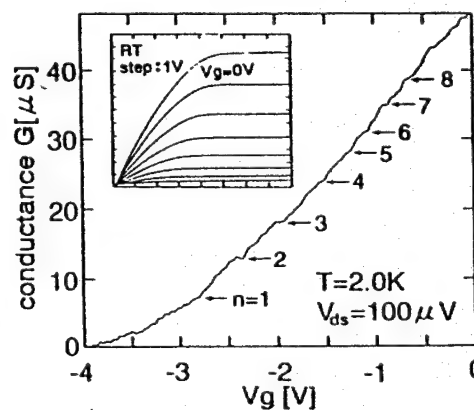


Fig.3

[1] T. Hashizume et al.: presented at 1994 PCSI-21, J. Vac. Sci. Technol. B12, 2660(1994).

Corresponding Author: T. Hashizume, Dept. of Electrical Eng., Faculty of Eng., Hokkaido Univ., North 13, West 8, Sapporo 060, Japan, TEL:+81-11-706-6509, FAX:+81-11-706-7890.

**Polarized-CL and CL wavelength imaging study of variations
in strain in $\text{In}_x\text{Ga}_{1-x}\text{As}/\text{GaAs}(001)$**

D.H. Rich, K. Rammohan, and Y. Tang
Photonic Materials and Devices Laboratory
Department of Materials Science and Engineering
University of Southern California
Los Angeles, CA 90089-0241
Ph/Fax: (213) 740-4329/7797; Email: danrich@usc.edu

R.S. Goldman, J. Chen, H.H. Wieder, and K.L. Kavanagh
Department of Electrical and Computer Engineering
University of California, San Diego
La Jolla, CA 92093-0407

We have examined μm -scale variations in strain and alloy composition in thin films of $\text{In}_x\text{Ga}_{1-x}\text{As}$ grown on $\text{GaAs}(001)$ using new variations in the cathodoluminescence (CL) imaging technique. A unique combination of scanning linearly-polarized CL (LPCL) and CL wavelength imaging (CLWI) measurements were performed. For LPCL measurements, a rotatable linear polarizer was mounted *in vacuo*. The strain-induced splitting of the heavy-hole (hh) and light-hole (lh) valence bands at $k=0$ can be examined by studying the polarization and energy dependence of the excitonic luminescence. LPCL imaging is observed to be sensitive to local deviations from biaxial stress and can be used to study stress variations near interfacial dislocations. In CLWI, the wavelength, λ_m , at which the intensity of luminescence is maximum is mapped as a function of spatial (x,y) position, and a false-color image is generated. CLWI enables a mapping of changes in defect-, strain-, and composition-induced changes in the bandgap on the scale of a $\sim 1 \mu\text{m}$, as limited by the minority carrier diffusion.

CL imaging shows the presence of dark line defects (DLDs). The DLDs are a result of nonradiative recombination caused by the presence of misfit dislocation cores and point defects left in the wake of dislocation propagation. Local variations in the polarization and energy of the excitonic luminescence are observed and found to correlate spatially with the DLDs observed in CL monochromatic imaging. The blue- and the red-shifted wavelength regions in the CLWI image correspond to regions of reduced- and enhanced-polarization anisotropy in the LPCL image. This correlation confirms that spatial variations in peak luminescence wavelengths are caused primarily by variations in strain in close proximity to the interfacial misfit dislocation as opposed to variations in In composition which would not yield a polarization anisotropy. The deviation of the polarization ratio from unity, indicates the presence of a quasi-uniaxial stress (σ) with a dominant longitudinal component, σ_{\parallel} , parallel to the DLDs such that $\sigma_{\parallel} > \sigma_{\perp}$. Transmission electron microscopy shows the existence of regions of varying asymmetries in misfit dislocation densities, consistent with the μm -scale variations in strain that is deduced from CL. LPCL and CLWI are also used to examine the influence of substrate misorientation on anisotropic properties of the luminescence. These results show that (i) large inhomogeneities in the stress of these InGaAs films are present on a μm -scale and (ii) DLDs in strained systems exhibit significant polarization and energy variations in addition to their more familiar nonradiative behavior.

The Investigation of Adsorbates on Si(100) with Photoelectron Holographic Imaging*

H. Yu, H. Wu, and G. J. Lapeyre

Physics Department, Montana State University, Bozeman, MT 59717-0350

The scanned energy method (CIS) of performing photoelectron diffraction measurements is used to determine images of individual atoms. The Fourier-like inversion of the data is based on the holographic principle and uses the Tong, Huang, Wie (THW) transformation [1]. Overlayers are made by vapor deposition of Se, ZnSe, and Mg onto single domain Si(100)- 2×1 surfaces. Upon inversion, the CIS data for the Se 3d and Mg 2p levels give high quality images of the neighboring Si atoms. Mg forms a 2×2 net and the image shows that the adsorption is in the four-fold hollow site. The Se net is 1×1 and the image shows adsorption in the bridge site, but unexpectedly two bridge sites, 90° rotated from each other, are found. The results indicate that significant Si diffusion occurs. A possible model is presented.

[1] H. Wu, G. J. Lapeyre, H. Huang, and S. Y. Tong, Phys. Rev. Lett. **71**, 251 (1993).

* Research supported by ONR-DEPSCoR and NSF. Wisconsin Synchrotron Radiation Center supported by NSF.

Effects of interface flatness and abruptness on optical and electrical characteristics of GaAs/Al(Ga)As quantum well structures grown by metalorganic vapor phase epitaxy

Masanori Shinohara, Haruki Yokoyama and Naohisa Inoue

NTT LSI Laboratories

3-1, Morinosato Wakamiya, Atsugi, Kanagawa 243-01, Japan

Phone: 81-(462)-40-2748, Fax: 81-(462)-40-2872, Email: shino@aecl.ntt.jp

Interface flatness and abruptness are controlled during metalorganic vapor phase epitaxy (MOVPE) and their effects on photoluminescence (PL) spectra halfwidths from quantum wells are clarified. Their effects on current-voltage characteristics of resonant tunneling diodes (RTD) are also investigated.

The quantum well structure consists of stacked 7 monolayer (ML), 11 ML and 14 ML thick GaAs wells and 100 nm thick $\text{Al}_{0.33}\text{Ga}_{0.67}\text{As}$ barriers. The RTD consists of a 14 ML thick GaAs well and 10 ML thick Al(Ga)As (Al content 0.5 or 1.0) double barriers. Various growth modes such as two-dimensional (2D) nucleation, step-flow and step bunching were realized by changing the growth temperatures and substrate misorientation angles within the range generally used conventional MOVPE. The growth modes were identified by observing the top surface of GaAs using atomic force microscopy. Atomic scale interface morphologies were characterized by observing the surface of a GaAs well on the Al(Ga)As barrier after growth was stopped. Each growth mode was found to be consistent throughout the whole structure since the variations in well thickness estimated from the halfwidth were the same among the three stacked quantum wells. PL was measured at 4.2 K using an Ar laser beam with a diameter of 0.1 mm. The current-voltage characteristics were measured at 300 and 77K.

The effects of various atomic scale morphologies such as 2D islands, step irregularity and bunched steps on PL linewidth were separately determined.

At relatively low growth temperatures, below 650°C , 2D nucleation growth occurs especially on a nominally oriented substrate surface (0.02° off) because the migration length of adatoms is small. The PL spectra halfwidth increases to that corresponding to effective thickness variations (ETV) of less than 2 ML thick with a density and size of 2D islands. Moreover, the smoothness of steps degrades and results in a difference of step-edge location between the top and bottom surfaces of the GaAs well. This position-shift increases the ETV to more than 2 ML and becomes the most serious among the above mentioned factors.

As the growth temperature increases ($> 700^\circ\text{C}$), step-flow growth mode dominates and regularly arrayed steps are formed without 2D nucleation. However, step bunching occurs on the highly misoriented substrate surfaces ($\geq 0.5^\circ$) and increases the ETV up to 1 ML.

The effects of interface abruptness were separately investigated from those of interface flatness. At extremely high temperatures, above 800°C , the growth mode is also step-flow and there is no difference in interface flatness. However, ETV increases to more than 2 ML due to the extreme degradation of interface abruptness by interdiffusion of atoms at the interface.

Thus, ETV is affected in order by interface abruptness, step irregularity, 2D nucleation and large step height. The proportion of areas with different ETV becomes larger in this order. For example, although the thickness difference is large for step bunching, it is limited within a small area at the step edge.

To reduce the ETV which increases halfwidths, a regular step array is the most suitable structure. This is attained using vicinal substrates ($0.1\text{--}0.5^\circ$) under medium temperature ($650\text{--}700^\circ\text{C}$), which also causes no 2D nucleation, step bunching or inter-face diffusion.

This can also be applied to get good RTD characteristics. The ratio of peak to valley currents was superior for RTD fabricated on vicinal substrates, showing about the best characteristics reported on MOVPE grown RTDs.

Gate-controlled modulation of charge transport in long channel, δ -doped,
heterojunction Hall bar structures.

H.H.Wieder[#], R.S Goldman[#], A.P.Young⁺ and Jianhui Chen^{*},
University of California, San Diego, La Jolla ,CA 92093

The charge transport properties of the two-dimensional electron gas (2DEG) generated by δ -doping lattice matched $\text{In}_x\text{Ga}_{1-x}\text{As}/\text{In}_y\text{Al}_{1-y}\text{As}$ heterojunctions, $x \leq 0.4$, grown on GaAs substrates by means of compositionally step graded, strain relaxed, $\text{In}_y\text{Al}_{1-y}\text{As}$ buffer layers were investigated by means of gate-controlled, long channel, eight-arm, Hall bridge specimens using Shubnikov de Haas (SdH) oscillatory magnetoresistance measurements, made at 1.6°K, low field Hall effect and resistivity measurements and field effect transistor measurements made on the same specimens at 1.6°K and 77°K. Fast Fourier transform analysis of the SdH data indicate that the displacement of the Fermi level produced by a quasi-static applied gate voltage can populate one, two or three subbands of the 2DEG in its quantum well. The experimental data is in good agreement with theoretical Poisson/Schroedinger simulations of the equilibrium properties of such gate-controlled heterostructures and the effective electron density, mobility and threshold voltage of the 2DEG are affected strongly by the density, distribution, time constants and field effect modulation of the deep level electron traps present in the $\text{In}_y\text{Al}_{1-y}\text{As}$ charge supply layer. Low frequency transistor characteristics are consistent with a simple, long channel, modulation doped field effect transistor model employing the parameters derived from the quasi-static measurements, gradual channel approximation rules and current saturation affected by electron diffusion.

[#]Electrical and Computer Engineering Department, UCSD-0407

⁺Physics Department, UCSD-0354

^{*}Present address: Thermawave Inc. San Jose CA.

H.H.Wieder, Electrical and Computer Engineering Department-0407

University of California, San Diego, La Jolla, CA-92093-0407

Phone (619) 534-3546

Fax (619) 534-2486

ANNEALING-INDUCED NEAR-SURFACE ORDERING IN DISORDERED LPE-GROWN $\text{Ga}_{0.5}\text{In}_{0.5}\text{P}$

J.S. Luo and J.M. Olson

National Renewable Energy Laboratory, Golden, CO 80401, U.S.A.

Meng-Chyi Wu

National Tsing Hua University, Hsinchu, Taiwan 30043, R.O.C.

Most samples of $\text{Ga}_{0.5}\text{In}_{0.5}\text{P}$ grown by metalorganic chemical vapor deposition (MOCVD) are partially ordered and exhibit distinctive reflectance difference spectral (RDS) features associated with the anisotropic properties of the ordered bulk structure. It is known that the ordering is not a ground-state property of the bulk but is surface-induced during growth. On the other hand, $\text{Ga}_{0.5}\text{In}_{0.5}\text{P}$ grown by liquid phase epitaxy (LPE) is completely disordered, and we have shown that its RD spectrum is essentially featureless. In this paper, we present a study of the effects of annealing (in a PH_3/H_2 atmosphere) on LPE-grown $\text{Ga}_{0.5}\text{In}_{0.5}\text{P}$ using *ex* and *in situ* RDS. The annealing temperatures and times used in this study (650°C and tens of minutes) have virtually no effect on the *bulk* optical or structural properties of MOCVD-grown $\text{Ga}_{0.5}\text{In}_{0.5}\text{P}$. For LPE-grown $\text{Ga}_{0.5}\text{In}_{0.5}\text{P}$, we find that annealing induces bulk-like RDS features at both E_0 and E_1 with lineshapes similar to those observed for MOCVD-grown ordered $\text{Ga}_{0.5}\text{In}_{0.5}\text{P}$. These bulk-like spectral features are, however, due to near-surface reconstructions since they are effectively quenched by exposure to air. Also, the E_0 feature becomes sharper and both the E_0 and the E_1 features red-shift as the annealing process is prolonged. This indicates that the reconstruction is kinetically limited, presumably by the slow interdiffusion process necessary to achieve the ordered bulk-like structure. We also observe at temperatures greater than 400°C a third spectral feature which, for MOCVD-grown $\text{Ga}_{0.5}\text{In}_{0.5}\text{P}$, has been attributed to surface P dimers and was used as evidence for a causal link between the Group V surface reconstruction and CuPt-like ordering in III-V alloys. This peak is not stable in air, but for MOCVD-grown $\text{Ga}_{0.5}\text{In}_{0.5}\text{P}$ it is stable in a reducing atmosphere at temperatures between 25° and 650°C . For the LPE-grown sample, this peak disappears at temperatures 300°C and lower. The implications of this and other observations are presented and discussed.

Corresponding author: J.M. Olson, NREL, 1617 Cole Blvd., Golden, CO 80401. (303) 384-6488, -6531:FAX, e_mail: olson@nrel.gov.

Surface Chemistry Evolution During MBE Growth of InGaAs

K. R. Evans, J. E. Ehret, R. Kaspi, and C. R. Jones

Solid State Electronics Directorate, Wright Laboratory, WPAFB OH 45433

The tendency of indium to segregate at the surface of InGaAs films during molecular beam epitaxy (MBE) is well documented¹ and results in significant vertical grading of composition profiles at nominally abrupt InGaAs/GaAs interfaces.^{2,3} The surface segregated indium population Θ_{In} is thought to be liquid-like¹ and thus should be relatively weakly bound to the crystal surface. Thus, thermal desorption of Θ_{In} is expected to be effected by simple temperature ramping, as was recently demonstrated.² In the present study we demonstrate the quantitative determination of the time and thickness evolution of Θ_{In} via in-situ temperature programmed desorption (TPD) measurements on various $\text{In}_x\text{Ga}_{1-x}\text{As}/\text{GaAs}$ structures, with nominal $x = 0.22$, produced under varying growth conditions. Knowledge of the evolution of Θ_{In} with film thickness allows the exact calculation of the vertical composition profile.

The TPD experiment is incorporated as a subroutine in our fully automated growth program, thereby facilitating systematic studies of the evolution of Θ_{In} during growth and its dependence on substrate temperature T_s and arsenic dimer flux $F_i(\text{As}_2)$. Selective thermal desorption and quantification of Θ_{In} is effected by interrupting growth, heating to 580°C in an arsenic dimer flux, and integrating the indium ($m/e = 115$ amu) peak on a calibrated mass spectrometer positioned in line-of-sight of the substrate. We find that Θ_{In} grows approximately linearly with InGaAs thickness during initial InGaAs growth until a steady state coverage $\Theta_{\text{In,ss}}$ is reached after about 10 monolayers (MLs) growth, resulting in a 10 ML graded $x = 0 \rightarrow 0.22$ bottom interface. The value of $\Theta_{\text{In,ss}}$ increases with growth temperature and is 1.3 and 1.6 ± 0.1 MLs for $T_s = 480$ and 530°C , respectively. Thermodynamics predicts that $\Theta_{\text{In,ss}}$ should decrease with T_s and thus kinetic limitation to the incorporation process is present, with an associated activation energy of 0.2 eV, consistent with a Ga-In surface exchange reaction. TPD results on GaAs-capped InGaAs layers show that In continues to segregate at the surface after up to 10 MLs of GaAs growth, resulting in a graded top interface. The degree of grading observed for both the top and bottom InGaAs/GaAs interfaces is in excellent agreement with the results of previous in-situ² and ex-situ³ studies. The evolution of Θ_{In} with thickness is independent of $F_i(\text{As}_2)$, and the activation energy for desorbing Θ_{In} is 1.5 eV; both of these results are consistent with the predicted¹ liquid-like nature of surface segregated indium.

These results and the ability to selectively remove the surface indium population suggest an improved approach for the growth of more truly square InGaAs/GaAs quantum wells has been conceived - based on predeposition of InAs at the bottom interface, with a dose equal to $\Theta_{\text{In,ss}}$, followed by thermal desorption of $\Theta_{\text{In,ss}}$ at the top interface - and verified by photoluminescence spectroscopy. Corroboration by high resolution cross-sectional TEM is in progress. The TPD approach for studying surface segregation in MBE and for affecting composition profiles is quite general and applicable to many different materials. The combination of predeposition plus thermal desorption represents a new step in advancing the capabilities of MBE for controlling composition profiles on the atomic distance scale.

¹J. M. Moison, C. Guille, F. Houzay, F. Barthe and M. Van Rompay, Phys. Rev. B **40**, 6149 (1989).

²J. Nagle, J. P. Landesman, M. Larive, C. Mottet and P. Bois, J. Cryst. Growth **127**, 550 (1993).

³J. F. Zheng, J. D. Walker, M. B. Salmeron and E. R. Weber, Phys. Rev. Lett. **72**, 2414 (1994).

Scanning Tunneling Microscopy with Large Band-gap Semiconductor Tips and Samples*

William E. Packard

*Department of Physics and Astronomy
Arizona State University, Tempe, AZ 85287-1504
Phone: (602)965-9326; FAX: (602)965-7954*

We fabricated a large band-gap scanning tunneling microscope tip out of p-type SiC and showed that it is possible to image the Si(111)- 7×7 surface with atomic resolution in ultra-high vacuum with such a tip. The semiconducting tip allows one to use the forbidden band gap as an energy filter to inhibit some tunneling transitions, and so raises the possibility of new and interesting surface spectroscopies. To investigate this, current-voltage (I-V) profiles were taken with a p-type SiC tip and an n-type Si sample. Band bending occurred and complicated the analyses. The main features, however, of the I-V profiles can be explained in terms of a simple Schottky barrier model of the tip/vacuum/sample interface region. A comparison between theory and experiment will be presented. These results caused us to study GaN, another large-gap (3.4 eV) semiconductor, for possible future use as a tip. However, our first scanning tunneling microscopy/spectroscopy experiments necessarily dealt with the GaN as a sample probed by a metallic tip. We have imaged GaN epitaxially grown on (0001) sapphire substrates[†] using a metallic scanning tunneling microscope tip. The GaN surfaces were prepared in vacuum by heating. Prior to sample heating, no steps or order were observed with the scanning tunneling microscope, although the native surface gives a 1×1 LEED pattern. Following several heating cycles, individual atomic steps separating terraces were observed, with some atomic disorder on the steps themselves.

*Supported by the U.S. Office of Naval Research (Contract No. N00014-92-J01425)

[†]GaN samples were provided by Kathy Doverspike at the Naval Research Laboratories, Washington, D.C.

COMPOSITION AND STRUCTURE OF InP AND GaAs {100} SURFACE PHASES FROM TIME-OF-FLIGHT SCATTERING AND RECOILING SPECTROMETRY (TOF-SARS)

J. W. Rabalais, M. M. Sung, and C. Kim
Department of Chemistry, University of Houston
Houston, Texas 77204-5641.

ABSTRACT

The polar {100} face of III-V semiconductors is the important surface for device fabrication, yet atomic structure models for the reconstructed phases of this crystal face are either unproved or totally unknown. Since the density and distribution of surface sites and their donor or acceptor nature depend on the atomic constituents and surface crystallography, establishing the surface structure of the III-V semiconductors is critical to understanding interfaces on an atomic level. In this work, the composition and structure of InP and GaAs {100} surfaces in the (1x1) and (4x2) reconstructed phases have been studied by time-of-flight scattering and recoiling spectrometry (TOF-SARS). In TOF-SARS, a monoenergetic, pulsed, rare-gas ion beam is directed onto a sample and the scattered and recoiled neutral plus ion flux is velocity analyzed by TOF techniques. Typical experimental parameters are: 2-5 keV pulsed He⁺, Ne⁺, and Ar⁺ beam, pulse width ≈ 20 ns, pulse rate ≈ 30 kHz, and average current density < 0.1 nA/cm². Elemental analysis is obtained by matching the observed TOF peaks to those predicted by the binary collision approximation for elements of various masses. Structural analysis is obtained from the anisotropy in the scattering and recoiling intensities observed as a function of crystal azimuthal angle δ and beam incident angle α . This anisotropy has its origin in the shadowing and blocking effects which originate from the repulsive potentials encountered in the collisions; such effects are strongly dependent on the atomic arrangement of the surface atoms. Classical ion trajectory simulations coupled with these anisotropic patterns are used to determine the surface periodicity and interatomic spacings. The advantages of TOF-SARS for surface structural analysis are that it is element-specific and sensitive to all elements (including hydrogen), has first-layer specificity, is sensitive to short-range (< 10 Å) order, directly probes atomic cores, and provides information in real-space. Both semiconductor and metal surface interatomic spacings can be measured (to an accuracy of 0.1 Å in favorable cases), surface reconstructions and relaxations can be determined, and subsurface structure can be delineated.

The results of these TOF-SARS studies on InP and GaAs {100}-(1x1) and -(4x2) surfaces, prepared by ion bombardment and annealing, provide the relative elemental compositions of the surfaces, surface elemental periodicities, and measurements of the intradimer spacings. Models for the reconstructed (4x2) phases are determined by coupling this data with trajectory simulations. For the InP{100}-(4x2) phase, it is shown that the reconstruction is an In *missing-row-trimer* P *dimer* model (MRTD) which differs considerably from the accepted GaAs *missing-row* (MR) model. Results obtained for both InP and GaAs samples in the form of wafers or MBE deposited films are compared and contrasted.

INDEX

Tu0920	A. H.	Al-Bayati	Th1035	J.	Chen
Mo1425	R. E.	Allen	Th1050	J.	Chen
Th0815	J.	Almeida	Tu1415	X. J.	Chen
Th0900	S. F.	Alvarado	Th0800	K.-Y.	Cheng
Th0805	A.	Antonelli	We1350	T. S.	Cheng
Mo1410	M.	Arens	We1355	T. S.	Cheng
Tu0910	V. Yu.	Aristov	Tu0810	S. J.	Chey
Tu1345	V. Yu.	Aristov	Mo0940	T.-C.	Chiang
Th0805	F. T.	Bacalzo	Th0950	C.-M.	Chiang
Th0805	K. K.	Bajaj	Th0950	R. J.	Chichester
Mo1435	A.	Bauer	We1605	J. O.	Chu
Tu0915	A.	Bauer	Tu1425	D. A.	Collins
We1615	A.	Bauer	Th0815	C.	Coluzza
Th0800	E. A.	Beam III	Tu1350	J. W.	Cook, Jr.
We1555	J. C.	Bean	We1345	J. W.	Cook, Jr.
We1550	L. D.	Bell	Th0815	D.	Courjon
Th0815	O.	Bergossi	Tu0915	M. T.	Cuberes
Tu0910	M.	Bjorkquist	Tu0820	J.	Dabrowski
Tu1350	C.	Boney	Mo1055	D.	DiMaria
Mo0840	T.	Boone	Mo0935	K. J.	Dickerson
Tu0925	P.	Bordone	Mo0935	D. J.	Dumin
Tu0920	K. J.	Boyd	Tu1350	D. B.	Eason
Mo0840	D.	Brasen	We1350	L.	Eaves
Tu1355	L. J.	Brillson	Mo1420	Ph.	Ebert
Mo1430	G.	Brown	We1345	J. A.	Edmond
Tu0805	E.	Burstein	Th1100	J. E.	Ehret
Tu0810	D. G.	Cahill	Tu0925	T.	Eldridge
Tu1350	G.	Cantwell	Tu0805	L.	Elissa
Mo1410	M.	Cardona	Mo1410	N.	Esser
Mo1415	M.	Cardona	Mo1415	N.	Esser
Mo1135	W. E.	Carlos	Th1100	K. R.	Evans
Mo1435	E.	Cartier	Mo0840	K. W.	Evans-Lutterodt
Th0810	R.	Caudano	We1550	R. W.	Fathauer
Th0955	N.	Cave	Tu1425	R. M.	Feenstra
Th0950	E. E.	Chaban	We1605	R. M.	Feenstra
Tu0905	E. E.	Chaban	Mo0925	D. K.	Ferry
Th0805	T.	Chang	Tu0925	D. K.	Ferry
Tu0815	Y.-L.	Chang	Su1940	C.	Fiegna
Tu1400	Y.-C.	Chang	Mo1410	B. O.	Fimland
Th0940	K.-J.	Chao	Mo1415	B. O.	Fimland
Mo1420	Xun	Chen	Mo1405	S. R.	Forrest
Th0805	R.	Chen	Tu1435	A.	Forster
			We1350	T. J.	Foster
			We1350	C. T.	Foxon

We1355	C. T.	Foxon
Tu1355	A.	Franciosi
Th0805	L. P.	Fu
Th0805	G. D.	Gilliland
Mo0935	S. M.	Gladstone
Tu1415	W. A.	Goddard III
Th1035	R. S.	Goldman
Th1050	R. S.	Goldman
Tu1420	H.	Goronkin
Tu0910	M.	Gothelid
Mo0940	M. J.	Graham,
Tu1425	R. W.	Grant
Mo0840	M. L.	Green
Tu1040	C. M.	Greenlief
Tu0910	M.	Grehk
Mo1425	J.	Gryko
Tu1400	Z.-Q.	Gu
Th0805	M.	Hafich
Tu1350	W. C.	Harsch
Mo1400	H.	Hasegawa
Th1030	H.	Hasegawa
We1600	T.	Hasegawa
Th1030	T.	Hashizume
Tu1430	S.	Heghoyan
Mo1420	M.	Heinrich
Su1900	K.	Hess
Th0820	H.	Hess
Mo0840	G. S.	Higashi
Mo1405	Y.	Hirose
We1615	A.	Hohr
We1350	S. E.	Hooper
We1355	S. E.	Hooper
Tu0815	E.	Hu
Tu1415	J.	Hu
We1350	X.	Huang
Mo0935	T. W.	Hughes
Tu1350	W. C.	Hughes
We1345	W. C.	Hughes
Th1045	N.	Inoue
We1605	K.	Ismail
Su1940	H.	Iwai
Mo1015	H.	Iwasaki
We1350	L. C.	Jenkins
We1355	L. C.	Jenkins

Th0945	D. E.	Jesson
Mo0920	Z.	Jing
Th1030	K.	Jinushi
Th0900	M. B.	Johnson
We1345	M. A. L.	Johnson
Th1100	C. R.	Jones.
Th0800	D.	Jovanovic
We1610	H. von	Känel
Mo1405	A.	Kahn
Tu0915	G.	Kaindl
We1615	G.	Kaindl
We1550	W. J.	Kaiser
Tu1405	B. A.	Karlin
Tu0910	U. O.	Karlsson
Th1100	R.	Kaspi
Th1035	K. L.	Kavanagh
Tu1430	M.-l.	Ke
Tu1430	A.	Kestle
We1300	A.	Khan
Th1110	C.	Kim
Th0805	J.	Klem
We1440	U.	König
Mo1400	S.	Kodama
Th0900	P. M.	Koenraad
Mo1400	S.	Koyanagi
Mo0840	K.	Krisch
Mo1410	M.	Kuball
Tu1305	L. H.	Kuo
We1355	D. E.	Lacklison
Mo1420	M. G.	Lagally
We1555	M. G.	Lagally
Th1040	G. J.	Lapeyre
We1400	F.	LeGoues
Tu0910	G.	LeLay
Mo0930	D. R.	Lee
We1610	E. Y.	Lee
Mo1425	G.	Lengel
We1340	Z.	Liliental-Weber
We1600	Z.	Liliental-Weber
We1600	X. W.	Lin
Th0955	G. S.	Loechelt
Mo0940	Z. H.	Lu
Mo0920	G.	Lucovsky
Mo0930	G.	Lucovsky

Mo1435	R.	Ludeke	Tu1405	J. G.	Pellegrino
Th1055	J. S.	Luo	Th0945	S. J.	Pennycook
Tu1435	H.	Luth	We1555	L. J.	Peticolas
We1605	M. A.	Lutz	Th0800	L. N.	Pfeiffer
Th0800	J. W.	Lyding	Th0900	M.	Pfister
Mo0935	J. R.	Maddux	We1555	Y. H.	Phang
We1350	P. C.	Main	We1550	W. T.	Pike
Th0950	R. A.	Malic	Tu0915	M.	Prietsch
Tu0905	R. A.	Malic	We1615	M.	Prietsch
Mo0840	L.	Manchanda	Mo1135	S. M.	Prokes
Tu1345	P. S.	Mangat	Th1110	J. W.	Rabalais
We1550	S. J.	Manion	Tu0920	J. W.	Rabalais
Tu0915	I.	Manke	Mo0925	M. J.	Rack
We1615	I.	Manke	Tu1355	A. D.	Raisanen
Th0815	G.	Margaritondo	Th1035	K.	Rammohan
Tu0920	D.	Marton	Tu1400	S.-F.	Ren
Tu1430	C. C.	Matthai	We1345	J.	Ren
Th0945	A. J.	McGibbon	Mo1415	U.	Resch-Esser
Tu1425	T. C.	McGill	Th1035	D. H.	Rich
Th0800	J.	Menendez	Tu1430	B. E.	Richardson
Th0955	J.	Menendez	Mo1410	W.	Richter
Tu0815	J.	Merz	Mo1415	W.	Richter
We1605	B. S.	Meyerson	We1345	W. H.	Roland
Mo0940	T.	Miller,	Th0950	J. E.	Rowe
We1550	A. M.	Milliken	Tu0905	J. E.	Rowe
Tu1415	A.	Mintz	Th0800	G.	S. Spencer
Tu1405	K. E.	Miyano	Su1940	M.	Saito
Tu1435	J.	Moers	Tu1305	L.	Salamanca-Riba
Mo0935	S.	Mopuri	Th0900	H.	Salemink
Tu0820	H.-J.	Mussig	Mo1410	P. V.	Santos
Tu0805	S.	Negm	Mo1415	P. V.	Santos
We1355	S. V.	Novikov	We1600	A.	Sasaki
Su1940	T.	Ohguro	Mo1410	J. A.	Schaefer
Tu1435	C.	Ohler	Tu1350	J. F.	Schetzina
Mo0800	K.	Ohmi	We1345	J. F.	Schetzina
Mo0800	T.	Ohmi	Mo0935	R. S.	Scott
Mo0800	Y.	Okada	Th0800	A.	Seabaugh
Th1030	H.	Okada	Tu1000	A.	Selloni
Th1055	J. M.	Olson	Tu1345	F.	Semond
Su1940	M.	Ono	Tu1405	P. S.	Shaw
Th0815	T. dell'	Orto	Tu1420	J.	Shen
We1350	J. W.	Orton	Tu0815	S.	Shi
We1355	J. W.	Orton	Th0940	C. K.	Shih
Th1105	W. E.	Packard	Th0940	Y. C.	Shih

Th1045	M.	Shinohara
Mo1420	M.	Simon
We1610	H.	Sirringhaus
Th0810	S.	Sivananthan
Th0800	S. L.	Skala
Th0940	A. R.	Smith
Th0950	N. V.	Smith
We1340	H.	Sohn
Tu1355	L.	Sorba
Tu1345	P.	Soukiassian
Tu1405	S. H.	Southworth
Th0815	M.	Spajer
Th0810	R.	Sporken
Mo1415	C.	Springer
Th0940	A.	Srinivasan
We1605	F.	Stern
Mo1410	F.	Stietz
Th0940	B. G.	Streetman
Mo0935	R.	Subramoniam
Th1110	M. M.	Sung
Tu0805	H.	Talaat
Mo0840	M.-T.	Tang
Th1035	Y.	Tang
Mo0940	S. P.	Tay,
We1555	C.	Teichert
Mo0925	P.	Thanikasalam
Tu0920	S. S.	Todorov
Tu1415	B.	Tsai
Th0800	J. R.	Tucker
Mo1420	K.	Urban
Mo0935	S.	Vanchinathan
Tu1355	L.	Vanzetti
Tu0810	J. E.	Van Nostrand
Tu0900	C. G.	Van de Walle
Tu0925	D.	Vasileska-Kafedziska
We1600	A.	Wakahara
Th0810	L.	Wang
Tu1425	M. W.	Wang
We1600	J.	Washburn
We1600	E. R.	Weber
Mo1425	M.	Weimer
Mo1430	M.	Weimer
Tu0815	W. H.	Weinberg
Tu0915	H. J.	Wen

We1615	H. J.	Wen
Th0800	K. W.	West
Tu1430	D. I.	Westwood
Mo0925	T. K.	Whidden
Mo0920	J. L.	Whitten
Th1035	H. H.	Wieder
Th1050	H. H.	Wieder
Tu1430	S.	Wilks
Tu1430	R. H.	Williams
Tu1405	J. C.	Woicik
Tu0820	G.	Wolff
Th0805	D. J.	Wolford
Th1040	H.	Wu
Th1055	M.-C.	Wu
Th0800	W.	Wu
Mo0800	T.	Yabune
Tu0900	Lin	Yang
Tu0815	S. I.	Yi
Th1045	H.	Yokoyama
Su1940	T.	Yoshitomi
Th1050	A. P.	Young
Th1040	H.	Yu
Tu1350	Z.	Yu
Mo1415	J.	Zegenhagen

NEXT YEAR, PCSI-23

PCSI-23 will be held next year in La Jolla, California (near San Diego) on January 21-25, 1996. The conference chair will be C. G. Van de Walle.

One-page nominations of invited speakers and of thrust areas for consideration at PCSI-23 should be sent to the conference chair at the following address:

C. G. Van de Walle
Xerox P.A.R.C.
3333 Coyote Hill Road
Palo Alto, CA 94304
FAX: 415-812-4140
Email: vandewalle@parc.xerox.com

Most decisions will be made in March and in May.

The deadline for one-page, any-format abstract submission for PCSI-23 will be October 6, 1995. Please send three copies of each abstract to J. Dow at the address below and include your phone, FAX, and E-mail on each abstract.

The contact point for registering for PCSI-23 will again be:

J. D. Dow, PCSI-22
6031 E. Cholla Lane
Scottsdale, Arizona 85253-6902.

In order to avoid confusion, all *registration* materials and *abstracts* should be sent *by mail* to J. Dow. All other communications should be directed to C. Van de Walle.

NAME: _____

BRIEF PCSI-22 MEETING SCHEDULE

SUNDAY, JANUARY 8, 1995

- Su1400-1700 Registration and check-in at Holiday Inn check-in desk.
- Su1700 Western cookout (dinner) at the pool.
- Su1900 Opening session (Banyan).
- Su2020 Put up posters (downstairs).

MONDAY, JANUARY 9, 1995

- Mo0800 Conference office is in Teakwood, downstairs.
- Mo0800 Oral presentations.
- Mo0945 Coffee break, downstairs.
- Mo1015 Oral presentations.
- Mo1140 Lunch (in bar).
- Mo1400 Oral presentations.
- Mo1515-1705 Poster viewing & discussion, downstairs. Mo & We posters.
- Mo2000 Rump session (Banyan).

TUESDAY, JANUARY 10, 1995

- Tu0800 Oral presentations.
- Tu0930 Coffee break.
- Tu1000 Oral presentations.
- Tu1125 Lunch.
- Tu1305 Oral presentations.
- Tu1440-1630 Poster viewing & discussion. Tu & Th posters.

WEDNESDAY, JANUARY 11, 1995

- We0700 Free for activities.
- We1130 Box lunch, in bar. You may order it from the hotel earlier.
- We1300 Oral presentations.
- We1520 Coffee break and poster viewing.
- We1550 Oral presentations.
- We1620 Poster viewing.
- We1830 Dinner (Banyan).
- We2000 Poster viewing and discussions.

THURSDAY, JANUARY 12, 1995

- Th0800 Oral presentations.
- Th1000 Coffee break.
- Th1030 Oral presentations.
- Th1115 Discussion.
- Th1150 Best Paper Awards.
- Th1200 Lunch.
- Th1250 Conference ends.